UNIVERSITATEA „POLITEHNICA” din BUCUREŞTI

FACULTATEA Ştiinţe Aplicate

CATEDRA Fizică I

Nr. Decizie Senat …….. din ……

TEZĂ DE DOCTORAT

TEHNICI DE PRODUCERE ŞI ACCELERARE A FASCICULELOR RADIOACTIVE

TECHNIQUES TO PRODUCE AND ACCELERATE RADIOACTIVE ION BEAMS

Autor: Ing. Liviu Constantin PENESCU

Conducător de doctorat: Prof. dr. ing. Gheorghe CĂTA-DANIL

COMISIA DE DOCTORAT

Preşedinte	Constantin UDRIŞTE	de la	Fac. Ştiințe Aplicate
Conducător de doctorat	Gheorghe CĂTA-DANIL	de la	Fac. Ştiințe Aplicate
Referent	Alexandru JIPA	de la	Fac. de Fizică
Referent	Ion M. POPESCU	de la	Fac. Ştiințe Aplicate
Referent	Şerban DOBRESCU	de la	IFIN-HH
Referent	Thierry STORA	de la	CERN

BUCUREŞTI

2009

CONTENTS

List of acronyms and abbreviations

CERN	–	European Organization for Nuclear and Particle Physics Research
CPO	–	Charged Particle Optics (commercial simulation code)
CRC-UCL	–	Cyclotron Research Center at UCL (Université Catholique de Louvain), Louvain la Neuve, Belgium
EBIS	–	Electron Beam Ion Source (ion source type)
EBGP	–	Electron Beam Generated Plasma (ion source type)
ECR	–	Electron Cyclotron Resonance (ion source type)
ECRIS	–	Electron Cyclotron Resonance Ion Source
EURISOL	–	EURopean ISOL radioactive beam facility
FC	–	Faraday Cup
FEBIAD	–	Forced Electron Beam Induced Arc Discharge (ion source type)
GANIL	–	Grand Accélérateur National d'Ions Lourds (Caen, France)
GPS	–	General Purpose Separator (located at ISOLDE)
HIE ISOLDE	–	High Intensity and Energy ISOLDE (facility upgrade)
HIGHINT	–	Marie Curie Project at CERN, aimed to find solutions (targets, ion sources and beam transport) for the future ISOL facilities dealing with HIGH INTensity primary beams
HRIBF	–	Holifield Radioactive Ion Beam Facility (located at ORNL)
HRS	–	High Resolution Separator (located at ISOLDE)
IGISOL	–	Ion Guide ISOL
IGUN	–	Commercially available code for the simulation of ion beam extraction from a plasma ion source
ISAC	–	Isotope Separator and ACcelerator
ISOL	–	Isotope Separation On Line (method)
ISOLDE	–	Experimental facility at CERN; acronym for Isotope Separator On Line
KENIS	–	Kinetic Ejection Negative Ion Source
KOBRA	–	Commercially available code for the simulation of ion beam extraction from a plasma ion source
LINAC	–	LINear ACcelerator
MK3,MK5,MK7	–	Acronyms used for the FEBIAD subtypes used at ISOLDE before the present work
ORNL	–	Oak Ridge National Laboratory
PSB	–	Proton-Synchrotron Booster (at CERN)
REX ISOLDE	–	Radioactive beam EXperiment at ISOLDE
REXTRAP	–	Radioactive beam EXperiment cooling TRAP
RF	–	Radio Frequency
RFQ	–	Radio Frequency Quadrupole
RIA	–	Rare Isotope Accelerator
RIB	–	Radioactive Ion Beam
RILIS	–	Resonant Ionization Laser Ion Source

SCALA	–	Commercially available code for the simulation of ion beam extraction and transport from a plasma ion source
SPIRAL	–	Système de Production d'Ions Radioactifs Accélérées en Ligne (facility at GANIL)
TIS	–	Target-Ion Source (compact unit employed in the ISOL method)
TrapCAD	–	Code for the simulation of the electron dynamics in an ECRIS
TRIUMF	–	TRI-University Meson Facility (Vancouver, Canada)
VADIS	–	Versatile Arc Discharge Ion Source (series of FEBIAD-type ion sources, implemented in 2009 at ISOLDE)
VD3, VD5, VD7	–	New acronyms used for the ISOLDE FEBIAD subtypes, employing the developments introduced by the present work (VADIS series)
VORPAL	–	Versatile Object oRiented Plasma Analysis code with Lasers (commercial simulation code)

Acknowledgements / Mulțumiri

There are many people that helped me, in one way or another, to find the way in the great maze that is a PhD thesis. Some of them have been crucial for my start-up or continuation on the research road; some of them I neglected sometimes due to the immersion into the ion sources world; some of them I only meet rarely, but they all have now a part of them with me and with this thesis and with all of them I would share a thought and a glass at any time (if I am not already doing it right now):

Cristina

Thierry, Jacques, Marie-Geneviève, Florin, Gheorghe

Titu, Ileana, Gabi, Ion, Dan, Maria, Franz, Andreea, Adi, Marius, Tibi, Dan, Dana, Cristi, Marius, Diana, Raluca, Andy, Maya, Robert, Roxana, Traian, Doina, Aurelia, Marian, Ovidiu, Ion, Marek, Renan, Pascal, Nathalie, Florent, Cynthia, Antony, Thibault, Gabriel, Jean Yves, Mickaël, Jean-Luc, Laurent, Cyrille, Guillaume, Christophe, Patrick, Françoise, Illina, Iolanda, Costin, Iulian, Mihai, Ruxandra, Stelian, Marius, Monica, Costin, Silvia, Richard, Mats, Luis, Alexander, Etam, Stefano, Elian, Herta, Sandrina, Martin, Roman, Luca, Bernard, Daniel, Ermano, Mike, Fredrik, Anna, Martin, Tania, Dennis, Erwin, Emiliano, Pascal, Magnus, Alexandre, Hanna, Pierre, Sarah, Melanie, Pekka, Cecile, Sophie, Julien, Thierry, Louis, Costică, Georgeta, Cristi, Alina, Corina, Răzvan, Cristina, Vlad, Fadmar, Adrian, plus all the imaginary friends (too many to be mentioned here).

Thanks a lot, my friends!

INTRODUCTION

The production and acceleration of the Radioactive Ion Beams (RIB) continues the long line of nuclear investigations started in the XIXth century by Pierre and Marie Curie, Henri Becquerel and Ernest Rutherford. The contemporary applications of the RIBs span a wide range of physics fields: nuclear and atomic physics, solid-state physics, life sciences and material science.

ISOLDE is a world-leading Isotope mass-Separation On-Line (ISOL) facility hosted at CERN in Geneva for more than 40 years, offering the largest variety of radioactive ion beams with, until now, more than 1000 isotopes of more than 72 elements (with Z ranging from 2 to 88), with half-lives down to milliseconds and intensities up to 10^{11} ions/s. The post acceleration of the full variety of beams allows reaching final energies between 0.8 and 3.0 MeV/u.

This thesis describes the development of a new series of FEBIAD ("Forced Electron Beam Induced Arc Discharge") ion sources at CERN-ISOLDE. The VADIS ("Versatile Arc Discharge Ion Source") series allows reaching better performances through the optimization of the source design for specific ISOL requirements, through the adaptation of the nominal operation parameters or plasma properties for each specific application; the best performances cannot be achieved with a single fixed design.

Several VADIS designs are proposed based on a new analytical model of the FEBIAD sources performances, inferred from extensive experimental investigations and refined through numerical simulation. Two of them have already been implemented, providing improved ionization efficiencies for the stable noble gas tracers and best yields for the investigated radioactive isotopes obtained so far (noble gases with half-lives from several milliseconds to several minutes).

The ion source development at ISOLDE is motivated not only by present demands (increased ionization efficiency and element selectivity, lower ionization time), but also by the demands of future projects (HIE ISOLDE, EURISOL) which will have to deal with increased gas loads due to higher beam power impinging on the production target. The proposed VADIS series also provides optimized designs of arc discharge ion sources to fulfill any of the above requirements.

All the stages of the development are described, including the justification of the choices followed during this study:

- The review of the methods employed to produce RIBs, with emphasis on ISOL (Chap.1);
- The review of the ion sources employed in ISOL facilities, with in particular the detailed description of the physical phenomena in the arc discharge ion sources (Chap.2);
- The description of the employed tools (experimental, analytical and numerical) (Chap.3);
- The extensive experimental investigations (Chap.5 and 6) that allowed the inference of a new theoretical model based on the different individual physical processes affecting the ionization of the neutral atoms (Chap.4), which can predict the source performance over a wide variation range of the operation parameters;
- The analysis of the observed performance limitations (Chap.7);
- The description of the VADIS concept, together with the possible applications (Chap.9);
- The production and use of the first designs of the VADIS series at ISOLDE, based on models which correct the limitations of the previous MK5 and MK7 standards (Chap.8).

We acknowledge the financial support from the EU through a Marie Curie Fellowship ("HIGHINT" Early Stage Training project at CERN).

CHAPTER 1

PRODUCING AND ACCELERATING RADIOACTIVE ION BEAMS (RIB). THE ISOTOPE SEPARATION ON-LINE (ISOL) METHOD.

In this chapter, the methods of producing and accelerating RIBs are described, with emphasis on the ISOL method and on the ion sources employed therein.

The main applications of RIBs are listed and the two main methods of producing RIBs are compared, with respect to beam intensity and quality. The existing ISOL facilities are introduced and linked to the future development plans.

1.1. Motivation for RIBs.

Historically, the study of radioactivity started in the XIXth century, with the pioneering research of Pierre and Marie Curie, Henri Becquerel and Ernest Rutherford. The study of the long-lived isotopes existing in nature required no special equipment, but to continue the research towards shorter-lived isotopes, efficient methods to produce them (and to study them before they decay) had to be developed.

The first approach was to produce the radioactive products in a target surrounded by detectors, by bombarding it with a beam of stable isotopes. Though, this approach only allows the study of the isotopes close to stability, due to the small production cross sections.

The need for radioactive ion beams appeared as the next step on this research field, for reducing the background from the other isotopes produced in the same time, by separating and sending to the detectors only the isotope of interest. The first radioactive beams have been produced more than 50 years ago, in Copenhagen, by the ISOL method (Krypton beams at 10 to 30 kV).

The progress continued with the post-acceleration of the RIBs: through the bombardment of a target (made of stable elements) by a RIB, isotopes even farther from the stability valley can be

produced. The first post-acceleration of the RIBs have been achieved in 1992, in Louvain-La-Neuve (at CRC-UCL), Belgium [1].

The methods spread fast to many laboratories around the world, thus creating a large user community, which insured the continued development of the production methods and of the applications.

The nowadays applications of the radioactive beams are spanning a wide range of physics fields:

- Interaction cross sections;
- Nuclear structure: systematic study of atomic and nuclear properties; exotic decays far from the line of stability; shell structure far from stability – doubly magic nuclei; new nuclei beyond Z=118;
- Nuclear astrophysics: the formation of the universe in the Big Bang and understanding the synthesis of elements – understanding the r-process and rp-process;
- Test of parity violation;
- Weak-interactions and beta-decay;
- Solid state physics: investigations using pure radioactive implants;
- Biomedical studies: use of radioactive isotopes for diagnosis and therapy;

More detailed descriptions of the various applications of unstable beams can be found in references [2][3][4].

1.2. RIB production: ISOL versus "in-flight" methods.

To produce beams of radioactive ions, two methods are employed at dedicated facilities worldwide: ISOL and "in-flight".

a) The ISOL method [5].

As presented in figure 1.1, the method consists in producing radioactive isotopes in a thick, hot target, through nuclear reactions occurring between the particles of a primary (stable) beam and the atoms of the target matrix. The radioactive products diffuse out of the target material, effuse (in gaseous form) up to an ion source (coupled to the target container through a transfer tube), where they are ionized, extracted and accelerated as a beam, separated according to their A/Q ratio and sent to the physics experiment or to a post acceleration.

There are three main reaction channels used in ISOL: spallation, fragmentation and fission. The cross section for each of them depends on the species and energy of the primary beam and on the target material and thickness; therefore for producing a specific radioactive isotope, the careful choice (if possible) of the target material and beam species will maximize the production cross section.

The target temperature is typically close to the melting point of the target material, for a fast diffusion of the reaction products out of the target material.

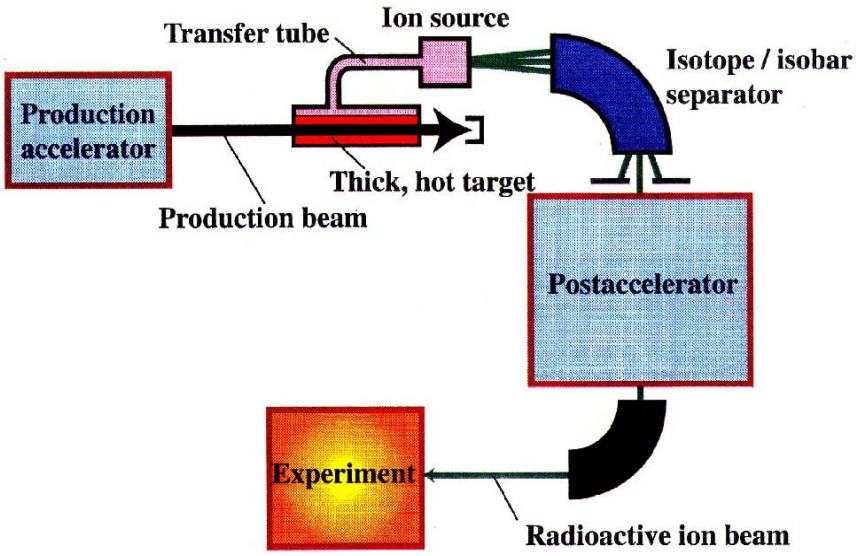

Figure 1.1. The ISOL method (schematic)

b) The in-flight method [6].

At facilities employing this method, the radioactive isotopes are produced through the fragmentation of the particles of a heavy ion beam, onto a thin target (figure 1.2).

The primary particles are not fully stopped into the target material and they are not losing their ionization state, therefore an ion source is not required and the beam is separated in A/Q and sent to the experiment.

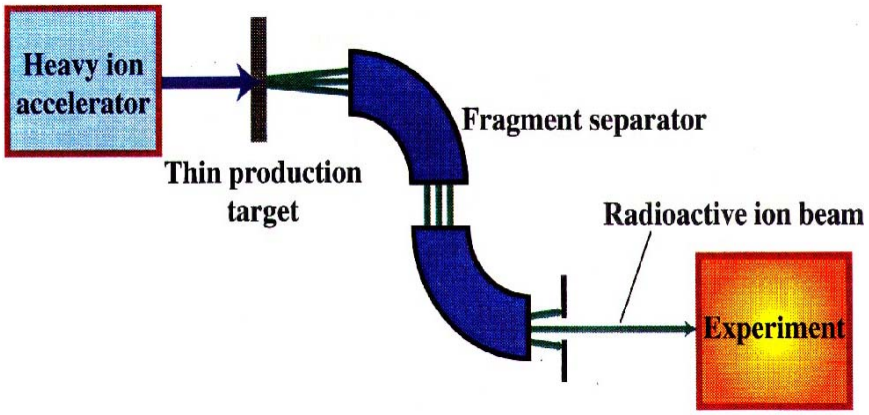

Figure 1.2. The "in-flight" method (schematic)

The two methods are complementary, as the properties of the resulting radioactive beams are significantly different: the ISOL delivers intense beams, but it is generally difficult to obtain high beam purities and the delay between isotope production and transport to experiment (due to the release process) can become limiting, while the in-flight method is faster and more selective but raises problems towards achieving high intensities and raises more problems for the beam transport to the experiments (due to the lower beam quality).

This can be easily understood by looking at the general properties of the two methods.

The main characteristics of the ISOL method are:

- High intensities are available, due to the high total cross sections, combined with a thick target.
- Difficulties in delivering refractory and reactive elements, which can hardly diffuse out of the target material or effuse to the ion source.
- Many elements are produced in the target in the same time. If, for an isotope of interest, the isobaric contaminants are not sufficiently reduced in intensity along the ISOL chain, the experiment can be hindered.
- The chemical reactions occurring in the ISOL chain from the production site up to the beam formation can play a significant role (positive if properly employed, negative if neglected). This is the case due to the high temperatures and of the production of a wide spectrum of elements in the target.
- There is a non-negligible delay in the transport of the produced isotopes to the experiment, due to all the successive phenomena that are occurring: diffusion (out of the target), desorption (from the surfaces), effusion (to the ion source), chemical reactions (eventually), ionization. Some of the products will decay on the way, thus reducing the overall efficiency of the method. The order of magnitude for the minimum isotope lifetime that can be delivered through the standard ISOL method is 1 millisecond.
- High beam powers can be achieved, as the primary beam can be defocused on the target to reduce the power density.

For the in-flight method, the main characteristics are:

- Instantaneous release from the target of the reaction products (which are already accelerated and generally in a high ionization state, due to the stripping at the passage through the target).
- Generally low intensities are produced, due to the use of thin targets.
- The beam quality is an issue, due to the large momentum spread and wide angle beam exiting from the target. This generally requires complex beam lines or different techniques of ion cooling (like absorbers or ion guides), to reduce the losses in beam transmission and isotope selection.
- A low level of isobaric contamination is produced, due to the selective cross sections (dependent on the energy of the primary beam) and of the separation of fragment products both by A/Q and by momentum (using the specific angular distributions and energy deposition in materials). Also, there are no stable contaminants in the beam from the impurities present in the system components (like target material or beam windows), as they cannot be accelerated.
- It is generally difficult to reach high beam powers, as the beam on the target needs to be small (for beam quality and intensity reasons) and consequently the targets have to be able to withstand very high power densities.

Starting from these two baselines, many variations have been developed at different facilities around the world, sometimes becoming difficult to separate between the two methods (figure 1.3):

- A converter target can be used to supply neutrons (by using primary beams of protons or deuterons), which will interact with a thick production target. The converter and the production target can even be assembled into one target.
- The transport of the particles from the target to the ion source can be achieved by using a directed flow of gas or through combination with an aerosol in a carrier gas.
- The two methods can be combined, by stopping the particles from the thin target in a solid catcher and then continue like in the ISOL method [7].
- The particles from the thin target can be stopped in a gas catcher and transferred to the ion source via a helium gas jet.
- Alternatively, after the particles are stopped in a gas, a helium gas ion guide systems can be used (method variation called IGISOL [8]). In this case, the particles are emerging as singly charged ions, therefore no further ionizer is needed.

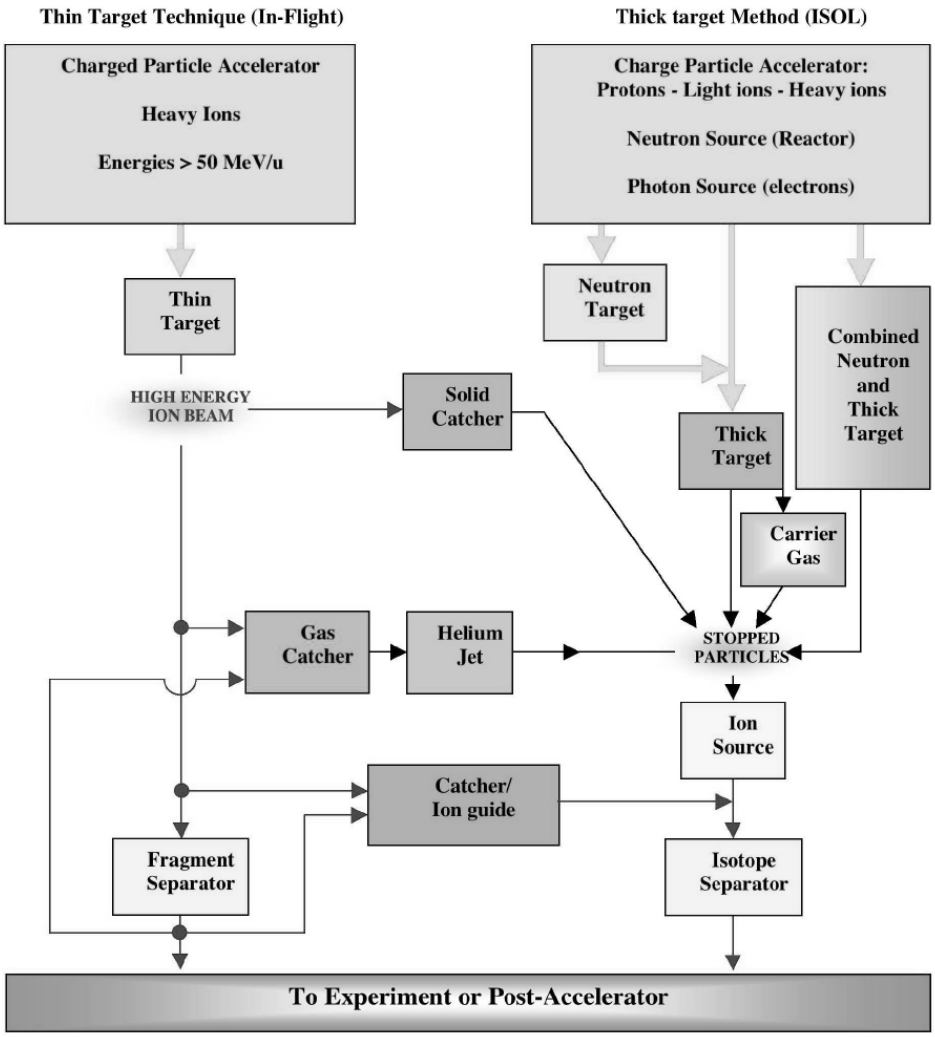

Figure 1.3. Variations and intertwining of the RIB production methods [9]

The facilities producing Radioactive Ion Beams are now spread all around the world (see figure 1.4) and the beams they deliver are more or less complementary. For the ISOL method, the most important ones are shortly described in section 1.3 and the trends towards the future are discussed in section 1.4.

Figure 1.4. A map of existing and planned ISOL and In-Flight facilities in the world [10]

1.3. Present of ISOL.

The representative facilities for the ISOL method currently operating worldwide are described in the following. A comprehensive list of ISOL facilities can be found on the webpage of the TARGISOL project [11].

1.3.1. **ISOLDE (CERN).**

Integrated into the accelerator architecture of CERN and operated by the ISOLDE Collaboration, ISOLDE [12][13] is historically the first ISOL facility (first experiments in 1967), playing a leading role in the development of new ISOL applications and technologies.

It offers the largest variety of radioactive ion beams in the world with, until now, more than 1000 isotopes of more than 72 elements (with Z ranging from 2 to 88 – see figure 1.5), with half-lives down to milliseconds and intensities up to 10^{11} ions/s. The RIBs are employed for a great number of different experiments (nuclear and atomic physics, solid-state physics, life sciences and material science).

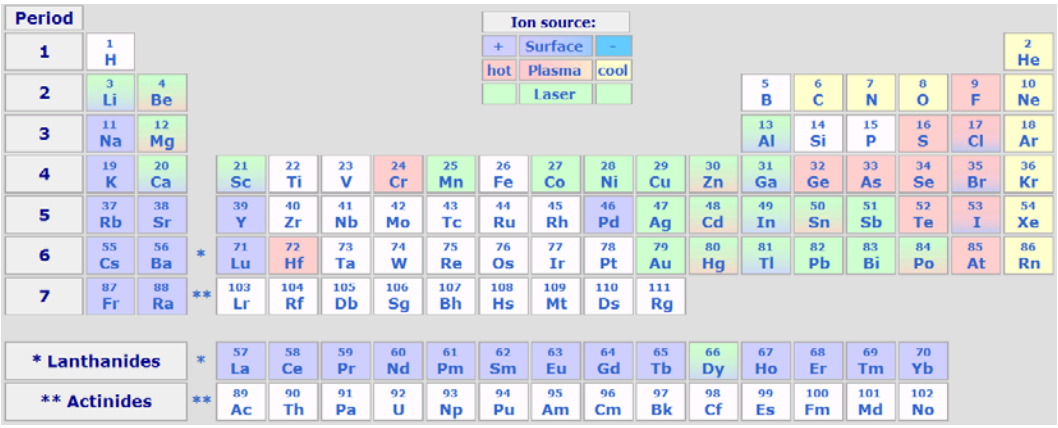

Figure 1.5. Elements produced at ISOLDE, with the corresponding ion sources [12]

At ISOLDE, radioactive nuclides are produced in thick high-temperature targets via spallation, fission or fragmentation reactions. The targets are placed in the external proton beam of the CERN PSB (figure 1.6), which has an energy of 1.0 or 1.4 GeV and an intensity of about 2μA. The target and ion source (coupled together in a compact unit – details in section 3.1.1) represent a small chemical factory for converting the nuclear reaction products into a radioactive ion beam. An electric field accelerates the ions, which are mass separated and steered to experiments.

Figure 1.6. The ISOLDE facility at CERN [12]

It has two different isotope separators, GPS (General Purpose Separator) and HRS (High Resolution Separator), with resolving powers of 2000 and >10000 respectively. The bending magnets are laminated with the possibility of running the two ISOLDE separators in parallel in a time-shared mode. The two separators are arranged such that a beam from either machine can be fed into a common beam distribution system to which almost all of the experiments in the 700 m^2 experimental hall are connected. Additionally, the GPS can select and deliver simultaneously three different beams within a certain mass range into the experimental hall via three different

beam lines (central mass, low mass and high mass beam lines); only one mass at a time can be delivered by the HRS.

Since 2001, REX ISOLDE [14]) allows the post acceleration of the full variety of beams available at ISOLDE. The final energy is variable between 0.8 and 3.0 MeV/u.

The targets employed at ISOLDE [15] span a broad range of elements and compounds: metals, metal powders, carbides, ceramics or even molten metals. The target selection criteria for a specific experiment are:

- the cross section of producing the radioactive isotope of interest;
- the chemical compatibility of the target material with the element to be produced;
- the characteristic release time of the target with respect to the element to be produced.

The ion source types available at ISOLDE are:

- The plasma ion sources, of FEBIAD type [16] (representing the central subject of the present work), employed for the production of any element (through one of the subtypes MK3, MK5 or MK7, that will be described in section 5.1), when the limited selectivity of the source complies with the experiment requirements;
- The surface ion sources [17][18], employed for the positive ionization of the alkali isotopes or for the negative ionization of the halogen isotopes. For these elements, they are very efficient and selective;
- The Resonant Ionization Laser Ion Source (RILIS) [19][20], employed for the selective ionization of the elements for which ionization schemes have been developed. The laser pulses are sent into a surface ionizer and therefore the possible contaminants are the alkali isotopes present in the ionizer tube (stable or radioactive).

Additionally to these standard options, other source designs can also be implemented for specific applications:

- MiniMono [21], an ECR-type ion source under development (employing a design developed at GANIL [22]) for the ionization of light noble gases and molecular compounds;
- KENIS ("Kinetic Ejection Negative Ion Source") [23], employing the design developed in Oak Ridge and aimed at the production of negative Fluorine beams.

1.3.2. **SPIRAL (GANIL).**

Since 2001, the SPIRAL facility, located at GANIL in Caen (France), delivers relatively intense radioactive ions of light elements from He to Kr (30 isotopes from 7 elements), mainly produced from noble or molecular gases. This "specialized" element spectrum is defined by the nuclear reactions used for production and by the employed ion sources.

The target-ion source system at SPIRAL (fig.1.7) consists in a graphite target (kept at ~2000°C), coupled (through a cold transfer line) with an ECR ion source (Nanogan III), which can provide charge over mass ratios ranging from 0.09 to 0.40.

The originality of SPIRAL lies in the use of an extended range of heavy ions as primary beams, accelerated by three cascaded cyclotrons up to the maximum energies available at GANIL (eg. 95 MeV/nucleon for ^{12}C). Such an approach differs from the proton (or light ion) beam technique in that the projectile rather than the target is varied in order to produce the

different radioactive species. This way one can use the most reliable and efficient production target for all cases.

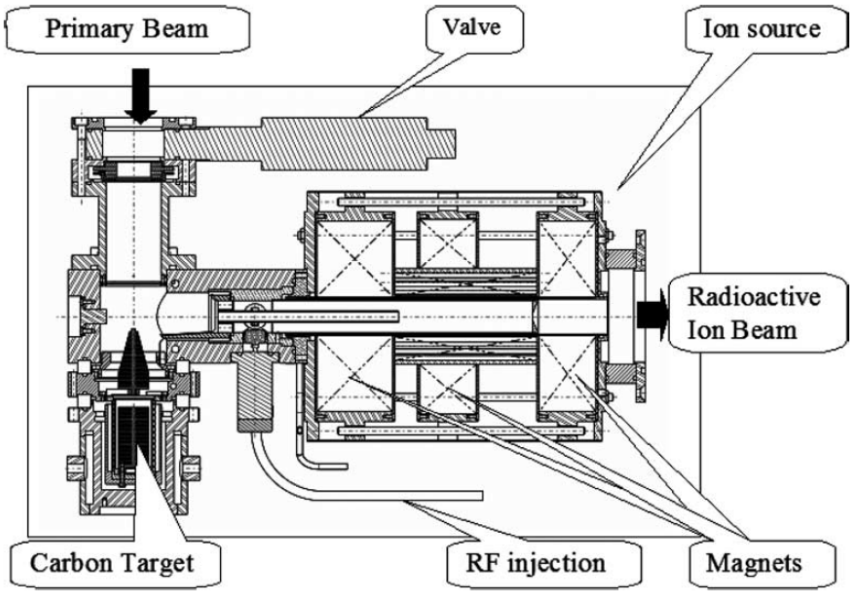

Figure 1.7. Radioactive ion production system of SPIRAL I at GANIL [24]

The RIBs are post-accelerated by the CIME cyclotron (to energies up to 25 MeV/u) and reaching the various experimental areas where they produce new reactions within the matter of a second target, placed close to specific detectors (like VAMOS and EXOGAM).

The advantages of using ECR ion sources are that high ionization efficiencies can be obtained for noble gases and generally high charge states can be obtained for the atoms reaching the source plasma. The difficulties are arising from the closeness to the hot target, which can lead to the demagnetization of the permanent magnets providing the plasma confinement, but also to lower ionization efficiencies during the target outgassing (by a factor of up to 3!). Also, changing a complex and expensive ion source every 15 days (the nominal operation time of a target-ion source unit, before being stored for 2 years for all the radioactive products therein to decay) is rather costly.

Different variations have been tried for increasing the overall performance or reliability, but they have not yet been adopted for the standard RIB production:

- "Mono 1000" [25], a compact 2.45 GHz ECR ion source, with permanent magnets, to efficiently provide 1+ ions to a second ECR for further ionization (the so called "1+/N+" method). Additionally, the advantage of such a scheme is that a 1+ source is less sensible to the pressure variations generated by the target compared to the N+ source.
- "MONOBOB" [26], a 2.45 GHz ECR ion source with electromagnets, for a radiation-hard and efficient solution of producing 1+ radioactive ion beams.

Extension of the beam choice to alkaline elements had been achieved recently, through the development of a surface ionization source [27]. Extending the RIB offer with ions of condensable elements is also foreseen for the future. FEBIAD ion sources are a strong candidate towards this development.

1.3.3. **ISAC (TRIUMF).**

The ISAC radioactive ion beam facility (fig.1.8) has been operational at TRIUMF (Vancouver, Canada) since November 1998.

It is the facility which can currently deliver the highest primary beam power (up to 100μA at 500MeV, from the H^- cyclotron of TRIUMF) and employs the targets that can withstand the highest power deposition. The standard targets are operated at 35-65 μA (different values for different materials) and can dissipate 4-5 kW, while the latest design [28] can dissipate up to 18 kW of beam power (and was operated at up to 70μA), due to an optimized radiative cooling of the target container. The target, made of Ta foils (thick of 400μm) is mounted to the Ta container equipped with radiative fins. The radiated power is absorbed in a water-cooled copper jacket. For further increase of the beam power, is it foreseen to install an ac magnet to rotate the beam on target.

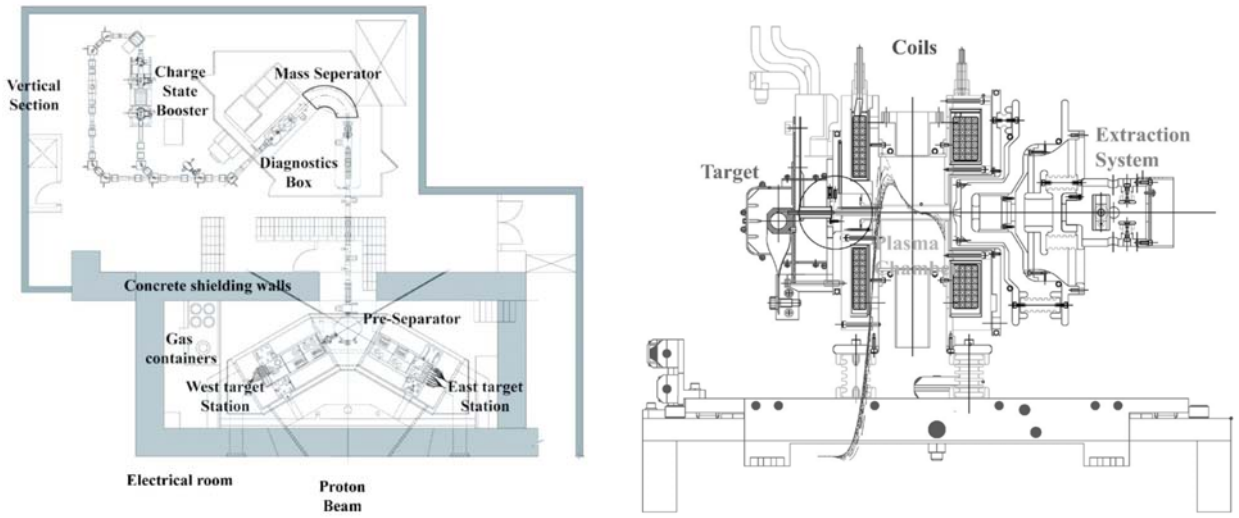

Figure 1.8. The ISAC facility at TRIUMF. Left: target stations and mass separator vault. Right: the ECR and target assembly [29]

The post acceleration of the RIBs is provided by a linear accelerator composed of a four-rod radio frequency quadrupole and a linear accelerator. The energy range is from 0.15 to 1.5 MeV/u, for A=3 to 30 amu. An accelerator upgrade is underway, which will allow to extend the mass range to A=150 amu and the energy up to 6.5 MeV/u.

An important stress is put at ISAC on the ion source development, especially towards the sources that can deal with high gas loads, as the high intensities of the primary beams are already available.

Since the beginning of ISAC most of the RIB production is done using the surface ion source. A 2.45 GHz ECR ion source was built and used on line with moderate success. In order to avoid large containment time, the ECR plasma volume is limited using a quartz tube of 12 mm diameter, located at the center of the cavity [30]. For achieving high selectivity, a laser ion source had been developed [31], in collaboration with the Mainz University.

A result of great interest for the present work is the observed effect of the gas load in the ECRIS on the ionization efficiency. The tests have been done by injecting Kr and Xe using a calibrated valve [29]. The ionization efficiency dropped by more than two orders of magnitude

when the pressure was increased from 2.0×10^{-6} to 3.9×10^{-6} mbar. The efficiency starts to decrease at about 5×10^{13} Xe atoms/s and 10^{14} Kr atoms/s, respectively.

To withstand the high pressure coming from the target material, a new ECR ion source (6 GHz and confinement provided by two sets of coils) is being developed. Also, a FEBIAD ion source has been tested at up to 70 μA proton intensity [32].

1.3.4. **HRIBF (Oak Ridge).**

The Holifield Radioactive Ion Beam Facility (HRIBF, fig.1.9) started producing RIBs in 1992. It is a test facility having as a primary purpose the development of targets and ion sources to produce radioactive ion beams using the ISOL technique [33].

The employed beam intensities are low (20-50 nAp of protons at 50 MeV, incident on UC_x targets), to allow easy access to the units for post-experiment investigations and also for enabling the reuse of ion sources and target materials after making modifications (eventually only one parameter is changed, not the entire ion source). This way, different concepts can be tested the optimum ion source parameters can be worked out, with the aim of developing new target materials and ion sources. At these facilities, direct measurements of release efficiency from target materials are available, as well as yields (ions/sec and efficiency) and hold up times from target/ion source configurations.

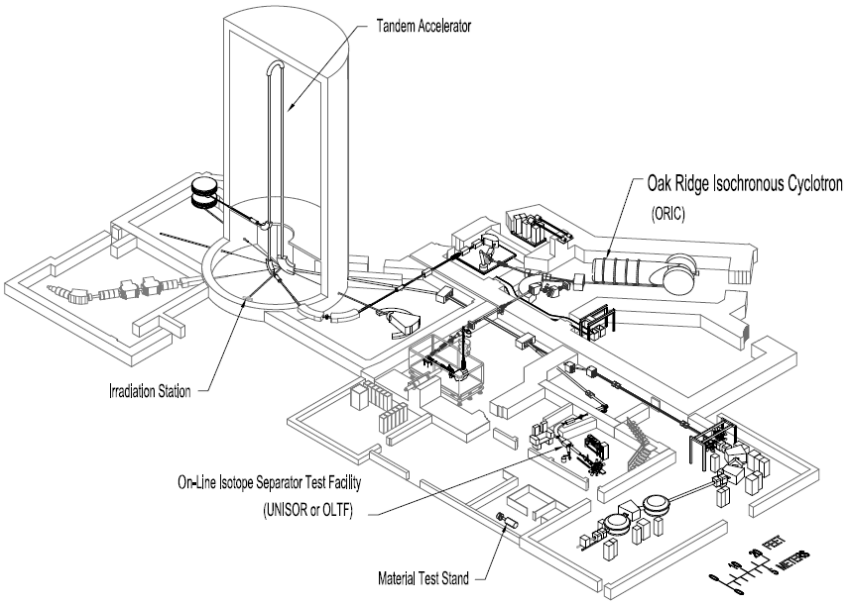

Figure 1.9. The Holifield radioactive ion beam facility (HRIBF) [33]

The light ion beam intensity from the tandem accelerator is limited to 50 nAp, for safety considerations. The separator can also accept a reaccelerated radioactive ion beam.

The specific equipments used for tests are: a tape station (for measuring yields for the various isotopes of interest; equipped for gamma ray spectrometry), offline irradiation chambers (where radioactive targets of materials of interest can be prepared), a material test stand (where offline release efficiencies can be measured), a charge exchange beam line (which allows accurate measurements of the charge exchange efficiencies, through the simultaneous measurement of the positive, neutral and negative beams following the charge exchange cell).

Since high intensity protons are the driver beams, a modified version of the ISOLDE target/ion source enclosure is used, therefore any of the ISOLDE ion sources can be implemented [34]. Both positive and negative ion sources can be tested.

1.3.5. **CRC (Louvain-la-Neuve).**

The radioactive beam facility at the Cyclotron Research Center (CRC) at Louvain la Neuve (Belgium) is the place where the first post-acceleration of the radioactive beams have been achieved, in 1992. A high-intensity cyclotron is employed as a driver and ECR ion sources to produce multiply charged ions for post-acceleration at the second cyclotron.

The primary proton beam has a power of 6kW (at 30 MeV) and the final energies of the RIBs are ranging from 0.4 to a few MeV/u.

Two very similar types of ECR sources [35][36] operated at 6 GHz are used to provide ion beams from elements ranging from He to Xe, metallic or gaseous, stable or radioactive.

For the radioactive beam production of the gaseous elements, the "classical" diffusion + effusion from solid targets is used. For the metallic or chemically reactive elements, a two step method is employed: the products are first produced in the target, after which the target (or a sample of it) is placed into the ion source, where the element to be ionized will be released from the target either through sputtering, either through evaporation in a high temperature oven. For sputtering, the bias electrode of the source serves also as the sputtering electrode, containing the material to ionize.

This approach presents the limitation that only long-lived elements can be used and the activity of the prepared probe has to be below 20mCi [36], for safe handling.

It was found [35] that the ionization efficiency of these sources is continuously decreasing at the increase of the operation pressure above 10^{-5} mbar, for all the investigated elements and support gases (efficiency decrease by about a factor 3 for every order of magnitude of pressure increase).

1.3.6. **IGISOL (Jyväskylä).**

The IGISOL ("Ion Guide ISOL") technique has been implemented and continuously improved at the accelerator laboratory of the University of Jyväskylä since 1985 [37].

This method allows the production of radioactive ion beams of mostly all elements, with half-lives down to 0.1 milliseconds.

The principle of the ion guide (fig 1.10) consists in slowing down and thermalizing the high charge state radioactive ions (energetic recoil ions from nuclear reactions in a thin target) in a noble gas (typically helium, but argon can also be employed), where their charge state is lowered through charge exchange reactions until the majority of the ions are extracted from the gas cell (with the gas flow) as singly charged. The typical carrier gas pressure varies from a few tens to a few hundreds of millibars, depending on the recoil ions that have to be stopped. After the exit nozzle of the gas cell, the neutral carrier gas is pumped away, while the ions are guided with electric fields through a further differential pumping section (with typical pumping speeds of up to 10^4 m^3/h) to an acceleration stage of a mass separator.

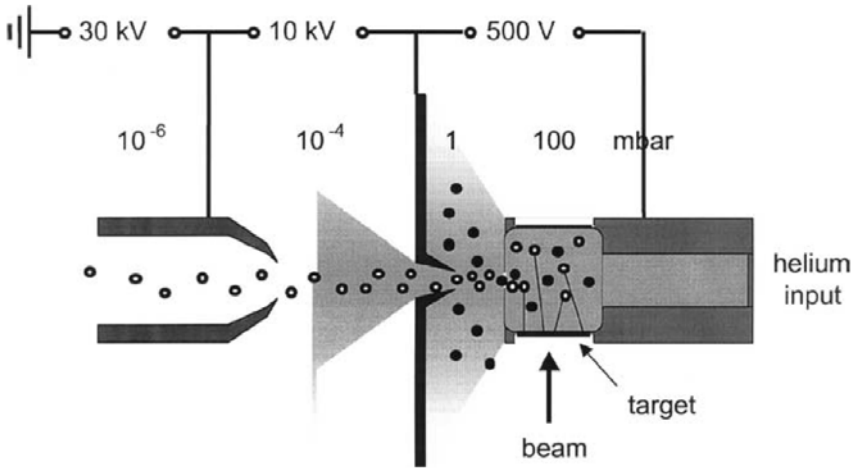

Figure 1.10. The principle of the ion guide [8]

Adaptations of the method have been designed specifically for fission [38], heavy ion induced fusion reactions (”HIGISOL” ion guide) [39] and also for deep inelastic transfer reactions [40].

In the basic technique, the reaction target is located inside the gas cell. In the fission ion guide the target is separated from the stopping volume by a thin metal foil (typically ~1mg/cm^2 of nickel), so that the plasma created by the primary beam cannot spread in the stopping cell. For both these ion guides, the gas flow also serves for target cooling.

In the HIGISOL version, the target is located outside the gas cell. The primary beam is stopped in a 7 mm diameter carbon block in front of the ion guide and only the reaction products from heavy ion induced fusion can enter the gas cell (through a large metal window), due to their larger angular distribution compared to the primary beam. The target is cooled only by conduction and radiation. Recently, a rotating target has been introduced for HIGISOL [41].

The ion guide for deep inelastic transfer reactions is a mixture of the fission and heavy ion guides, using in its design the large emittance angle of the transfer reaction.

The IGISOL technique is limited to thin targets with a thickness equal to the maximum range of a recoil ion in the target material, this being of the order of 1 mg/cm2 for fusion evaporation residues and 15 mg/cm2 for fission fragments [8]. Another limitation arises from the limited ability of a gas to stop energetic ions.

The most important mechanisms for losses of ions are diffusion to the walls of the target chamber, the formation of molecular ions with impurities in the gas, as well as the three-body recombination (involving electrons, ions and neutral gas atoms).

1.4. Future of ISOL. Motivation for ISOL ion source development.

In addition to the constant developments integrated to the existing facilities, many of these facilities have planned major upgrades of their accelerators and performances, which (as can be seen in figure 2.11) will be implemented by 2015.

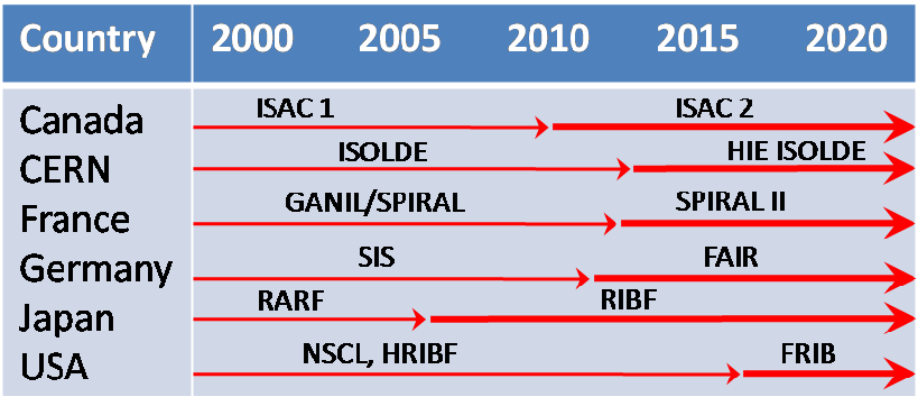

Figure 1.11. Evolution of the existing RIB facilities (both ISOL and In-Flight) [42]

Also, the on-going studies of RIA [43] and EURISOL [44] will cover aspects specific to the design and implementation of the next-generation facility, which would provide radioactive ion beams of unmatched intensity, variety and quality. The intensities of the primary beams will have to reach 100 kW (and beyond) and the post-acceleration should be at least to 100 MeV/u.

The development challenges are to produce:

- The high RIB intensity.
- The full range of isotopes.
- Very highly charged ion beams, ideally fully stripped.
- Simple, long lived targets that can withstand high primary beam powers.
- Targets, transport systems and ionizers, which provide overall particle transmission that is fast compared to the decay times.
- High selectivity.

For the targets, the main issues to be addressed are the heat dissipation and material ageing.

For the ion sources, the main (additional) issue is the ion source overloading by the increased amount of gas arriving from the target, which can deteriorate the source performances (especially the ionization efficiency and the beam quality). As was pointed out in section 1.3, this limitation has already been reached as some of the existing facilities (depending on the primary beam power and on the employed ion sources). This represents the main motivation of the work that will be presented here.

For the overall accelerator, the increased radiation level requires special attention with respect to safety regulations.

CHAPTER 2

ISOL ION SOURCES

The ion sources will have to follow the evolution of the requirements set by the different projects for future facilities worldwide (see figure 1.11). The operation and the physics parameters of the ISOL sources are described. As the physical phenomena characterizing the source operation are today well understood, a solution for future source optimizations is to change the nominal operation point (characterized by the balance between the different phenomena) by the enhancement or inhibition of some of the phenomena. This can be achieved through the adjustment of e.g. ion source geometry, materials, temperature, applied external fields – electric and magnetic, operating gas composition and pressure.

2.1. ISOL requirements for the ion sources.

The ideal ISOL ion source would have to efficiently ionize any isotope of any element reaching its enclosure, while still being able to provide isobaric selectivity and good beam quality. Shortly, this can be resumed as: fast, efficient, selective, neat and universal.

This source does not exist, as these requirements cannot be fulfilled by the same design. The requirements can therefore be split in several categories, and solutions can be found that fulfill at least one of them. Generally, the stress is put on the first three requirements:

- **Fast ionization**: for ionizing (and extracting) the short lived isotopes before they decay;
- **Efficiency**: the source should be able to ionize a fraction as high as possible of the limited amount of radioactive atoms reaching its volume;

- **Selectivity**: the mass separation depends on ΔM/M of the elements present in the beam, on the beam emittance and on the separator resolution. For the isotopes far from stability, the amount of isobaric contaminants (with low ΔM/M) closer to stability will be significantly higher, up to several orders of magnitude, therefore this selectivity should be provided either by the ion source, either by other (dedicated) ISOL components – if the source alone cannot do it.

For the future facilities or upgrades of the existing ones, the ISOL ion sources will have to fulfill the same requirements, but the operation conditions will change: the gas load coming from the production target will increase by more than one order of magnitude.

By taking the example of a primary beam of 100 kW (as is foreseen for the EURISOL direct targets), compared to the present input for a FEBIAD ion source employed at ISOLDE, the evolution of the gas load is presented in table 2.1.

Table 2.1. Evolution of the gas input composition for a ISOL FEBIAD ion source [45].

Gas input	Present day (ISOLDE)	Future (100 kW target)
Buffer gas	~13^{13} at/s	>10^{14} at/s
Radioactive products	<10^{11} at/s	~10^{14} at/s
Target evaporation; impurities	~10^{4} mbar	~10^{-3} mbar

The pressure inside the source is the result of the buffer gas load (injected through a calibrated leak), of the radioactive products released from the target and of the residual gas given by the target evaporation and impurities (see table 2.1).

Presently at ISOLDE, the buffer gas load is on the order of 10^{13} atoms/s, higher than the radioactive load (for a 2.6 kW proton beam, of less than 10^{11} atoms/s). The increase of the beam power to 100 kW would increase the radioactive gas load up to 10^{14} atoms/s [46], which will require a comparable buffer gas load.

The typical target vapor pressure is on the order of 10^{-6} mbar (which for SiC corresponds to an operating temperature of 1650°C). Considering the current ISOLDE ratio between the target and ion source volumes (62.8 cm^3 to 2.6 cm^3) the resulting pressure in the ion source given by the target evaporation can reach 10^{-4} mbar. The increase of the target volume (for the 100 kW EURISOL SiC target, a factor up to 5 was estimated [46]) will lead to a higher pressure, of 10^{-3} mbar or even more (as a too efficient impurity pumping would also reduce the time that the atoms of interest will stay in the ionizing electron beam and therefore reducing the ionization rate).

In these conditions, maintaining the same ionization efficiencies, the extracted current will have to be of 1-10 mA/cm^2, outside the present operating domain of the FEBIADs [47], but not outside the domain of other versions of hot cathode ion sources, as will be presented in section 2.2.2. More than this, it will be shown in this work that the FEBIAD sources can also be adapted for high gas loads (section 9.3.5).

Additional to the decrease of efficiency, a specific problem for the ion sources requiring a large support gas flow for sustaining the plasma is that the required pressure in the plasma chamber is typically higher than the pressure in the target container (generated by the target evaporation and diffusion of the radioactive products) and consequently the radioactive products from the target can have increased difficulties in reaching the plasma chamber.

Our approach to solving these problems is that an increased gas flow doesn't necessarily mean a higher pressure in the plasma chamber. With a careful design, the same values can be

maintained for the internal source pressure even at the increase of the gas load; for such an approach, the optimization have to be done by reducing the confinement time of the neutral atoms inside the source, while maintaining (at least) the same ionization efficiencies (through the enhancement of the ionization).

2.2. Available ion sources.

There are several types of ion sources that have been of are currently employed for the 1+ ionization of the radioactive isotopes produced through the ISOL method. These solutions have been well reviewed in the past [48][49][50][51] and we will only mention here their main characteristics and typical use.

2.2.1. **Surface ion sources.**

They have been introduced in the early 70s [52][53] and modeled analytically since then [54][55][56].

They are hot cavities (typically tubes or very small cavities) of specific materials which provide efficient thermo-ionization of elements with ionization potentials up to 6.5 eV. If the neighboring elements of a given isotope to ionize have the ionization potential above this threshold, the source is also selective.

The commonly used materials are refractory metals (niobium, tantalum, tungsten or rhenium) for positive ionization and low work function materials (ceramics e.g. LaB_6, or metallic alloys e.g. Ir_5Ce) for negative ionization.

2.2.2. **Arc discharge ion sources.**

They are typically employed for the generation of 1+ ion beams of any element volatile at ~2000°C (corresponding to an enthalpy of adsorption ΔH_a<6eV).

Their operation principle relies on the generation of a plasma in the hot, gas-tight enclosure defined by a 2 or 3 electrode system: a cathode generating the primary electrons and one or two anodes providing the accelerating potential for the electrons and eventually serving to the plasma confinement (together with a solenoid-magnet field).

Several efficient source types have been developed worldwide:

- the Nielsen source [57];
- the Hollow Cathode Source (HCIS) [58];
- the Bernas-Nier source [59];
- the FEBIAD source [47][16];
- the Electron Beam Generated Plasma (EBGP) source [60];

The first three sources are all characterized by the same base design: the cathode (a filament in all cases) and the anode are on opposite sides of the plasma chamber; only the ion extraction is different, being performed axially through a hole on anti-cathode side, cathode side, or radially through a slit in the anode, respectively.

The FEBIAD source is an optimized Nielsen source, where the implementation of a grid in front of the cathode (to accelerate the primary electron beam) allows a stable operation for a wide range of operating pressures (especially towards the low pressures, which were not

accessible to the other cathode sources, due to the threshold pressure below which the arc discharge cannot be sustained – as defined by the Bohm theory [61])

The EBGP source is an optimized hollow-cathode source, providing better performances through the implementation of a radial grid facing the internal side of the hollow cathode.

The operation pressures of the Nielsen, hollow cathode and Bernas sources are typically 1 or even 2 orders of magnitude higher compared to the FEBIAD and EBGP (10^{-3} mbar compared to 10^{-4} to 10^{-5}), which leads to higher current densities of the extracted currents (1 to 100 mA/cm^2 compared to 0.1 mA/cm^2, respectively) and also instabilities and short component lifetimes. This is the reason why the FEBIAD type is currently the most employed source from this category.

2.2.3. **ECR ion sources.**

They are employed in the ISOL method for the 1+ ionization of gaseous or molecular elements, but also as charge breeders (for further ionization of a 1+ ion beam provided by a primary ion source, as part of the approach 1+/N+ to produce RIBs).

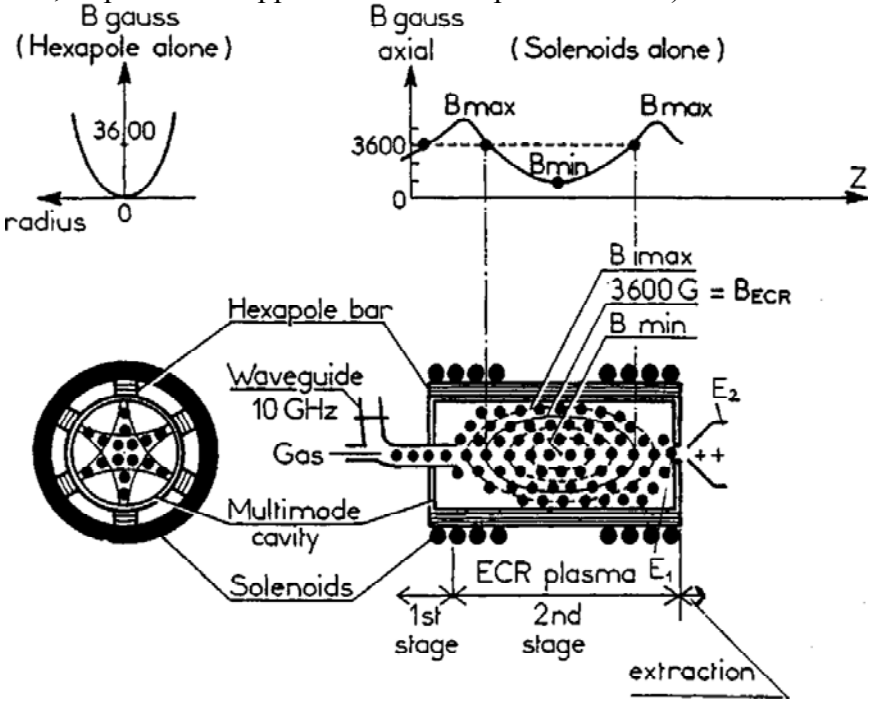

Figure 2.1. The operation principle of an ECR ion source (see text) [62].

The plasma is generated through the injection into the plasma chamber of microwaves with a defined frequency, which will transfer their energy to the electrons having the same gyration frequency (due to the Lorentz forces) as the microwave frequency (see figure 2.1). These electrons will acquire sufficient energy to produce multiply charged (up to fully stripped) ions; the resulting plasma is confined by a magnetic field created through the superposition of a hexapole magnet (placed axially around the plasma chamber) and two (or three) solenoids, placed on the injection and on the extraction side (the eventual third one in the middle) of the plasma chamber.

2.2.4. **EBIS ion sources.**

In the ISOL method, EBIS (Electron Beam Ion Sources) are only employed as charge breeders, due to their large volume which would not allow the efficient 1+ ionization for short-lived radioactive isotopes.

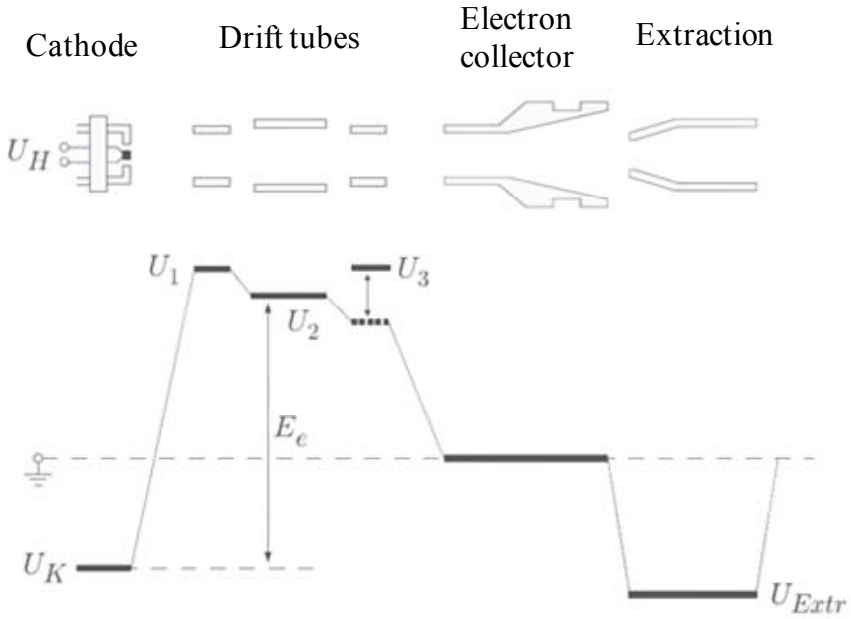

Figure 2.2. The operation principle of an EBIS ion source (see text).

The ionization is provided by an intense electron beam (see figure 2.2), maintained focused by a strong axial magnetic field and accelerated by a complex system of successive electrodes (polarized at increasing potentials, corresponding respectively to the successive ionization potentials – from 1+ to N+ – of the atoms to be ionized). The radial ion confinement is provided by the negative space charge of the electron beam, while the axial confinement is provided by the electrostatic barrier produced by the electrodes situated on the two sides of the plasma chamber. This electrostatic barrier can also allow the operation of this type of ion source in the so called "trap mode", when the generated ions can be kept confined (and eventually accumulated) in the plasma for a longer time before being extracted.

2.2.5. **RILIS (Resonant Ionization Laser Ion Source)**

The introduction of the laser ion sources into the ISOL method [19][63] brought up the possibility of selectively ionizing one element at a time, by sending into a confined cavity laser pulses with a precise wavelength scheme to produce a resonant ionization.

Generally, the cavity providing the confinement for the produced ions is a surface ionizer, due to their high operation temperature, allowing low sticking times for the isotopes of interest (see section 9.1.2) and providing a confinement to the laser produced ions. The drawback is that the ionizer will also ionize the alkali elements reaching its enclosure, which can this way affect the source selectivity.

For summarizing, there are several ion source solutions to the ISOL requirements that have been developed and implemented worldwide, for different chemical classes of elements:

- Ionization of the noble gases: can be done basically through all the ion sources, but the ECR can additionally provide selectivity against all the condensable contaminants. Still, the typically large volume of the ECR can be a drawback towards a fast ionization.
- Ionization of the metals: is achieved typically through hot cathode ion sources with small volumes and operated at high temperatures; it can also be done using RILIS sources, with more selectivity.
- Ionization of the alkalis: is achieved selectively in surface ionizers; it can also be done employing the hot cathode ion sources, but with less selectivity.
- Ionization of the halogens: is done employing surface ionizers (for negative ionization) or special sputter sources (like KENIS [23])
- Use of molecular sidebands (with Fluorine, Sulphur, Oxygen, Chlorine, etc.). The isotopes of interest are extracted as molecular compounds (ionized 1+ or 2+). Typically hot cathode ion sources are used, saturated with the gas providing the reactive element (CF_4, SF_6 etc.).

2.3. Physics of arc discharge ion sources

The main phenomena occurring in an arc discharge ion source are described in the following. Not all of them will dominate the source operation for any ion source design or for any operation parameters. For a good modeling of an ion source, their partial contribution and the parameters they depend on should be well known. This kind of analysis will be done for the FEBIAD sources in chapter 4.

2.3.1. **Neutral feed of the ion source.**

The measured variation of the radioactive ion-beam intensity as a function of time after the proton impact was fitted [64] using the empirical expression below:

$$R(t) = C \cdot \left(1 - \exp\left[\frac{t}{\tau_f}\right]\right) \cdot \left(\alpha \cdot \exp\left[-\frac{t}{\tau_f}\right] + (1-\alpha) \cdot \exp\left[-\frac{t}{\tau_s}\right]\right) \qquad (2.1)$$

This release function is a result of all the physical processes involved in the transport of radioactive atoms from their production place inside the target to their detection on the tape station, in the experimental line: diffusion from the target material, desorption from the material surface, effusion to the ion source, eventual chemical reactions all along the high temperature target-ion source unit, radioactive decay, ionization, extraction from the ion source and beam transport. Therefore, the constants C, α, τ_r, τ_f, τ_s, are dependent on the analyzed element, the target, the ion source parameters and on the associated temperatures.

In our approach, we consider that the effect of ionization and ion extraction from the ion source does not influence the shape of the release function and therefore we assume that the radioactive load in the ion source follows the relation (2.1).

The other two components of the ion source neutral load (presented in table 2.1) are not time-dependent.

2.3.2. **Electron emission.**

The characteristic construction element of the FEBIAD ion sources is the accelerating grid placed in front of the cathode, which eliminates the space-charge limitation of the cathode electronic emission. Therefore, the emitted electron current is not affected by the gas pressure or the ion production rate, and can be obtained using the Richardson-Dushman equation:

$$j_{cath} = A \cdot T^2 \cdot \exp\left[-\frac{W}{kT}\right][mA/mm^2] \tag{2.2}$$

where A is Dushman's constant (≅120 mA/mm^2K^2) and W [eV] is the work function of the cathode material.

On the contrary, because of the direct contact with the plasma, the electron emission from the anode walls is space-charge limited; therefore, it is estimated by the Child-Langmuir relation:

$$j_{th} = \left(\frac{4}{9}\right) \cdot \varepsilon_0 \cdot \left(\frac{e}{m}\right) \cdot \frac{V^{3/2}}{d^2}[mA/mm^2] \tag{2.3}$$

where V is the potential difference between the plasma and the anode walls, and d is the plasma sheath dimension (on the order of a few Debye lengths).

2.3.3. **Electron impact ionization.**

The electron beam produced by the accelerating grid will oscillate inside the anode body, confined by the applied potentials and magnetic field. The impact ionization cross section is estimated by using the Lotz semi-empirical formula [65]:

$$\sigma_{q \to q+1} \approx 4.5 \cdot 10^{-14} \sum_{nl} \frac{\ln\left(E_e / E_{q+1,nl}\right)}{E_e \cdot E_{q+1,nl}}[cm^2] \tag{2.4}$$

where E_e [eV] is the electron energy, nl are the quantum numbers defining the electrons to be stripped and $E_{q+1,nl}$ [eV] is their binding energy.

The generated ion current density inside the ion source, n_{ioniz}, is then calculated by taking into account the accelerated electron flux and the gas parameters inside the ion source.

The ionization probability for the maximum beam ionization ("beam ionization" limit) is given by:

$$p_e = 1 - \exp\left(-n_e \cdot \sigma_{q \to q+1} \cdot \tau_0\right) \tag{2.5}$$

where n_e is the electron beam density [el/cm2s] and τ_0 is the time that the neutral atom remains in the beam.

2.3.4. **Charge exchange.**

The **charge exchange** cross section between different particle species is estimated by using the Muller and Salzborn formula [66]:

$$\sigma_{q \to q-1} = 1.43 \cdot 10^{-12} \cdot \frac{Z_q^{1.17}}{E_i^{2.76}}[cm^2] \tag{2.6}$$

where Z_q is the ion charge state and E_i [eV] is the ionization potential of the neutral atom.

The resulting ion current density, $n_{ch\text{-}exc}$, can be hence deduced for specific particle densities.

When occurring, this phenomenon favors the charge transfer towards elements with lower ionization potential; therefore (qualitatively) the degree of ionization for a given element will be affected by the ratio between the particle density of the elements with a higher ionization potential to the one of the elements having a lower ionization potential.

Generally, it is the buffer gas that establishes the value for the ionization potential above which the ionization efficiency will drop, but when the radioactive gas loading becomes important, that value can be shifted.

The importance of this effect will depend on the residence time of the species: heavier elements will spend more time in the source and consequently the probability for a charge exchange collision will be higher.

2.3.5. **Ion recombination.**

The **ion recombination** is occurring by two mechanisms: radiative recombination, in the volume of the ion source, and surface recombination, on the walls of the ion source.

The volume recombination is estimated by the Bethe and Salpeter formula [67]:

$$\sigma_n = 2.1 \cdot 10^{-22} \cdot \frac{q^4 \cdot E_0^2}{nE_e \cdot \left(q^2 E_0 + n^2 E_e\right)} [cm^2] \tag{2.7}$$

where E_0 [eV] is the Rydberg energy, E_e [eV] is the free electron energy, q is the ion charge state and n is the main quantum number of the ion vacancy.

The drain current density from this kind of interaction, n_{recomb}, can hence be deduced. Nevertheless, this term is generally negligible.

The surface recombination is strongly dependent on the electron temperature, T_e, which is setting the plasma sheath properties. The ion current density through the plasma boundary can be expressed by the relation [68]:

$$j^+ = n^+ \cdot \sqrt{\frac{kT_e}{2\pi eM}} [ions / cm^2 \cdot s] \tag{2.8}$$

2.3.6. **Surface ionization.**

Depending on the element, on the nature of the surface material and its temperature, a probability β of ionization per impact can be defined (Saha-Langmuir):

$$\beta = \frac{\alpha}{1+\alpha}, \text{ with } \alpha = \frac{\sigma_i}{\sigma_0} \cdot \exp\left(\frac{W - E_i}{kT}\right) \tag{2.9}$$

where W [eV] is the work function of the ionizer material, T [K] its temperature and Ei [eV] the ionization energy of the atoms.

This probability applies to neutral atoms hitting the wall, but also to the ions recombining on the wall (if their adsorption enthalpy is low enough to let them leave the surface).

2.4. Overview. Motivation of the choices followed during this study.

Typically, the best performances for a fixed ion source design are only obtainable for a limited variation range of the operation parameters. This range is always smaller than the range for which the phenomena driving the ionization occur. Therefore, the performance limitations for any ion source type are defined by the implementation (i.e. technical choices, materials, operation parameters) and not necessarily by the principle design of the ion source.

The approach for the present work is to investigate the operation behavior of the performance of the FEBIAD ion sources for the widest possible range of variation of the operation parameters, with several goals:

- Identifying the dominant phenomena inside ion source for the current design, for allowing an accurate modeling of the source;
- Identifying the performance limitations given by the source design;
- Optimization of the source performance by eliminating the identified limitation causes and extending the range of the operation parameters to reach the best performance.

The FEBIAD ion sources have been selected for this study due to several reasons:

- Availability at CERN-ISOLDE, where this work has been done.
- Universality: they have been confirmed for the ionization of the largest number of elements, gaseous, condensable and chemically reactive.
- The high variation range of operation pressures which can still allow the source operation.
- Stability and reliability: their performances are reproducible for the same set of operation parameters and are the less affected by the inevitable variation of the gas load coming from the target container.

CHAPTER 3

INVESTIGATION TOOLS EMPLOYED IN THE PRESENT STUDY.

The results that will be presented in this work have been obtained through various approaches: experimental, analytical and numerical.

The developments that will be described, proposed or already implemented, have been justified through a self consistent analysis of all the accumulated results.

All the employed tools are described in this section, while all the analysis and data interpretation is generally distributed to the sections treating the respective investigations.

3.1. Experimental tools.

3.1.1. **The target-ion source unit.**

The target-ion source unit (TIS) employed at ISOLDE (figure 3.1) has a compact design, allowing a close coupling between the target container (a cylinder of 2.0 cm internal diameter and long of 20 cm) and the ion source. On the left side of figure 3.1, the aluminum casing can be seen, presenting no window for the protons entering from one side (centered on the target). On the right side, a view from the separator side; an air-tight valve is mounted for a safe transport and isolation of the unit (which has to be kept impurity-free before experiment and accumulates an important amount of radioactive products during operation on the online separator).

The target and ion source employed for a specific experiment are selected according to the element(s) whose RIB will have to be produced (details in section 1.3.1).

For some of the ion source investigations that will be presented in this work, the TIS unit was used without a target material filling the target container, or even completely without the target container (with the transfer line corked).

Figure 3.1. The ISOLDE target-ion source unit (exterior view)

3.1.2. **ISOLDE offline mass separator.**

The ISOLDE offline mass separator is a fully equipped separator serving several purposes:

- The test of all the target-ion source units before installation on the online separator for the production of radioactive beams;
- The commissioning of any newly-developed device or prototype (like the diagnostic device described in section 3.1.4 or of the prototypes described in chapter 8);
- Development-aimed investigations of the existing systems.

The main components of the offline separator are (figure 3.2):

- The target-ion source unit (described in section 3.1.1);
- A pair of X deflectors;
- A pair of Y deflectors;
- An Einzel lens;
- A Faraday cup for the total current extracted from the ion source;
- A 60° dipole magnet, able to separate 1+ ions up to mass 220;
- A diagnostics box (described in the following).

The geometry of the puller electrode is identical to the one existing at the online separators (GPS and HRS).

The gas required for the source operation and performance characterization is injected through fixed calibrated leaks (compressed powder calibrated leaks produced by BOC EDWARDS; now out of production). The standard values are between 10^{-5} and 10^{-7} mbarl/s; for dedicated investigations that will be presented in this study, values up to 10^{-3} mbarl/s (home-made) have been employed.

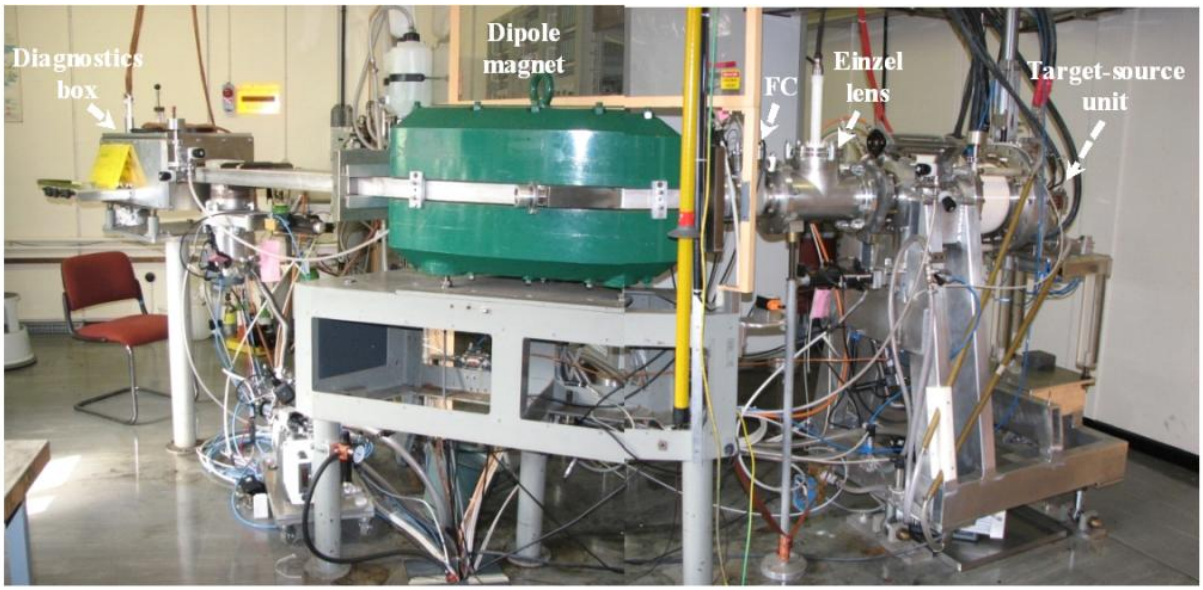

Figure 3.2. The ISOLDE offline mass separator

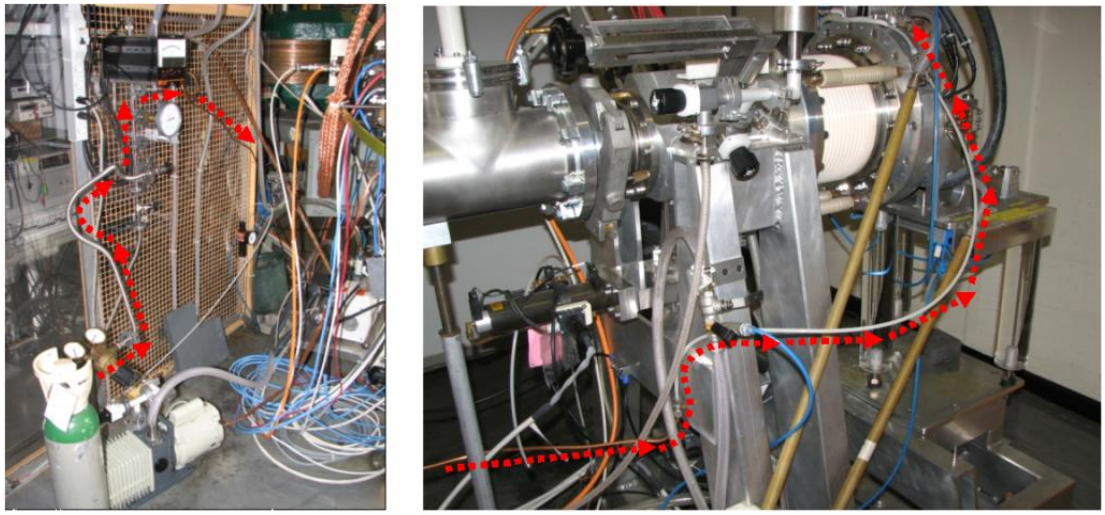

Figure 3.3. The gas injection system

These leaks are mounted in the TIS unit and a pressure of typically 1 to 1.2 bar is applied on them, supplied by an injection system presented in figure 3.3. The buffer gas bottle is installed outside the Faraday cage around the high tension platform (left side of fig.3.3) and the gas is transmitted to the TIS through a copper tube of 5 mm internal diameter (the last part is in plastic, for insuring the electrical insulation of the TIS unit – at 30 kV during operation – with respect to the rest of the separator, which is grounded). During some of the tests that will be presented in this work, the pressure of the input buffer gas was varied from 0.15 to 3 bar, to probe the variation of the injected amount of gas and consequently of the pressure inside the ion source.

The diagnostics box mounted at the end of the separated beam line contains (as indicated on figure 3.4):

- A horizontal wire scanner;
- Two horizontal slits;

- A standard Faraday cup (with a resolution on the order of milliseconds; horizontal insertion into the beam);
- A fast Faraday cup (resolution on the order of nanoseconds; vertical insertion);
- A device for the measurement of the beam energy (described in section 3.1.4).

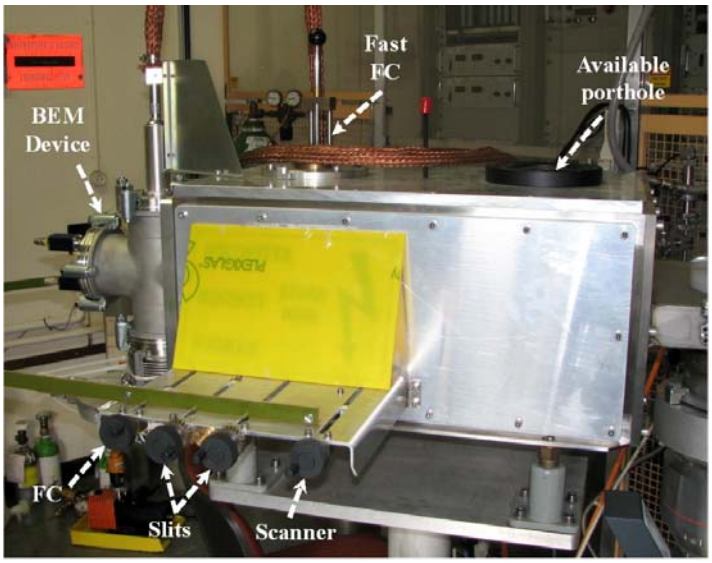

Figure 3.4. The diagnostics box allowing the characterization of the separated beam

3.1.3. **ISOLDE online mass separator.**

As most of the developments and investigations have been done on the offline separator, the instruments installed on the ISOLDE online separator that are relevant for the present study are limited:

- The beam profile monitors (scanners and grids);
- The Faraday cups;
- The tape station employed for the measurement of the yields of the radioactive isotopes.

3.1.4. **Beam energy meter.**

A beam energy analyzer developed in Jyväskylä [69] was adapted to the ISOLDE offline separator. This device can be employed to measure the beam energy distribution for a broad range of beam intensities (from a few nA up to several mA).

The detailed layouts of the devices in use at Jyväskylä and ISOLDE are presented in figures 3.5 and 3.6. The device components are:

- Front electrode with a round collimator with an opening of 5 mm (connected to vacuum-BNC at back flange);
- Center HV-electrode with mesh at center;
- Back electrode for current measurement (connected to vacuum-BNC at back flange);
- Main insulator made of plexi-glass.

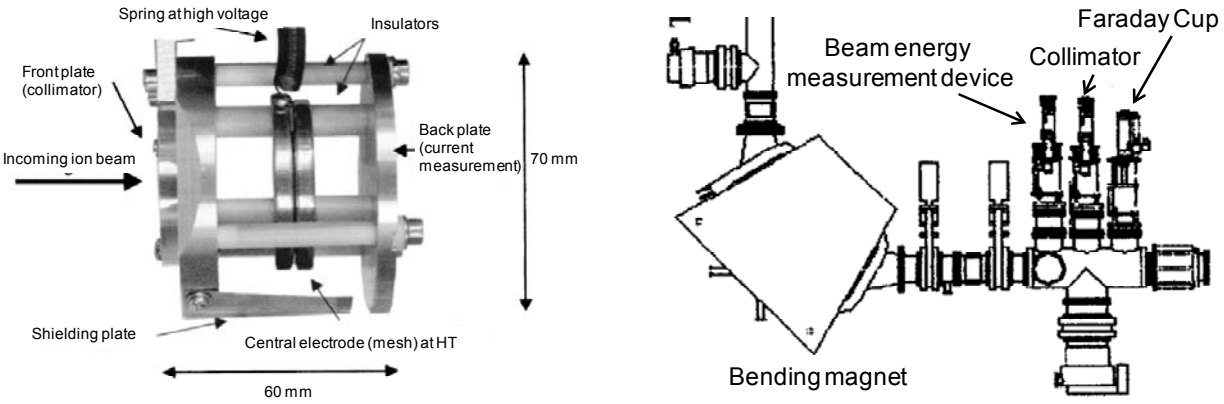

Figure 3.5. The beam energy meter used at Jyväskylä [69] and serving as base design for the device build at ISOLDE. **Left**: Main parts of the instrument. **Right:** Insertion in the beam line. The quoted dimensions are compatible with an operation at 15kV; for higher potentials, the dimensions can be scaled up linearly (as confirmed at ISOLDE).

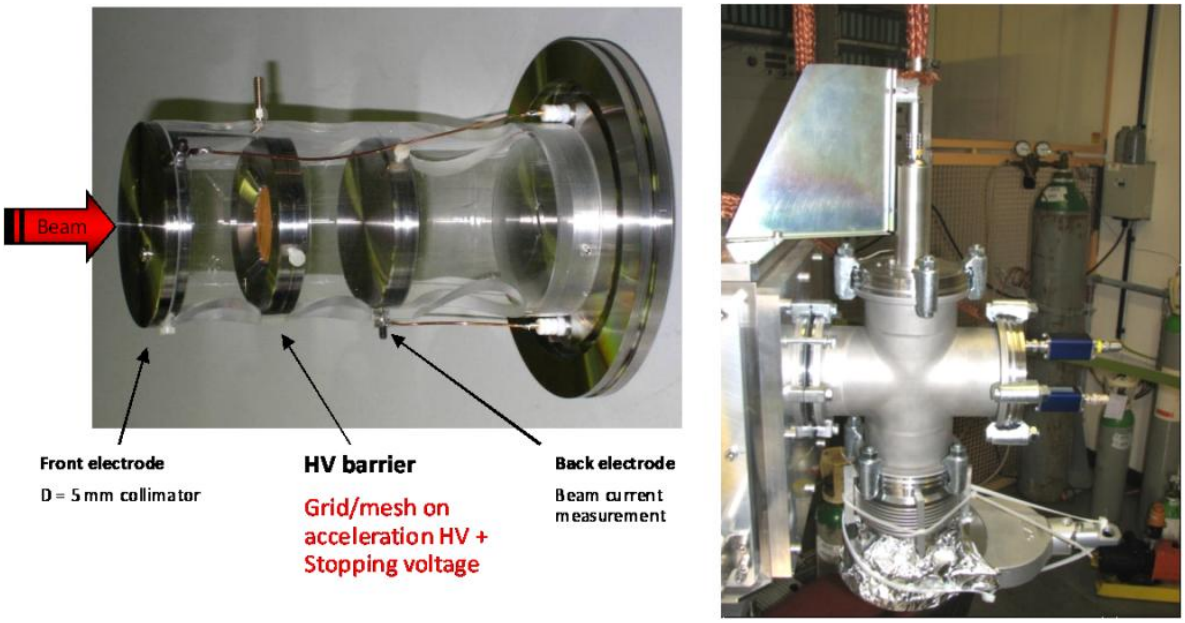

Figure 3.6. The beam energy meter installed on the ISOLDE offline separator. Left: electrode configuration. Right: installation on the diagnostics box.

The operation principle consists in applying a decelerating potential (starting from the reference value of the acceleration high voltage) into the central (mesh) electrode, which will progressively stop the beam particles having lower energies. The measurement of the beam intensity reaching the back electrode as a dependence on the applied decelerating potential is giving access to the beam energy distribution (details in chapter 6). The front electrode (collimator) is typically selecting a beam fraction of 10% to 90%.

An important requirement is the presence of a vacuum pumping unit in the beam line close to the device location, to reduce the risk of sparking but also the measurement background.

At ISOLDE, the device was attached to the diagnostics box and is used in a fixed configuration (compared to Jyväskylä, where it is only inserted into the beam line during the measurements).

3.2. Analytical calculations.

For all the phenomena occurring into an ion source (described in section 2.2.3), the parametric influence of all the contained terms has been studied analytically, for identifying all the inflexion points characterizing the respective phenomena.

As the possible range of variation for every parameter in a given ion source design is limited, this kind of investigation helped for two important results:

- The identification of the dominant (but also of the negligible) phenomena inside an investigated source, for a given design and operation conditions;
- The identification of the design limitations (when a point of maximum cannot be reached due to the fixed design).

Also, the theoretical analysis served to the construction and validation of the ion source model that will be introduced in chapter 4.

More details on the analytical approach and results are given in the corresponding sections.

3.3. Simulation tools.

Two simulation programs have been employed for the present study, with the goal of checking the feasibility of the proposed analytical model and ion source designs.

3.3.1. **VORPAL ("Versatile Object-oRiented Plasma Analysis code with Lasers").**

VORPAL is a plasma simulation code employing the PIC ("Particle-In-Cell") method, which allows a full simulation of the plasma dynamics in the presence of electromagnetic fields [70].

The PIC method consists in dividing the volume of the ion source in distinct cells, having a sufficiently small dimension in order to resolve the smallest scale phenomena. For plasma simulation, this dimension is set to the Debye length scale.

The particles, charged and neutral, can then be generated or removed in these cells, according to the theoretical input. Their motion will be determined by their momentum and by the existing field (sum of the defined external electrostatic fields and of the instantaneous space charge field). After each time step, the fields are updated, to include the new space charge distribution. The time step is chosen so that any particle (or wave) won't traverse more than one cell at a time.

VORPAL can generate ions by electron impact ionization, but its cross section library only includes a few of gases of interest; also, the impact ionization module can only treat the ionization of a buffer gas, one at a time, treated as a fluid with a constant pressure. To study the ion source behavior in the presence of a complex gas composition, with the pressure depending on the ionization rate, which is of interest in the present case, the particles will have to be generated and removed explicitly, according to the reaction rates introduced in section 2.3.

All phenomena generating particles can be implemented using particle sources with specified densities, energies and positions. The particles can be removed from the simulation when hitting defined boundaries or uniformly from the volume (with a given probability). For a better follow-up, the same type of physical particles can be treated as a sum of several different simulation particles, according to the phenomena through which they were created.

For a FEBIAD, the fastest moving particles are the grid accelerated electrons. Considering a typical accelerating voltage of 150 V, the required time step will be of about 10^{-10} s so a

simulation over 1 ms will require 10^7 steps which, depending on the particle densities, will demand several hundred hours of simulation on a single processor.

Such a simulation is only required to estimate the timescales of different effects (residence times, pulsed operation, change of ionizing efficiency produced by the variation of the operating pressure, laser pulse effect). When one wishes to simulate only the extracted current or the emittance in the steady state regime, the calculated equilibrium state can be reached faster, by setting up the initial conditions of the simulation close to the equilibrium state, as estimated by theoretical and experimental investigations.

VORPAL has been initially tested to reproduce the plasma dynamics, up to the ion extraction from the ion source [45]. The conclusion was that it can treat well the ion extraction in space charge conditions and can thus allow accessing the plasma parameters from the internal side of the plasma meniscus, where most of the extraction codes are stopping their prediction capacity.

This approach has not be pursued further in the present developments, as the code was requiring as input confirmed results for the particle generation and removal rates, which only became available in the last months of the PhD, through the investigations that will be presented in the following chapters. Therefore, by employing the results from this thesis, VORPAL can allow future refined investigations of a multi-component plasma dynamics (like selective element trapping into a multi-component plasma or plasma-laser interactions).

3.3.2. **CPO ("Charged Particle Optics").**

CPO [71] is a simulation code employed to trace the particle trajectories, under space charge conditions, in a combination of electrical and magnetic fields. It uses the Boundary Element Method for the electrical field calculation. This method consists in substituting the applied potentials with the surface charges generated; these surface charges will become the only source of all the potentials in the analyzed space. The principal advantage of this approach is that no mesh is needed for the space enclosed within the electrodes; also, there is no need to define the external boundaries (which can affect the calculations by other methods, if not properly addressed).

The field calculation in a given point is done taking into account all the contributions of the distributed charges.

The particles are defined either as individual rays (defined through their mass, charge and current) or as a beam (containing only one type of particles).

There are two methods for the ray tracing: the direct method (the field is calculated at each ray step, using the distributed charges) and the mesh method (when the field for a given point is calculated only when a propagating particle passes closer than the defined spacing between the mesh points).

The space charge is taken into account through successive iterations of the particle trajectories, where at every iteration the particles will move into the superposition of the electrical fields generated externally and generated by the space charge of the particle rays traced at the previous iteration (scaling factors can be used for the ray currents, for limiting computational instabilities). These iterations are repeated until the required accuracy is obtained.

The code is generally employed for the multi-component beam transport trough complex beam optical elements; it cannot be used for the beam extraction from an electrically neutral plasma, as it cannot treat self-consistently the plasma meniscus.

The code has been employed to investigate the dependence of the internal electrical field distribution of the ISOLDE FEBIAD sources on the densities of charged particles generated inside the source (section 8.1.2).

CHAPTER 4

MODELING OF THE IONIZATION EFFICIENCY

In this chapter, a global model for the ionization efficiency of FEBIAD sources is developed. Chronologically, the model was proposed after the interpretation of the detailed experimental investigations that will be presented in chapters 5 and 6 but, to provide a better theoretical support for the experimental results included in this work and to ease the reading of the manuscript, the model is presented beforehand. This structure also permitted the discussion on the model applicability for all the experimental results that will be presented in the following.

4.1. Existing models for electron impact ion sources and their limitations.

The arc discharge phenomena was well investigated since the beginning of the 20th century ([72][73][61]) but the general theory was developed for simple systems, where each phenomena can be identified, while each ion source type represents a unique set of phenomena, with specific applicability ranges and saturation behavior. More than that, the requirement to extract a beam from the generated plasma strongly affects the source design, making the plasma confinement imperfect on purpose and often affecting the plasma density and energy distributions.

Therefore, for meaningful results, a separate model including the significant phenomena has to be developed for each type of ion source, and eventually refined for each practical realization of the considered type.

The existing models for the overall behavior of an ion source are limited, mostly due to the limited diagnostic tools that can be employed on an operating source, to access its internal parameters. More than that, a model can only be developed (and useful) if the source performance is stable and reproducible for a given set of operation parameters, not only during different operation sessions but also for different units built after the same design.

For example, the ion source behavior can be affected by many parameters depending on the source manufacturing process or on the particular implementation of the plasma chamber to the ion source bench. The most important of these parameters are:

- The elementary composition of the employed materials;
- The vacuum conductance of the connections to the separators or within the source components;
- The stability and reproducibility of the critical input or output components (gas injection, power supplies generating the plasma or contributing to the beam extraction);
- The thermal properties and evolution of the systems connected to the plasma chamber.

Due to the different factors mentioned above, even for the same design the operation regime of an ion source (characterized by the full set of plasma parameters for stable operation) can be different for the same input parameters and therefore the ion source can reach a performance limitation because of a specific process affecting the ionization and/or beam extraction. Therefore, the range of applicability of the model is also conditioned by the specification of all the limits that can affect its application, with the corresponding parameters (operational or physical) that have to be considered.

The limitations described above led to different development solutions for different types of ion sources:

a) For the **ECR ion sources**, representing the most complex cocktail of phenomena, the general behavior can be understood through the use of several "scaling rules" developed through extensive experimental investigations and linking the most important design parameters (i.e. the magnetic field configuration and/or the frequency and power of the microwave generator) to the ion currents generated by the source ([74][75][76][62]). An exhaustive theory has been developed relatively recently [77], which treats each phenomena in detail but cannot fix all the floating parameters characterizing the global operation of a real source. The available simulation tools are limited and only treating partially the source performance. More precisely, there are codes treating the ion extraction from a plasma with given parameters (KOBRA [78], IGUN [79], SCALA [80]), codes for electron dynamics in magnetic fields (TrapCAD [81]) and codes to treat the interactions within the plasma components (VORPAL [70]), but there's no confirmed code to treat the global ion source behavior. Also, there are many codes developed in-house at various laboratories, to represent punctual aspects of an ECR operation (RF heating of the electrons, time evolution of the charge state distributions inside the plasma, etc.).

b) For the **EBIS ion sources** employed for the multiple ionization of a wide range of elements, the phenomena can be better put together in a global model, as there are fewer sources of instabilities. Also, the electron energy and the loss currents from the plasma are better controlled. The global behavior of the ion source can be globally contained in a set of analytical equations ([82][83][84]), but the resulting system requires numerical solving.

c) For the **arc discharge ion sources** employed for the generation of **1+ ion beams** (the category of interest for this study), the complexity is generally given by the small volume (making the plasma boundary effects dominant and maximizing the effect of non-uniformities) and by the extreme operation conditions (high temperature, complex gas composition, chemical reactions). Several efficient source types have been developed

worldwide (the Nielsen source [85], the hollow cathode source [58], the Bernas-Nier source [59], the FEBIAD source [47], the EBGP source [60]), but without a full model attached to justify the good performances. This led to the impossibility of implementing the same design to a different facility with the same ion source performances.

As this study is dedicated to 1+ arc discharge ion sources, we will only detail the history and limitations of the models in this category. We describe in the following the most complete models for these ion sources, linked to the most efficient designs (referenced above).

4.1.1. **The Nielsen model.**

It was developed for the Nielsen source [85]. It is based on the following assumptions:

- The ion source operates at a pressure p above the minimum pressure p_{min}, required for sustaining an arc discharge following Bohm's theory [61];
- The electrons generated by the source filament are oscillating inside the source and generating electron-ion pairs until they are slowed down below the energy corresponding to the ionization potential;
- The average electron temperature in the plasma is $T_e \approx 5eV$;
- The average ion temperature in the plasma is $T_i \approx 500°C$ (0.05eV);
- The ion density inside the source is much below the density of the neutral atoms.

In these conditions, the ionization efficiency could be expressed as:

$$\eta_{max} = C \cdot l \cdot \nu \cdot \sigma_{ie} \qquad (4.1)$$

where l = the length of the plasma chamber;
ν = number of oscillations carried out by a primary electron;
σ_{ie} = effective ionization cross section (including all processes of ionization);
C = constant depending on the acceleration gap and potential.

The model quotes only the maximum achievable value for the ionization efficiency, value that can be attained (for a fixed source and extractor geometry) through the optimization of the anode potential E_a and of the magnetic field B.

This was a very simple model, used only for qualitative analysis, as it was not including some important factors defining the plasma (n_e, n_i, T_e, T_i).

4.1.2. **The Kirchner model**

It was employed by Kirchner for the FEBIAD ion source type, developed in 1976 [47]. Later, it was also used by Nitschke, for the EBGP source that he developed in 1985 [60]. The model assumptions are:

- There is no more threshold pressure, p_{min}, required for the operation of the arc discharge, due to the introduction of an accelerating grid in front of the cathode;
- The plasma is assumed to be uniform;
- The current density extracted from the plasma is given directly by the Bohm criterion for a stable plasma sheath [61].
- Plasma parameters: $n_e \approx n_i \approx 10^{10}$ cm^{-3} ; $T_e = 10^6$ K (~100 eV) ; $\lambda_D = 0.7$mm [17].

The ionization efficiency is expressed as:

$$\eta = \frac{j_i}{j_i + j_0} \tag{4.2}$$

The gas flow of the operation gas through the outlet hole when no discharge is maintained, j_0, is expressed as:

$$j_0 = n_0 \sqrt{\frac{k \cdot T_{is}}{2\pi \cdot M_i}} \tag{4.3}$$

The ion current through the plasma boundary, j_i, can be expressed as:

$$j_i = \gamma \cdot n_i \cdot \sqrt{\frac{k \cdot T_e}{M_i}} \tag{4.4}$$

The parameters from the previous equations are:

γ = Bohm's correction factor [61], $\gamma \in (1/3;2/3)$;
n_i = ion density ;
n_e = electron density ;
T_{is} = ion source temperature (assimilated with the ion temperature);
T_e = electron temperature ;
M_i = ion mass.

Consequently, the ionization efficiency is approximated as:

$$\eta = \gamma \cdot \sqrt{2\pi} \cdot \sqrt{\frac{T_e}{T_{is}}} \cdot \frac{n_i}{n_0} \tag{4.5}$$

The use of this formula led to the conclusion that the ionization efficiency decreases with the increase of the ion source temperature or with the increase of the pressure. This is practically inaccurate, as the ion source temperature is coupled to the cathode temperature, and an increase of the latter will lead to an increase of the electron beam intensity and consequently of the ionization efficiency. But this effect was not included in the model.

This approach was only used for giving the general behavior of the source and could not fit the ion source behavior at the variation of all the parameters over more than one order of magnitude. It could also not fit the results from this study, as it does not include all the relevant parameters (compare with the model introduced in section 4.2.3).

4.1.3. **The Alton model.**

This model was proposed by Alton [86] for fitting the results obtained with the Kirchner's FEBIADs and Nitschke's EBGP (Electron Beam Generated Plasma) source.

We cannot really speak about the model assumptions, as the proposed formula for the ionization efficiency is semi-empirical:

$$\eta_{calc} = \frac{4D_0 \cdot \frac{\langle l \rangle}{S_{out}} \cdot \sqrt{\frac{\pi \cdot M_i}{8kT_i}} \cdot l_e \exp\left[\frac{-I_p}{< kT_e >}\right]}{1 + 4D_0 \cdot \frac{\langle l \rangle}{S_{out}} \cdot \sqrt{\frac{\pi \cdot M_i}{8kT_i}} \cdot l_e \exp\left[\frac{-I_p}{< kT_e >}\right]} \tag{4.6}$$

Where the parameters are:

$\langle l \rangle$ = the average path length for a particle in the plasma;

S_{out} = the emission area of the source;
D_0 = constant (cm^2/s);
I_p = the ionization potential;
l_e = number of electrons in the valence shell of the atom with a given I_p;

This model is good for fitting the maximum performances of these sources; the only confirmed parameter is the ionized element (represented through M_i and I_p), as any variation of the plasma properties was beyond the model purpose.

The model was employed using the following values for the plasma parameters: $\langle kT_e \rangle$ = 3.029 eV; T_i = 2273 K (0.17eV); $4\langle l \rangle D_0/S_{out} = 5.39 \cdot 10^3$ cm/s, without any detailing on the choice.

The expression (4.6) contains a term proportional with the **ionization cross section** ($l_e \exp\left[\frac{-I_p}{<kT_e>}\right]$), a term inversely proportional with the **ion velocity** ($\sqrt{\frac{\pi \cdot M_i}{8kT_i}}$), a term proportional with the **plasma density** ($\langle l \rangle$) and a term related with the **neutral gas effusion** (S_{out}) but the way they are mixed together is empirical and can lead to confusions if one would look for source comprehension based on this formula.

If we take a closer look at the formula (4.6), we can see that the efficiency is expressed through a monotone increasing function (of the type A/(1+A)), having the minimum equal to 0 when A=0 and increasing asymptotically towards 1 when $A \to \infty$.

The factor $A = 4D_0 \cdot \frac{\langle l \rangle}{S_{out}} \cdot \sqrt{\frac{\pi \cdot M_i}{8kT_i}} \cdot l_e \exp\left[\frac{-I_p}{<kT_e>}\right]$ can be equivalently expressed as:

$$A = C \cdot \frac{\langle l \rangle}{S_{out}} \cdot \frac{1}{v_i} \cdot \sigma_i \tag{4.7}$$

By replacing the average path length in the plasma using the formula 4.10, which will be introduced later (section 4.2.1), the factor A becomes:

$$A = \frac{C}{S_{out}} \cdot \frac{v_n}{v_e} \cdot \frac{1}{\sigma_i \cdot n_e} \cdot \frac{1}{v_i} \cdot \sigma_i \tag{4.8}$$

Considering that:

- the ion velocity is approximately equal to the neutral gas velocity ($v_i = v_n$);
- the product between the volume electronic density (n_e) and the electron velocity (v_e) is equal to the current density emitted by the cathode surface ($v_e \cdot n_e = j_{cath}$),

A and η_{calc} are becoming:

$$A = \frac{C}{S_{out} \cdot j_{cath}} \Rightarrow \eta_{calc} = \frac{\frac{C}{S_{out} \cdot j_{cath}}}{1 + \frac{C}{S_{out} \cdot j_{cath}}} \tag{4.9}$$

Put in this equivalent form, the formula 4.6 reveals its limited applicability:

- It only depends on two independent parameters, even though in the first form was apparently including all the relevant phenomena;
- It makes sense that an increase of the extraction aperture S_{out} leads to a decrease of the ionization efficiency (due to the increase of the effusion losses), but not that an increase of the current density of the primary electrons leads also to an efficiency decrease. This

error is appearing due to the fact that the model was developed for constant operation conditions (constant temperature, electronic flux, electron energy) and some of the proportionality factors which should contain the dependence on these parameters were inaccurately included in the constant leading the expression.

To put it together, the main limitations of the existing ionization efficiency models are:

- They cannot predict the response of the ion source performance at the variation of any of the external parameters. More than that, some of them are even punctual, being able to describe only the performance at the nominal parameters (the only available input being the element to be ionized);
- They cannot offer an insight on the (internal) plasma parameters, leaving some of them floating (fitting parameters); they are only aiming at characterizing the plasma boundary and therefore are not representative for the bulk of the plasma;
- They cannot be used for extrapolating the ion source performance outside the present variation range of the operation parameters;
- They don't allow an accurate estimation of the extracted beam emittance, as the ion temperature and plasma potential (the main parameters defining the emittance) are floating parameters in the model;
- They don't allow the accurate estimation of the ionization and response time of the ion source (due to the floating plasma parameters);
- The analysis of the selectivity properties is not possible, as it would require the knowledge of the specific times (confinement, wall sticking, ionization, ion lifetime) for all the investigated species.

In one sentence, the conclusion on the presented models is that they cannot serve for ion source development.

4.2. An operation-oriented model.

Any model that can explain and predict the ion source behavior is welcome and very useful for the comprehension of the ion source performances and limitations.

In particular, a model for the ionization efficiency requiring as input only the operation parameters that are set externally is presenting the additional advantage that it allows a better comprehension of the source response at the change of the operation conditions, while still permitting a quick and reliable diagnose of the source plasma.

In this section, the deduction process of such a model is being detailed.

4.2.1. **Typical parameters of a FEBIAD plasma and model assumptions.**

The FEBIAD plasma is a highly non-uniform plasma, constituted by a mixture of several populations of neutral and charged particles, with different spatial and energetic distributions.

The main components are:

a) The neutral atoms volatile in the ion source volume.
b) The primary electrons, generated through the cathode emission.
c) The ions generated through electron impact.

d) The secondary electrons, generated by the ionizations occurring in the source volume.

Other possible populations are:

e) The ions generated through surface ionization in contact with the source walls at high temperature.
f) The electrons generated by the thermal emission of the ion source walls.
g) The secondary electrons generated by the ion impact on the walls.
h) The ions generated through charge exchange in the ion source volume.

In the following, the properties of each of these populations are detailed.

a) *The neutral atoms.*

They represent a complex mixture of elements. They can be differentiated in three categories:

- The atoms of the injected buffer gas (noble gas);
- The radioactive atoms effusing from the target coupled to the ion source;
- The vapor atoms of the component materials of the target-ion source unit (becoming volatile at the operating temperature).

Their **energy** is the thermal energy at the given operation temperature.

Their **density** inside the ion source represents the equilibrium between the input flux and the effusion flux through the ion source extraction aperture (as it will be detailed in the paragraph 4.2.3.c).

The dominant inelastic collision they are suffering inside the FEBIAD is the 1+ ionization. Their average free path with respect to this interaction can be expressed as following:

$$\lambda_n = \frac{V_n}{\nu_n} = \frac{V_n}{n_e \cdot \sigma_i \cdot V_{rel}} = \frac{V_n}{(V_e - V_n)} \cdot \frac{1}{\sigma_{ioniz} \cdot n_e} \qquad (4.10)$$

where V_n, V_e, V_{rel} = neutral, electron and relative (e-n) velocities;
ν_n = collision (ionization) frequency between neutrals and electrons;
n_e = electron density;
σ_{ioniz} = ionization cross section.

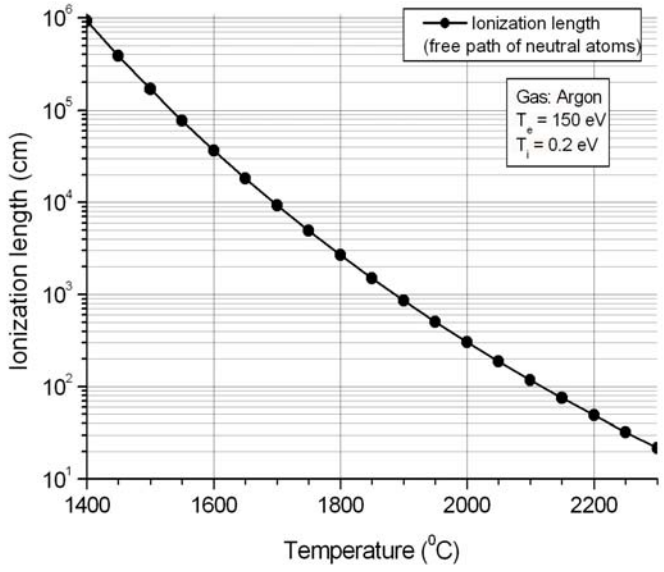

Figure 4.1. Temperature dependence of the neutral free path.

For a given element, the ionization length will therefore depend on the operation temperature, as presented in figure 4.1.

It can be seen that for the standard operation temperature of 2000°C, the neutral free path is of about 3m, corresponding to ~200 wall collisions of the neutral atoms inside the plasma chamber (considering the averaged dimension of the plasma chamber of 1.5 cm). The ionization time can therefore be deduced from this ionization length, by taking into account the thermal velocity distribution for a given operation temperature.

b) *The primary electrons.*

Their **energy** is controlled by the potential of the accelerating grid situated in front of the cathode (at approximately 1mm distance). Typically, an accelerating potential of around 150V is employed. Their energy spread will be generated by the passage through the grid geometry, through the space charge accumulations in the ion source volume and by the collisions they will suffer in their path. In this work, this energy spread is neglected.

Their **density** is controlled by the cathode temperature and by the grid accelerating potential. In the absence of the grid potential, most of the electrons emitted by the cathode will not enter the anode body (which in the FEBIAD ion sources is serving as plasma chamber) and the cathode emission will be space charge limited (therefore independent on the cathode temperature). When sufficient potential is applied to the grid, the space charge limitation can be raised to sufficiently high electron currents, so that the cathode emission can reach the thermal emission limit.

The temperature limited emission is the most efficient operation mode, as it makes full use of the cathode emissive properties and also makes the cathode emission independent on the properties of the generated plasma. The cathode emission at the thermal limit is described by eq. (2.2).

As the source geometry is fixed (and therefore the electron acceleration distance is constant), the threshold acceleration potential is dependent on the operation temperature: the higher the operation temperature, the higher will be the threshold acceleration potential required for achieving the thermally limited mode. This dependence will be detailed in section 7.2.6.

Even though the cathode surface emission (j_e) will only be controlled by the cathode temperature, the electron volume density (n_e) will still be affected by the accelerating potential, through their velocity ($n_e[cm^{-3}] = j_e[cm^{-2}\cdot s^{-1}] / v_e[cm\cdot s^{-1}]$).

The mean free path of the primary electrons depends directly on the neutral gas density inside the ion source. This dependence is presented in figure 4.2, as computed analytically.

One can see that even at operation pressures of 10^{-3} mbar (the highest values that will be employed in this study), the electron free path is still of about 10m, which is almost three orders of magnitude higher than the length of the plasma chamber (~2cm). As for a FEBIAD ion source there is no significant trapping of the electrons (and therefore they most of them only pass once through the source volume), this means that less than 1% of the primary electrons will interact in the ion source. This justifies the neglecting of the energy spread of the primary electrons.

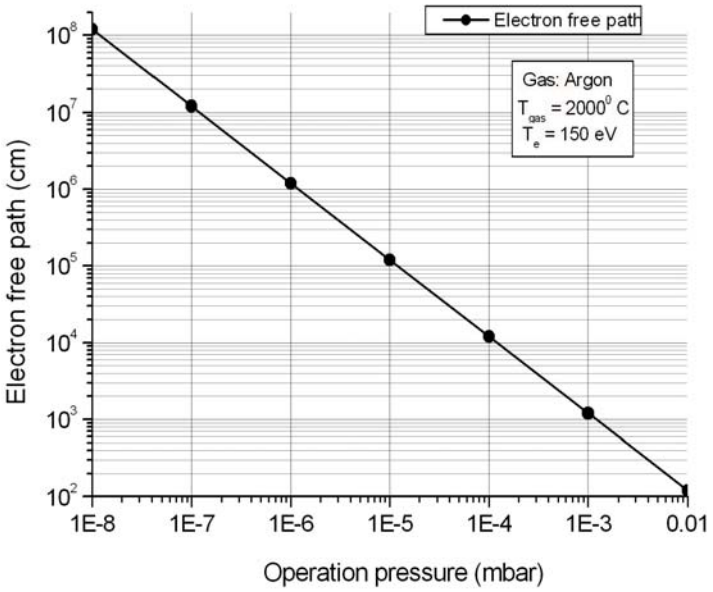

Figure 4.2. Pressure dependence of the electron free path.

Other interactions of the primary electrons (recombination, elastic scattering) are neglected in this work, due to the very low cross sections (relative to ionization) for the FEBIAD case.

c) *The ions generated through electron impact.*

This is the most important species for an efficient operation of the FEBIAD sources.

Their density is the result of the interaction between the primary electrons and the background gas. The analytic description of the ionization rate will be presented in section 4.2.3.

Their energy is considered to be the thermal energy of the neutral gas (equivalent with about 0.2eV at 2000°C). This is justified by the fact that there is no significant ion trapping mechanism inside FEBIAD sources and consequently the ion lifetime in FEBIAD plasmas is short enough for not allowing any heating mechanism (elastic collisions).

d) *The secondary electrons* (generated through ionization).

Their density is equal to the density of the generated ions (and therefore can be expressed though the same formula for the production rate).

Their energy can be estimated using the parameterization developed in reference [87], adapted for the FEBIAD energies in figure 4.3.

It can be seen that less than 20% of the secondary electrons will have energies higher than 10 eV (which could allow ionizations produced by these electrons). More than this, their velocity is about 10 times smaller than for the primary electrons and the ionization cross section is more than two times lower at the energies of the secondary electrons (compared to the primary electrons).

As will be detailed in the following (section 4.2.3), the important factor for an electron species to produce ionization is the product $n \cdot v \cdot \sigma$ (density, velocity and cross section), therefore

the ionization produced by the secondary electrons is representing less than 1% of the ionization generated by the primary electrons.

Also, their lifetime in the FEBIAD source is not sufficiently long for producing significant elastic collisions.

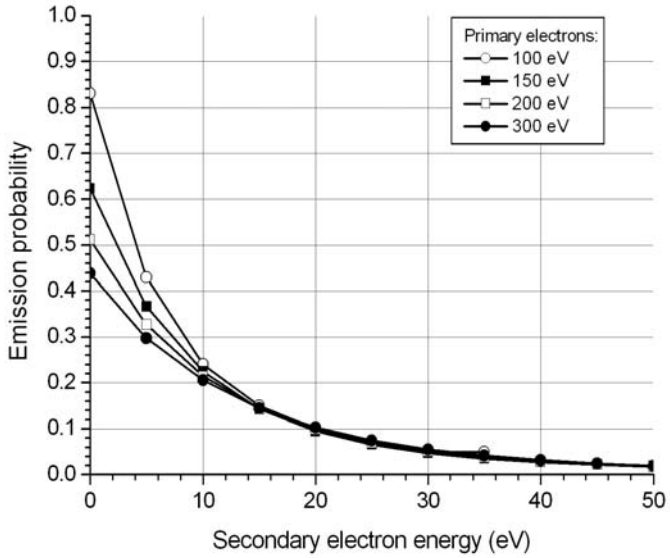

Figure 4.3. Energy distribution of the secondary electrons (as obtained from [87]

Therefore, the secondary electrons are negligible for any binary interaction occurring in the ion source volume, but they are important when considering the total space inside the ion source.

e) *The ions generated through surface ionization.*

Their contribution to the ion source behavior can be important, as some impurities that can be typically encountered in significant amounts in ISOLDE FEBIADS (Potassium and Sodium) can be surface ionized.

As the impurity amount is not well known, the ion density in the plasma can only be estimated from the intensity of the extracted current. Saha's formula (2.9) can be used for relating the ionic volume density to the neutral volume density for the impurity element. The neutral volume density at a given temperature is controlled by the vapor pressure of the element in cause.

Their initial energy is equal to the thermal energy of the neutral atoms but, considering that these ions are generated at the source walls and the FEBIAD plasma potential is negative (see chapter 6), they will be accelerated to up to 10-30 eV towards the source center, where they can affect the useful electron impact ionization.

In most of the experimental investigations presented in this study (more precisely, for the cases where the surface ionization was not among the investigation goals), the ion source was carefully outgassed of the contaminants that could be surface ionized, so that their contribution to the total beam was less than 1%. In this cases, the surface ionization was neglected.

f) *The electrons thermally emitted by the ion source walls.*

This emission is space charge limited, due to the direct contact of the plasma with the walls. The space charge limitation is enforced by the fact that the plasma potential is negative with respect to the ion source walls (see chapter 6).

Based on this justification, this population was neglected in the present study.

g) *The secondary electrons generated by the ion impact on the walls.*

There are negligible in the FEBIAD case, considering the electron and ion energies discussed above, which are far from those required by this emission phenomena.

h) *The ions generated through charge exchange.*

Their density is insignificant for normal operation of FEBIAD sources (as will be justified in section 7.2.1); therefore they are neglected in this study.

In conclusion, the FEBIAD plasma is generated and controlled by the electron beam produced by the cathode emission. For showing the wide range of plasma properties that this kind of source can cover, we present in figure 4.4 the variation of the Debye length determined by these electrons, as a function of the operation temperature. The Debye length is considered to be limited by the primary electrons and was computed using the formula:

$$\lambda_D^2 = \frac{\varepsilon_0 k T_e}{e^2 n_e} \quad \Rightarrow \quad \lambda_D(cm) = 743 \cdot \sqrt{\frac{T_e(eV)}{n_e(cm^{-3})}} \tag{4.11}$$

where n_e (the electron density generated by the cathode emission) is the only temperature dependent unit.

One has to keep in mind that this graph is presented only for qualitative reasons, as the velocity distribution of the FEBIAD electrons is neither Boltzmannian, neither isotropic.

It can be seen that below 1800°C, the Debye length is higher or equal to the source diameter; therefore no electrical shielding can be possible in this range. After 1800°C, even though some shielding can start to appear towards the source center, it will not be very effective for the ions produced in a FEBIAD, due to their very low energy (<0.2eV). Considering that the applied electrical potentials are on the order of 150V (the potential applied to the anode body), a sufficient shielding for these ion energies will only be produced after a distance of about $3.5\lambda_D$. This means that the center of the plasma is not sufficiently shielded from the wall potential if the source diameter is smaller than $7\lambda_D$. Considering that the real electron density will be smaller than the one considered in figure 4.4, this means that an important part of the FEBIAD plasma will not be electrically shielded even up to 2200°C, which represents the highest values that can be employed at ISOLDE.

This will be confirmed by experimental measurements presented in the following sections, where the source behavior with respect to temperature variation is following the same trend up to the highest tested temperatures (~2250°C).

Based on these considerations, the main assumption for the ionization efficiency model developed in this work is that there is no trapping effect of the ions in the plasma; once ionized, the ion will follow the electrical potential distribution present inside the ion source and will end either by being extracted, either by recombining on the ion source walls.

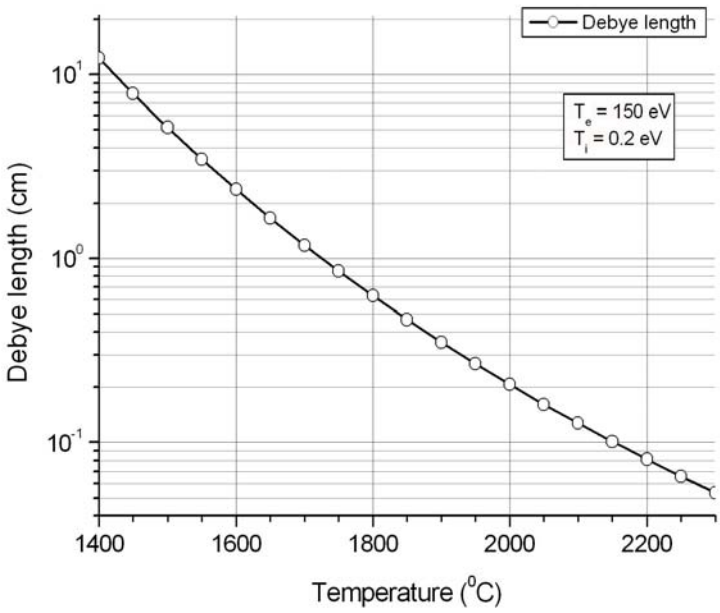

Figure 4.4. The estimative (see text) temperature dependence of the Debye length

There are two big consequences to this:

a) The ion lifetime in the ion source is much shorter compared to the ionization time; therefore, most of the limitations of the source performances are related to the relation between the ionization time and successful extraction as ion. This is the main direction of investigation in this work.
b) The ion lifetime is short enough for not having other collisions (charge exchange, elastic collisions); therefore, the model remains simple enough for not requiring numerical solving.

In other words, the electrical field penetration into the source volume is an important parameter for the FEBIAD ionization efficiency. In the following, we will characterize this field penetration in two equivalent ways, depending on situation:

a) Through the fraction f_{extr} of the generated ions that are successfully extracted, before recombination on the walls. This adimensional unit is also representing the average extraction probability for an individual ion, after one ionization.
b) Through the "active volume" of the ion source, V_{active}, defined as the fraction of the total ion source volume from where the generated ions are successfully extracted.

The relation between these two equivalent factors is $f_{ext} = V_{active} / V_{total}$.

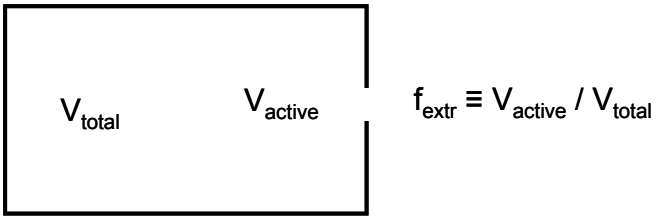

Figure 4.5. Geometrical definition of the extraction factor, f_{extr}

Considering that the typical dimensions of an ion source with a high density plasma (ECR, EBIS) are about two orders of magnitude higher than the Debye length, the usual value of f_{extr} for such a source is on the order of 10^{-6} (through proportionality with $(\lambda/L)^3$), which would make this approach inaccurate, as the ion beam extraction will only be controlled by the plasma meniscus properties.

But for the FEBIAD low density plasma described above, f_{extr} is only on the order of 10^{-1}; in this case, V_{active} is defined primarily by the electrical field distribution inside the ion source and is therefore affected by all the operation parameters.

4.2.2. **Influence of the operation parameters on the ionization efficiency.**

The FEBIAD operating parameters are acting on several phenomena at once – either directly or through charged particle dynamics inside the source. Therefore their influence on the ion source performance cannot be studied independently.

The parameters available for FEBIAD tuning are:

- The temperature;
- The magnetic field;
- The anodes potentials ;
- The operating gas parameters (pressure and composition).

The figure 4.6 presents qualitatively the way the operating parameters are acting on the ionization efficiency. Even when their direct influence is only on one internal property of the ion source their effect is being transmitted, through the particle dynamics inside the source, to all the other internal properties.

The ideally controllable ion source should have every parameter acting on only one effect described in figure 4.6.

Theoretically, this can be achieved, but the resulting ion source can become too complicated to build and operate. Therefore, it is important to identify the critical limitations for specific operating conditions and to act directly on them, using eventually different ion source designs for different operating conditions.

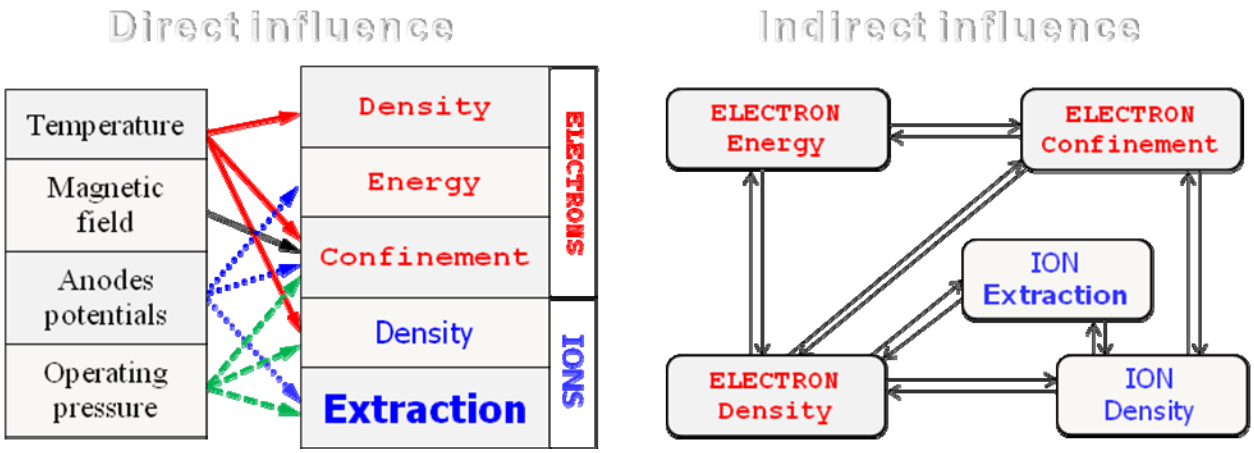

Figure 4.6. The influence of the FEBIAD operating parameters on the ion extraction (and consequently on the ionization efficiency).

We detail in the following the role of the above parameters on the source operation.

a) *The temperature.*

Presently is the crucial parameter for generating an ionizing electron beam into the source from the cathode surface.

Therefore, it influences directly the density of the primary electrons (and consequently the density of the generated ions), but also their confinement, as the percentage losses of the generated electron beam will depend on its density.

But the cathode is the only heating element in the ion source volume, therefore the heating of the anode is obtained by direct radiation from the cathode and its temperature cannot be controlled independently on the cathode temperature. The interest on doing that would be to improve the confinement of the primary electron beam by emitting more thermal electrons from the anode body into the ion source volume, independently on the primary electron density. The ionization of the noble gases would also benefit from the cooling of the source anode, through the reduction of the impurity level inside the source.

b) *The anodes potentials.*

Presently, they have several functions:

- providing the accelerating potential for the electrons (through the grid);
- determining the primary electron trajectories in the ion source volume and consequently affecting the electron confinement and the electric potential distribution inside the ion source (see the beam energy measurements presented in chapter 6).
- determining the ion trajectories in the ion source, thus influencing the extraction efficiency from the ion source volume.

It has already been tried by Kirchner [47][17] to separate all these functions, but without a clear improvement of the ion source performance. Nevertheless, the extraction efficiency cannot be optimum without the presence of a potential gradient in the ion source volume, as was also noted by Nietzsche [60].

For a plasma dense enough, where the Debye length is small compared to the source dimensions, the extracting gradient is provided by the plasma sheath and is not much affected by the anode potentials. But, as is was estimated in section 4.2.1 and will be confirmed by the experimental measurements in chapters 5 and 6, this is not the case for the present FEBIAD operating conditions.

The big challenge in optimizing the electrical field distribution inside the source is that the solution has to be optimal for both electrons and ions; any accelerating field for ions will be a decelerating field for electrons and therefore the optimization of the ion extraction can reduce the electron density in the active volume and therefore reduce the ionization rate.

For example, at ISOLDE the design of the MK3 sources (figure 5.1) is optimized for the ion extraction, but this is done at the expense of repelling an important part of the primary electron beam from the outlet plate region.

c) *The magnetic field.*

As will be justified by experimental measurements (presented in section 5.2), the main influence of this parameter is on the electron beam confinement. Therefore, any influence on the extracted ion beam is induced through the variation of the primary electron density.

d) *The operating pressure.*

Its primary effect is on the ion density, but as a result, more primary electrons will be also confined towards the centre of the ion source and consequently, through the change of the plasma density, the efficiency of the ion extraction from the ion source volume will change.

When willing to keep the ion extraction efficiency unaffected by an increased operating pressure, the main goal has to be to adapt the ion source design for being able to extract an ion current on the same order with the ionization rate inside the source (see section 9.3.5).

4.2.3. **The inference of an ionization model based on the operation parameters.**

Generally speaking, the two critical aspects that are primarily affecting the efficient operation of the ion source are:

- The ionization rate, R;
- The fraction of successfully extracted ions.

A good comprehension on the effect of the operation parameters on the ion source efficiency can be achieved by expressing the efficiency in the following manner:

$$\varepsilon = \frac{n_{i\_out}}{n_{n\_in}} = \frac{R_{ioniz} \cdot V_{source} \cdot f_{extr}}{n_{n\_in}} \tag{4.12}$$

where: ε = ionization efficiency (%);
n_{i_out} = number of extracted ions (pps);
n_{n_in} = number of injected atoms (pps);
R_{ioniz} = rate of ionization ($cm^{-3}s^{-1}$);
V_{source} = volume of the ion source (cm^3)
f_{extr} = fraction of the generated ions that are successfully extracted before recombination on the walls (adimensional).

For developing the formula (4.12), the **rate of ionization** can be expressed as:

$$R_{ioniz} = n_e \cdot n_n \cdot \sigma_{ioniz} \cdot v_{rel} \tag{4.13}$$

where: n_e = electron density (cm^{-3});
n_n = neutral gas density (cm^{-3});
σ_{ioniz} = ionization cross section for the considered gas (cm^2);
v_{rel} = relative velocity between electrons and neutrals (cm/s).

For the assumptions presented in section 4.2.1, we can express these factors in the following way:

a) *The particle relative velocity.*

v_{rel} is with a very good approximation equal to the primary electrons speed:

$$v_e = \sqrt{\frac{2eU}{m_e}} \Rightarrow v_e(cm/s) = 5.9 \cdot 10^7 \cdot \sqrt{U(V)} \tag{4.14}$$

where U is the accelerating grid potential;

This is valid because the neutrals are only having the thermal energy, therefore:

$$\langle v_n \rangle = \sqrt{\frac{8kT}{\pi M}} \tag{4.15}$$

$$\Rightarrow \langle v_n \rangle = 1.46 \cdot 10^4 \cdot \sqrt{\frac{T[K]}{M[amu]}} [cm/s] \tag{4.16}$$

which is more than three orders of magnitude lower than the primary electron speed, for a typical operating temperature of around 2300°C.

b) *The electron density.*

The electron density established in the ion source volume, n_e, depends on the electron flux sustained by the cathode emission and on their energy:

$$n_e(electrons/cm^3) = \frac{f_{elec} \cdot j_{e\_cath}(electrons/cm^2 s)}{v_e(cm/s)} \tag{4.17}$$

$$j_{e\_cath}(el/cm^2 s) = \frac{j_{cath}(A/cm^2)}{e(C)} = j_{cath}(mA/cm^2) \cdot 6.25 \cdot 10^{15} \tag{4.18}$$

where f_{elec} = correction factor applied to the electron flux, comprising the grid transparency and the electron beam confinement in the ion source volume;
j_{cath} is given by eq. (2.2).

c) *The neutral gas density and the internal pressure*

The density of neutrals is given by:

$$n_n = \frac{p_{int}}{k \cdot T} \Rightarrow n_n[cm^{-3}] = 7.25 \cdot 10^{18} \cdot \frac{p_{int}[mbar]}{T[K]} \tag{4.19}$$

The pressure inside the ion source can be estimated from the equality between the gas fluxes getting in and out of the ion source:

$$Q_{in} = Q_{out} \tag{4.20}$$

but $$Q_{out} = C_{out} \cdot p_{int} \tag{4.21}$$

with $$C_{out} = \frac{1}{4} v_{av} \cdot S_{out} = \frac{1.128}{4} \cdot v_p \cdot S_{out} = 0.282 \cdot \sqrt{\frac{2kT}{M}} \cdot S_{out} \tag{4.22}$$

or, in practical units: $$C_{out}(l/s) = 3.64 \cdot \sqrt{\frac{T(°K)}{M(amu)}} \cdot S_{out}(cm^2) \tag{4.23}$$

where C_{out} = conductance of the outlet hole;
S_{out} = surface of the outlet hole;
v_{av} = arithmetic average molecular velocity;
v_p = the most probable velocity;

From (4.19) and (4.21-23), we have:

$$n_n(cm^{-3}) = 2 \cdot 10^{18} \cdot \frac{Q_{in}(mbarl/s) \cdot \sqrt{M(amu)}}{T^{3/2}(°K) \cdot S_{out}(cm^2)} \tag{4.24}$$

Furthermore, n_{n_in} can be linked to n_n, by expressing them both as a function of the throughput of the calibrated leak, Q_{in}:

$$n_{n\_in} = \frac{Q_{in}}{k \cdot T_0} \quad \text{or} \qquad n_{n\_in} = Q_{in} \cdot N_{mbarl} \tag{4.25}$$

with Q_{in} = the throughput of the calibrated leak (mbarl/s);
T_0 = operating temperature of the calibrated leak (300°K);
$N_{mbarl} = 2.4 \cdot 10^{19}$, number of particles per 1 mbarl.

d) *The ionization cross section.*

The ionization cross section is given by the Lotz formula, (2.4).

By putting all together, the ionization efficiency becomes (in SI units):

$$\varepsilon = 2.33 \cdot 10^4 \cdot f \cdot V_{source} \cdot A \cdot \exp\left[\frac{-W}{kT}\right] \cdot l \cdot \frac{\ln\left(\frac{U}{V_{ioniz}}\right)}{U \cdot V_{ioniz}} \cdot \frac{\sqrt{M}\sqrt{T}}{S_{out}} \tag{4.26}$$

with the efficiency factor f having two components, $f = f_{extr} \cdot f_{elec}$, where f_{extr} is the component characterizing the ion extraction and f_{elec} characterizing the electron beam transport from the cathode to the ionization volume. These two factors cannot be easily split due to the limited diagnostics available for the plasma parameters, therefore in the following they will be taken together for the fitting of the experimental data and taken separately only for theoretical justifications of the observed effects.

Even if in this formula the operating pressure is not appearing explicitly, it does affect the ionization efficiency through the f_{extr} factor, which is a measure of the electrical field penetration inside the ion source and therefore can depend on all the ion source parameters, if they are varied over a wide range. Also, at high operating pressures, the formula taken for the outlet conductance can become inaccurate. The range of application of this formula and the subsequent correction factors will be deduced from the experimental investigations presented in this chapter.

CHAPTER 5

EXPERIMENTAL INVESTIGATIONS OF THE IONIZATION EFFICIENCY OF ISOLDE FEBIAD ION SOURCES.

Even in the case of carefully engineered models, an ion source is far from being a turnkey device which provides the optimum performance just by turning it on.

The optimal performance of an ion source can be obtained through a careful variation of the operating parameters ("tuning"). As presented in section 2.4, the tuning possibilities are generally limited by the available operating parameters allowed by the ion source design. When in need of a better performance, generally a customization of the ion source is needed: the design of the ion source has to be modified for providing the required operating conditions that were not available only through tuning.

Through tuning alone, the ion source performance can be changed by a considerable factor (up to more than one order of magnitude). For that reason, a certain ion source performance is not attached to the ion source type itself, but to a specific set of operating parameters.

More than that, there can be several sets of parameters leading to the same ion source performance and generally the parameters providing the best ionization efficiency can be different of those providing the best selectivity or the best confinement times.

For a good operation of the ion source it is sufficient to only know the parameters corresponding to the best performance but, for an ion source development, the full variation of the ion source performance on the operating parameters is mandatory, in order to identify the ion source limitations.

Therefore, the ion source customization can benefit from the results provided by the ion source tuning.

We present in this chapter the detailed experimental dependence of the ISOLDE FEBIAD ion sources performances on the operation parameters. These results served to the identification of the dominant phenomena (out of all the possible phenomena presented in section 2.3) inside the ion source for the present design. This was the basis of the inference of the source model introduced in section 4.2.3 (which will be applied here to explain the observed behavior).

Several performance limitations are evidentiated. They will be analyzed in chapter 7 and the removal of their origin lead to the developments presented in chapter 8.

5.1. FEBIAD ion sources in use at CERN-ISOLDE

As presented in section 2.2, there are several big categories of arc discharge ion sources, each of them implemented in several facilities around the world (section 1.3) and presenting a widespread variation of their performances from facility to facility, but also from one subtype to another.

At ISOLDE there are presently used 3 subtypes of FEBIAD ion sources [16]:

- **MK3 subtype** (figure 5.1): dedicated to the molten metal targets. It presents two anodes, both made of graphite, for avoiding sparking induced by the condensing of the metal vapors coming from the target;

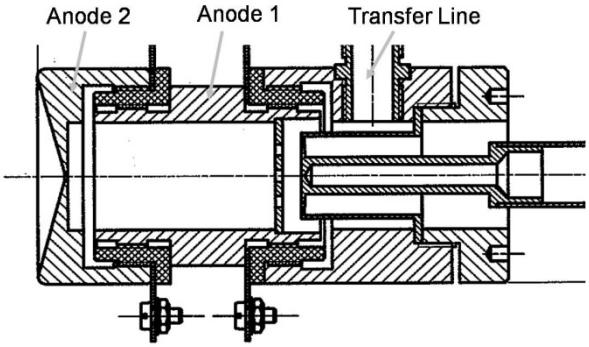

Figure 5.1. ISOLDE FEBIAD: MK3 subtype

- **MK7 subtype** (figure 5.2.): so called "**cold plasma**", it is dedicated to the ionization of noble gases and molecular compounds. It presents a water cooled transfer line, for condensing all the refractory elements;

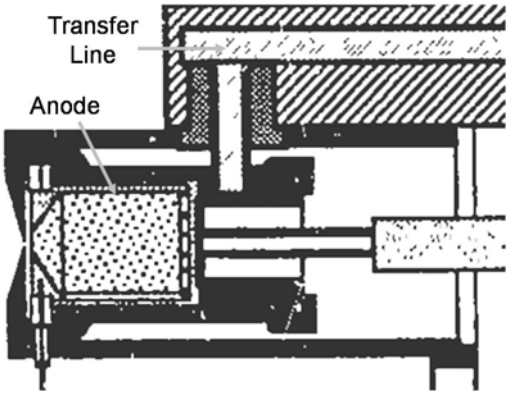

Figure 5.2. ISOLDE FEBIAD: MK7 subtype

- **MK5 subtype** (figure 5.3.): so called "**hot plasma**", it is dedicated to the ionization of refractory elements. For that, its operating temperature should be as high as possible, but practically it is being limited by the maximum operating temperature of the electrical insulators (made of BeO or BN) to about 2200°C (but typically operated only at around 2000°C).

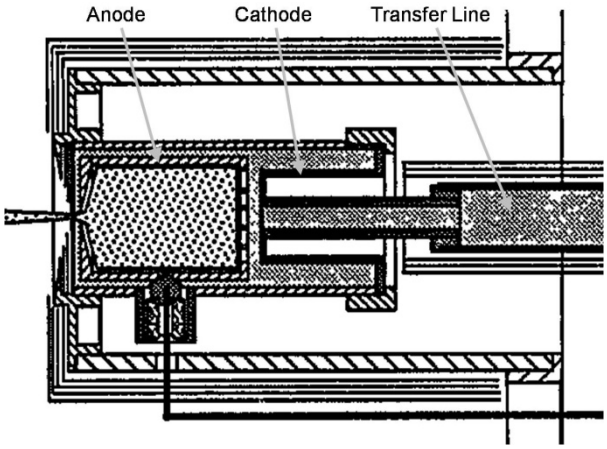

Figure 5.3. ISOLDE FEBIAD: MK5 subtype

5.2. Dependence of the ionization efficiency on the internal magnetic field

The magnetic field is generated transversally in the ion source volume by a solenoid installed around the source. The field strength is controlled through the intensity of the current applied to the solenoid, and it can vary from 0 to a few hundred gauss.

The specific dependence of the extraction current on the internal magnetic field is a succession of maxima and minima, with a peak-to-peak variation of the extracted ion current within typically a factor 2, as it is being presented in the following.

This modulation effect is present only due to the source nonlinearities, as in a plasma of uniform density and temperature, an uniform magnetic field cannot introduce a nonlinearity (the Larmor radius, $r_L = \frac{mv_\perp}{QB}$, is depending linearly on the magnetic field). As it will be detailed and justified below, the primary origin of these nonlinearities is the anode grid, producing an electron beam with a non-uniform density.

The typical variation for an **MK3** FEBIAD source is presented in figure 5.4, a) and b), corresponding respectively to an operation with both anodes at the same potential and with a difference between the two anodes ΔV=60V (value optimized for the highest Argon current).

The 3 curves are representing 3 element classes:

- a **surface ionized impurity**, Potassium, originating from the ion source materials;
- a **condensable impurity**, Lead, coming from the target material;
- a **gas tracer**, Argon, introduced in the system through a calibrated leak.

It can be seen that there is no difference between the 3 elements concerning the position of maxima and minima, therefore the intensity modulation is an effect induced by the electron beam (as will be confirmed for the MK5 case, below).

The way the electrons can transmit the magnetic field influence on the extracted ion current is connected to the variation of the density distribution of the primary electrons with the varying magnetic field:

- On one hand through the variation of the ionization rate in the central volume of the ion source (through f_{elec});
- On the other hand through the variation of the extracting field seen by the ions, affected by the negative space charge of the primary beam (through f_{extr}).

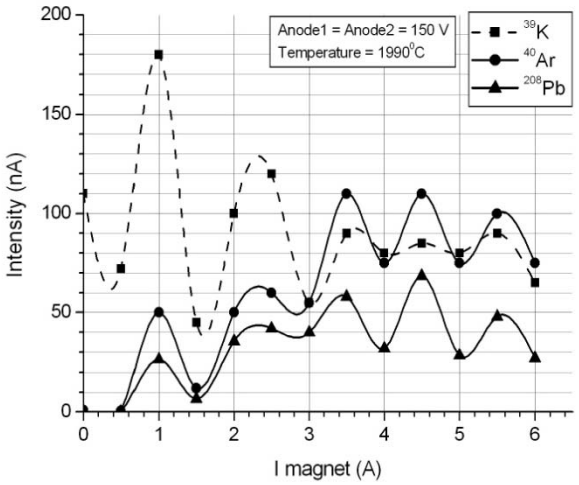

Figure 5.4.a) Dependence on the magnetic field of different classes of elements, for an MK3 source operated with both anodes at the same potential.

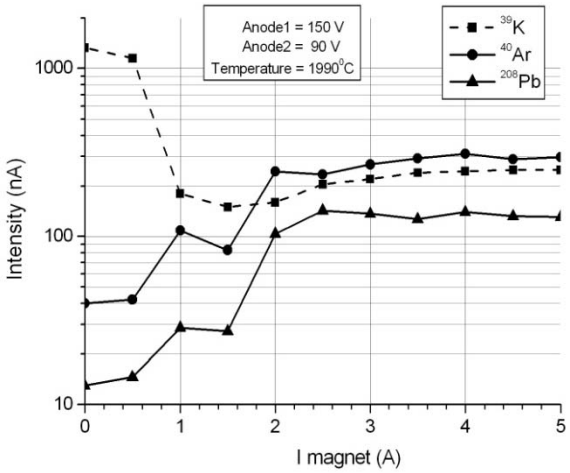

Figure 5.4.b) Dependence on the magnetic field of different classes of elements, for an MK3 source operated with 60V difference between the anodes.

An interesting effect is that when $\Delta V \neq 0$, the intensity modulation is much attenuated towards higher magnetic fields, which is not the case for $\Delta V = 0$.

Concerning the ion source performance, it can be seen that both elements ionized only through electron impact (Argon and Lead) are better ionized (by up to a factor 3) when using a potential difference between the two anodes.

This is justified by the fact that the ions are better extracted when the outlet plate ("Anode2") is at a lower potential than the plasma potential (imposed mainly by the potential of the cylindrical anode – "Anode1").

The situation is different for the surface ionized Potassium:

- The extracted intensity <u>without magnetic field</u> is about 10 times higher for the case $V_{anode1} > V_{anode2}$. This can be explained by the fact that most of the Potassium ions are produced through surface ionization (following Saha's formula (2.9), the probability of surface ionization of K at contact with a Mo surface at 2000°C is about 80%) and the primary electron concentration is not affecting the surface ionization, but only the successful extraction of the produced ions. In the absence of the magnetic field, the electron beam ionization is strongly reduced (as noted above for the Argon and Lead) and therefore most of the ions produced through surface ionization can reach the central volume for being extracted.

  This difference factor is strongly dependent on the amount of K contamination, on the place inside the source where it is being produced and on the other ion source operation parameters.

  For example, the dependence of this difference on the potential difference V_{anode1}-V_{anode2} is presented in figure 5.5. It can be seen that the measurement presented in figure 5.4. b) is corresponding not only to the optimum ΔV value (60V) for the maximum Argon current at high magnetic fields, but also to the maximum Potassium current with no magnetic field.

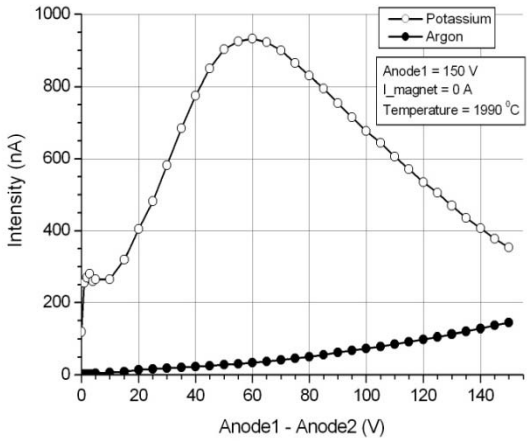

Figure 5.5. Dependence of the Ar and K ionization on the potential difference between the two anodes.

- The extracted intensity towards the high magnetic fields is about 3 times higher for the case $V_{anode1}>V_{anode2}$. This behavior is similar to the Argon behavior.
- For $V_{anode1}>V_{anode2}$, there is a strong intensity decrease when increasing the magnetic field (opposite to the behavior of Ar and Pb), by about a factor 5. This is opposite to the Argon behavior, but strongly correlated with this one. More precisely, the more ions will be produced in the central volume of the ion source (mainly Argon ions in this case), the less Potassium ions will reach the extraction volume. This was also confirmed by operating the ion source at a lower Argon pressure, when more Potassium ions could be extracted instead, for the same operation conditions.

A side effect not visible in these plots is that the beam emittance is increasing proportionally with the potential difference between the anodes, similar to the behavior of Kirchner's sources [47]. This is mainly generated by a broader energy distribution of the extracted ions (given the increase of V_{active}).

A more detailed investigation of the magnetic effect has been done for an **MK5** source, as can be seen in figures 5.6. a) to d).

The measurements have been done for an operation gas composed of 40% Helium, 20% Neon, 20% Krypton and 20% Xenon. The other operation parameters are specified in the figures.

Figure a) confirms that the magnetic behavior is not element dependent. Therefore the measurements in figures b), c) and d) are only done for one element, namely Krypton. Figure b) shows that the main dependence is on the anode potential, therefore on the electron energy. As the electron acceleration is done axially, but the electron Larmor radius is dependent on their radial velocity, it is not clear where are the electrons gaining their radial velocity and what is its exact dependence on the axial velocity.

There are several locations in the ion source where the electrons can gain a radial velocity:

- during their acceleration, at the passage through the grid (figure 5.7.); the difficulty in analyzing this effect is that the direction of deviation of the electrons depends strongly on the crossing position through any of the grid holes;
- in the ion source volume, as an effect of the space charge expansion of the electron beamlets; this effect is not quantifiable;

in the outlet plate region, due to the electron repelling by the ion extraction electrodes.

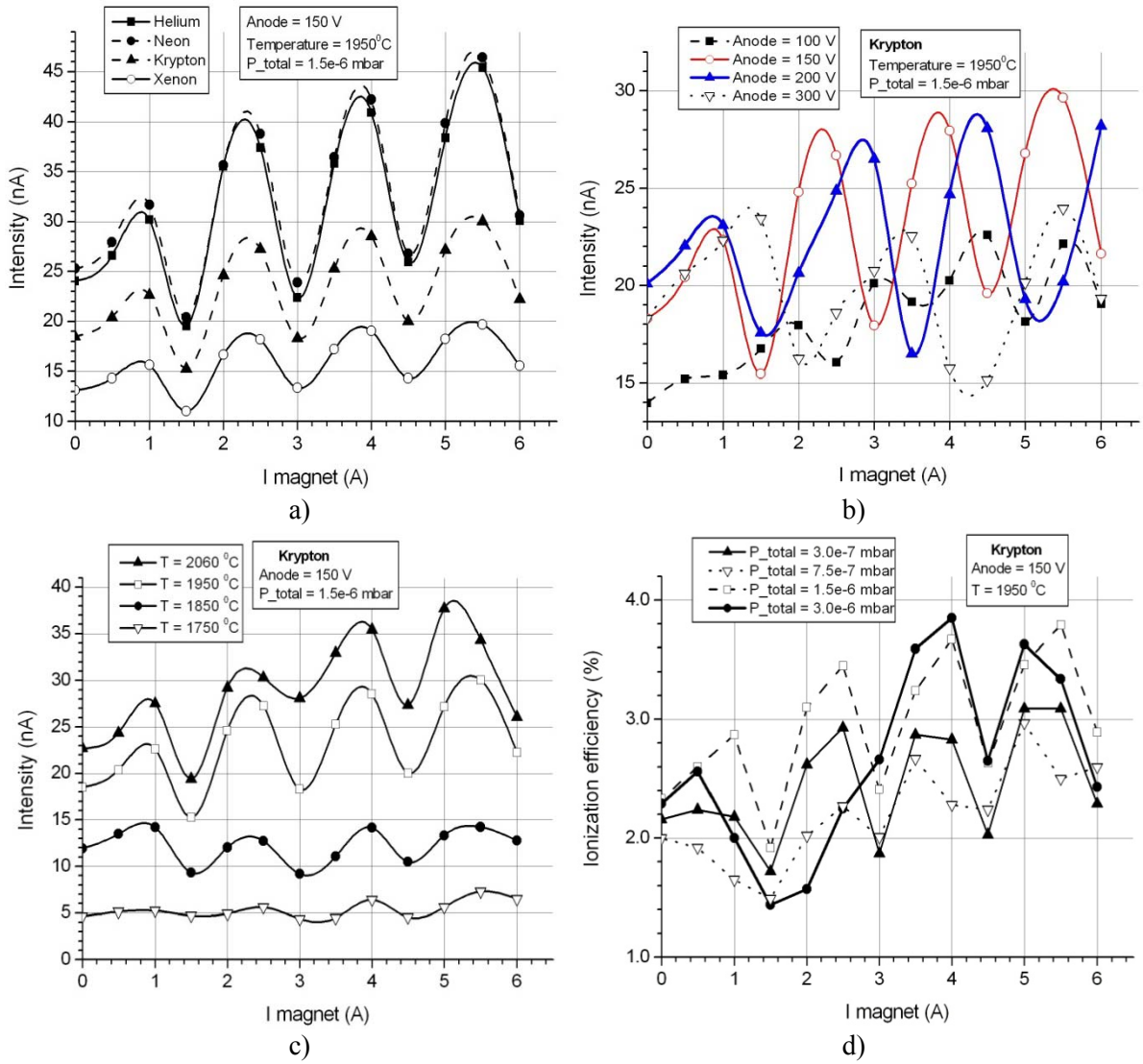

Figure 5.6. Investigation of the magnetic effect in a MK5 source. **a)** Element dependence; **b)** Anode potential dependence; **c)** Temperature dependence; **d)** Pressure dependence.

The fact that the positions of the maxima and minima are not shifting when increasing the temperature (and consequently the electron density) – as shown in figure 5.6 c) - is a proof that the radial velocity is not gained through the space charge expansion of the electron beam (which is stronger at a higher temperature).

From the measurements presented in figure 5.6 d), it can be seen that the operation pressure affects mainly the position of the first maxima. Also, there is in the presented data a notable efficiency increase wit\h the increase of the injected gas amount (increase by up to 50% in efficiency for a gas increase of 10 times), which can be justified by the fact that the ion source temperature was optimized for the highest pressure (3e-6 mbar). The ionization efficiency is reaching its maximum at higher operating temperatures for smaller operation pressures, therefore it is not yet saturated for the presented data at 3.0e-7 mbar and 7.5e-7 mbar.

In figure 5.6.d) can also be seen a source instability observed often in ISOLDE FEBIAD ion sources: sometimes, for the same operating parameters, the extracted current can have two

distinct values, different by about a factor 2. In the figure, this instability appears in the case of 700 nA Kr injected (3.0e-6 mbar total pressure), where the second maxima is no longer stable due to the increasing plasma density. This effect has only been observed for the second maxima and can be avoided either by increasing the electron beam density (therefore the operating temperature), either by operating the ion source at a higher magnetic field (corresponding at least to the 3rd maxima).

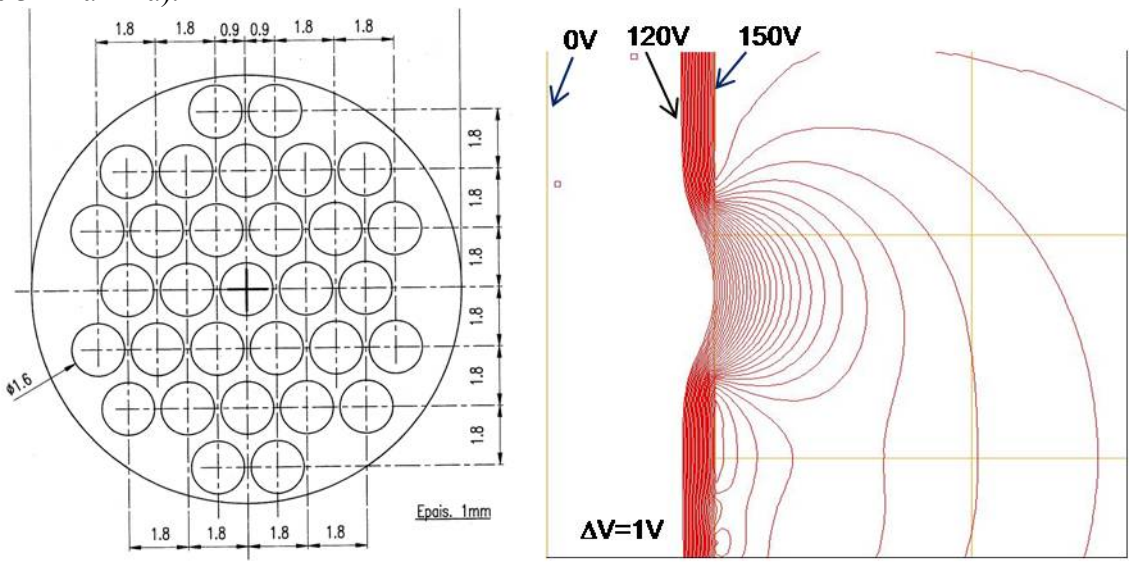

Figure 5.7. The effect of the accelerating grid on the electron velocity. **Left**: grid geometry. **Right**: detail of the electric potential distribution around a grid hole (CPO) for the grid at 150 V.

A notable difference between the MK3 and MK5 types is that the MK5 can be operated even without a magnetic field (by losing maximum a factor of 2 in the ionization efficiency compared to the values with a magnetic field), while the MK3 loses about a factor of 10 in the efficiency when the magnetic field is not applied. This can be explained by the fact that the primary electron beam is having a bigger expansion in the MK3 source compared to the MK5, which leads to a lower ionization rate in the active volume when no magnetic field is applied.

This effect has been successfully applied for increasing the selectivity of a MK5 ion source [88], by taking advantage of the fact that a lower f_{extr} (characterizing the operation without the magnetic field) means a higher residence time, thus disfavoring the ionization of the refractory elements.

Historically, several grid geometries have been tried at ISOLDE before choosing the present one (which is the same for all the ion source subtypes), but no systematic data on their characterization was published. Kirchner [47] also tried different types of electron acceleration, going from a fine mesh to no grid at all. But, considering that the influence of this parameter on the ion source performance is limited, the main selection criterion remained the grid lifetime.

5.3. Dependence of the ionization efficiency on the ion source potentials

As described in section 4.2 (and concluded in eq. 4.26), the anodes potentials are influencing the ionization efficiency through:

- the ionization cross section;

- the electron beam confinement factor, f_{elec};
- the extraction field imposed to the ions (characterized by f_{extr})

The resulting effect for a standard MK5 source is presented in figure 5.8 a) to c). The data in figure 5.8 d) was obtained using a source prototype described in section 8.2, developed with the goal of reducing the partial pressures of the impurities inside the ion source.

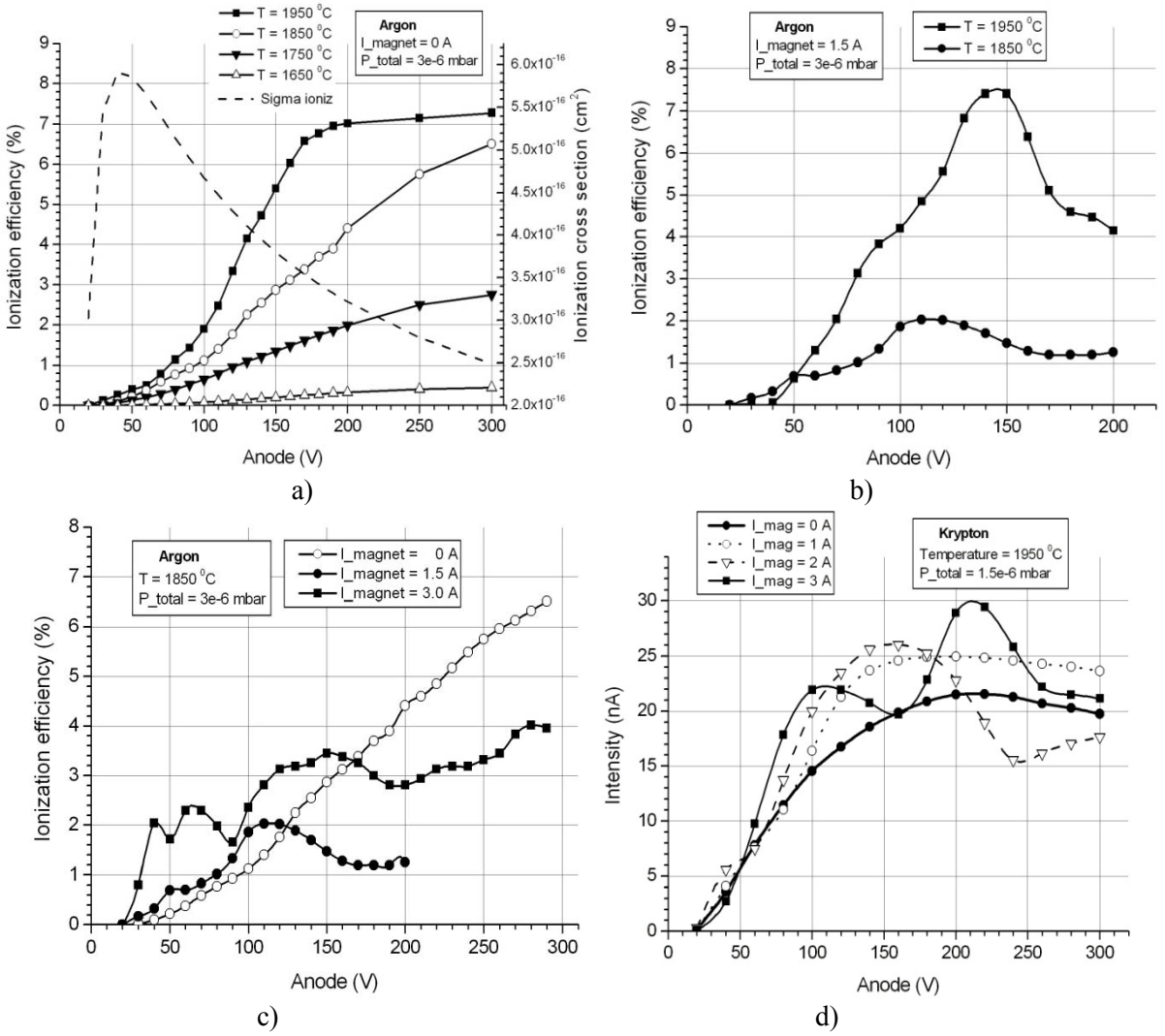

Figure 5.8. Influence of the anode potential on the MK5 efficiency. **a)** Anode and temperature dependence without magnetic field; **b)** Anode and temperature dependence with magnetic field; **c)** Anode and magnetic field dependence in the presence of impurities; **d)** Anode and magnetic field dependence without impurities in the ion source (prototype).

As expected from the presented theory, the ionization efficiency is increasing with the operation temperature (figure a), due to the intensity increase of the primary electron beam, but this effect will always mix with the effects induced by the anode potential and by the magnetic field. It can be seen in figure b) that the temperature increase not only improves the ionization efficiency, but also shifts the point of maxima towards higher values of the anode potential. This effect is showing that the ionization efficiency is not continuously increased when increasing the

primary electron density (a higher temperature increases the electron density, while a higher anode potential decreases the electron density, when all other parameters are kept constant).

The results in figure c) are bringing more information on this aspect: when increasing sufficiently the magnetic field, the dependence on the anode potentials starts to present the same succession of maxima and minima as the dependence on the magnetic field (presented in section 5.2), which confirms that the radial velocity of the electrons (and therefore the magnetic modulation of the extracted current) is directly depending on their axial velocity (given by the anode potential). This effect could be pointed out more clearly in figure d), for a unit presenting a very low level of impurities (and therefore presenting a behavior dominated only by the parameters externally controllable).

The same figure c) may suggest that the best ionization efficiency is obtained without a magnetic field but, by comparing the results with those in figure a) and b), one can see that this is only valid for low operation temperatures. For temperatures in the nominal range at ISOLDE, the ionization efficiency is saturating towards the increase of the anode potential, while it can be further increased through the modulation given by the magnetic field.

It can be seen that in none of the measurements, the efficiency variation on the anode potential does not follow only the dependence of the ionization cross section on the electron energy (dotted curve in figure 5.8. a). In equation (4.26), the remaining factor with a dependence on the anode potentials (other than the ionization cross section) is the factor f ($=f_{elec}*f_{extr}$). For a better understanding of the superposition of the phenomena, we express here $f=f_{nomag}\cdot f_{mag}$, the product of two independent factors, one characterizing the dependence of f purely on the anode potential, the other purely on the magnetic field (for this investigation, no difference is made between the electronic component f_{elec} and the ionic component f_{extr}). These two factors can be extracted from the measurements presented in figure 5.8, by using the formula (4.26).

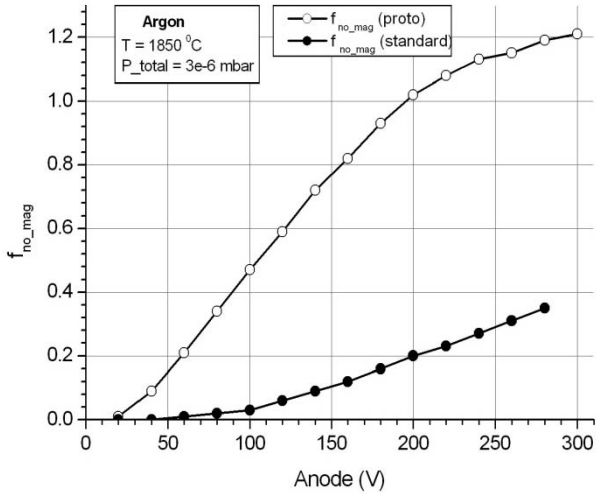

Figure 5.9. Dependence of the $\mathbf{f_{nomag}}$ factor on the anode potential

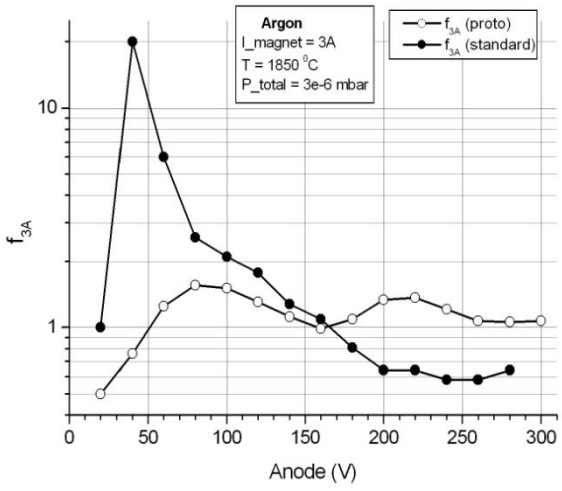

Figure 5.10. Dependence of the $\mathbf{f_{mag}}$ factor on the anode potential

The component f_{nomag} is obtained directly from a measurement in the absence of the magnetic field (in this case, $f = f_{nomag}$). The component f_{mag} can then be deduced from a measurement with magnetic field, as $f_{mag} = f / f_{nomag}$.

The continuous increase of f_{nomag} presented in figure 5.9 can be explained in the following way: a higher electron energy for the same cathode emitted intensity will lead to a lover volume density of primary electrons, which can both improve the electron confinement factor, f_{elec} (through the decrease of the space charge repulsion of the electron beam) and the ion extraction factor, f_{extr} (through the increase of the Debye length of the plasma and therefore of the active volume).

The fact that the improvement is bigger when having less impurities in the ion source (hollow circles curve in figure 5.9) is suggesting that out of these factors, the most important one is the f_{extr} contribution. Less impurities means lower total operation pressure and therefore lower plasma density, which is not helping the confinement of the primary electrons, but will lead to a bigger active volume.

Figure 5.10 confirms this approach, showing that the magnetic field is adding a periodical dependence to the f factor defined primarily by the anode potential. More than this, the magnetic dependence can be rapidly damped in the presence of important impurity partial pressures.

Therefore, the dependence on the anode potential can be dissociated in 3 parts:

1) The dependence given by the ionization cross section (already included in eq. 4.26);

2) A dependence given by the electron energy, which can be included in the f factor;

3) A periodical dependence given by the magnetic field, which can also be included in the f factor.

The components 2) and 3) are directly related to the variation of the primary electron density inside the ion source.

The MK3 ion source can provide more information on the internal properties of ISOLDE FEBIADs, as it presents two anodes that can help dissociating between the electron acceleration function and the confinement/extraction functions.

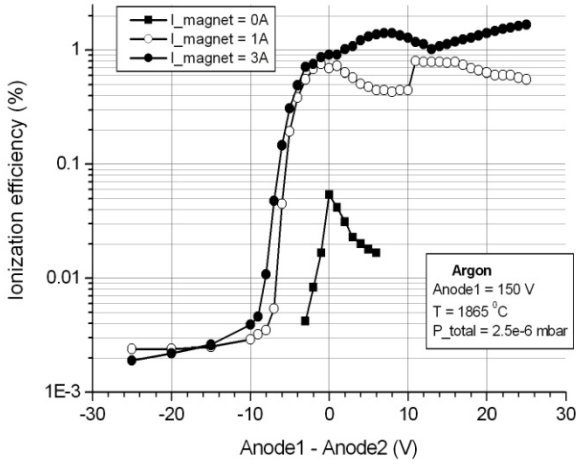

Figure 5.11. Influence of the anodes potentials on the MK3 efficiency. Anode1=150V (constant).

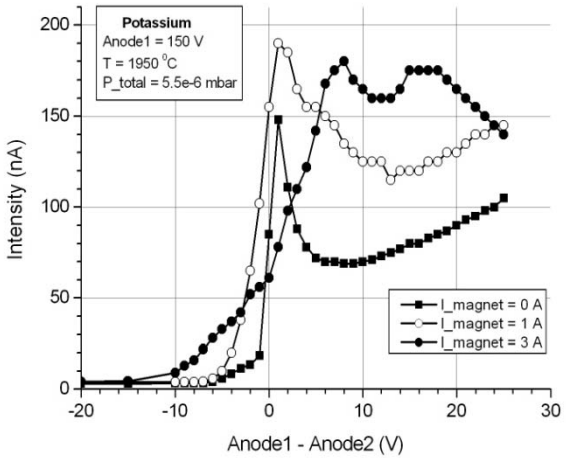

Figure 5.12. Influence of the anodes potentials on the K impurity ionization. Anode1=150V.

The figures 5.11 and 5.12 are presenting the typical behavior of this kind of source against the polarization of the anodes.

Namely, the source efficiency for tracer elements (Argon in the presented case) can be increased by a factor of 2 to 3 by operating the Anode2 (the outlet plate) at a lower potential than the potential of Anode1 (the cylindrical plasma chamber). This is a consequence of the increase of f_{extr}, as the produced ions will see this way a higher accelerating field towards the source exit.

The behavior is different for potassium, as an important part of the ionic current of this element is produced through surface ionization, therefore starting at the anode potential. As their kinetic energy is roughly the thermal energy (~0.2eV), a potential difference of only 1V between the anodes is already enough for directing them towards the exit (leading to the observed maximum in figure 5.12), while a bigger increase will not be favorable to their extraction, as an increasing part of them will be attracted to the outlet plate itself.

Important information is lying on the other direction of variation of Anode2. The fact that the decrease of Anode2 potential below Anode1 is leading to the rapid decrease of the extracted current is a proof that the plasma density inside the source is not enough for shielding the potential variation imposed by the anodes. This information gave the direction towards the development of the ionization efficiency model proposed in chapter 4. Also, this means that the source does not need a buffer gas to operate, as both the ionization and the extraction are controlled by the anode potentials and not by the plasma density. The stable gas introduced in the source is therefore useful mainly for the tuning of the ion source (therefore it is more accurate to call it "tracer" instead of "buffer" gas).

More than this, the measurement in figure 5.11 is giving information about the energy spread of the MK3 beam: considering the additional potential required for Anode2 in order to stop 99% of the extracted beam, the energy spread is on the order of 8 eV in the presence of the magnetic field and of about half this value in the absence of it. As for the plasma potential, it appears to be very close to Anode1 (as the extracted intensity is strongly decreasing as soon as ΔV is becoming negative).

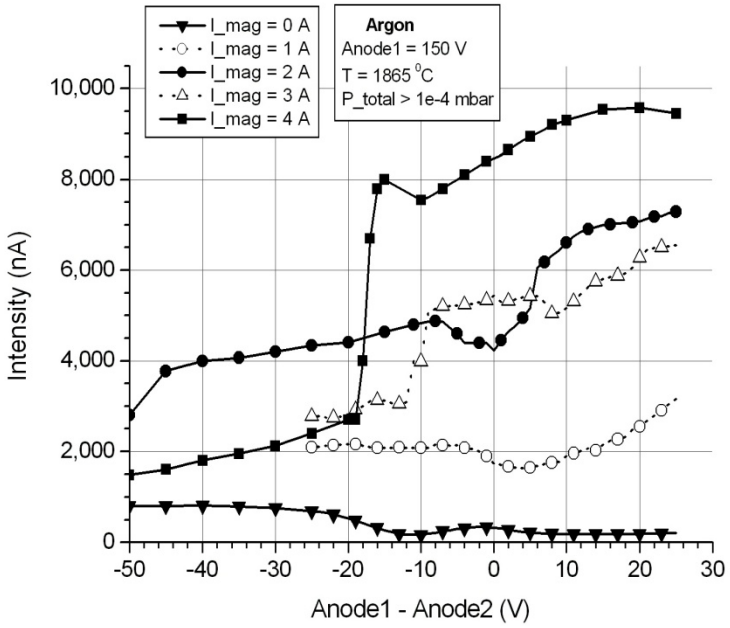

Figure 5.13. Influence of the anode potentials on the MK3 ionization efficiency, for an operating pressure of $>10^{-4}$mbar.

This interpretation is confirmed by the measurement presented in figure 5.13, where the source was operated at a pressure about two orders of magnitude higher than usual. It can be seen that in these conditions, the potential difference between the two anodes is no longer determinant for the ion beam extraction. The plasma density becomes high enough for shielding the anodes

potentials and the beam extraction depends only on the ion density generated in the ion source volume. In these conditions and considering that the ion density is directly proportional with the electron density, the intensity variation presented in figure 5.13 is generated mainly by the variation of the electron density. As the temperature is kept constant, the electron density can only be increased through the increase of their lifetime in the source volume: by repelling them through the Anode2 (left side of the curves at low magnetic field, I_mag=0A and I_mag=1A, opposite effect compared to low pressure discharge!) or by curling them around the magnetic field lines, by increasing the magnetic field.

When applying a stronger magnetic field, the current for $\Delta V<0$ increases further but in that case the bigger advantage lies on the side of $\Delta V>0$, where the ion source can sustain a denser plasma, with a positive plasma potential with respect to both the anodes (with up to 15V for the curve at I_mag=4A).

These estimations are only giving the general variation trends of the FEBIAD plasmas; a detailed investigation of the beam energy and of the energy spread of the FEBIAD ion sources used at ISOLDE is presented in chapter 6.

5.4. Dependence of the ionization efficiency on temperature

The FEBIAD ion sources used at ISOLDE are generally operated at temperatures ranging from 1800°C to 2100°C. There are several reasons for choosing this range, both for the lower and for the upper limit.

The lower limit is imposed by the electronic flux generated by the Tantalum cathode. At a too low temperature, the decrease in the cathode emission is leading to low ionization efficiency. Nevertheless, the ion sources are not always operated at their maximum possible temperature, as sometimes the beam composition is a critical issue; by reducing the temperature, some of the contaminants in the beam can be reduced, due either to the change in the chemical equilibrium inside the source, either to the change of their sticking time on the walls of the ion source. An important remark is that even for the so called “cold plasma” MK7 ion source, the cathode has to be operated at the same temperature as for a “hot plasma” MK5, in order to achieve the optimum ionization efficiencies.

The maximum temperature limit is imposed mainly by the materials used for insulating the source anodes, but more generally by all the materials present in the hot enclosure. The limiting parameter is the pressure generated inside the ion source as a sum of the partial pressures of the component materials. Generally, the partial pressures generated by the source materials have to remain below the partial pressures of the tracer gas. Above that limit, the ionization efficiency of the tracer gas will go down (see section 5.6). Considering the difference in partial pressure (see table 2.1), it is possible that the ionization efficiency for some of the radioactive products (depending on their half-life and sticking time) will still remain high, but there will be no precise real-time prediction of that from the efficiency measured for the stable tracer.

Of course, even if the ion source could withstand higher partial pressures, there is another limit for the partial pressure of a specific material, given by the maximum evaporation rate allowed for maintaining the desired lifetime of the corresponding part.

At ISOLDE, the insulators that are being used are BN (for MK3 and MK7) and BeO (for MK5). For the BN, the temperature limit is of about 1800°C, when no chemically aggressive elements are present in the source [89]. These elements can be either SF_6 or CF_4 as buffer gases,

either vapors coming from the target container, or even other source materials in direct contact with the BN insulator (as the Molybdenum, commonly used in the FEBIAD sources). The temperature limit for the BN is not arising from the increase of its partial pressure inside the source, but from the decrease of its specific resistance towards higher temperatures, which can lead to the insulator self-destruction. The BeO can be operated at higher pressures (~2050°) than the BN, but it has a lower resistance to mechanical stress. It has also been observed [89] to be a source of Oxygen for the formation of CO in the presence of graphite (up to pressures of $\sim 3 \cdot 10^{-4}$ mbar), but that is also the case for the Tantalum (which presents a TaO layer at the surface), an irreplaceable element for the standard FEBIAD ion sources.

It is important to note that the temperatures mentioned for the measurements in this work are the temperatures of the cathode, which is the hottest part of the ion source. The temperatures at the level of the insulators can easily be lower with more than 100°C, as they don't have a direct view towards the cathode and they are closer to the surrounding stainless steel case. The temperature is only measured for the cathode, as the measurement is done with a pyrometer, through the ion source extraction hole, which offers limited visibility. This precision is sufficient for the study of the noble gas ionization efficiencies, where only the cathode temperature is important; but for refractory elements - having a sticking time on the ion source walls strongly dependent on the temperature – the existence of some cold spots can lead to longer residence times of the neutral atoms and consequently to lower lower ionization efficiencies compared to those estimated using the uniform temperature hypothesis, especially for the stort-lived radioactive isotopes (see sections 9.1.2 and 9.1.3).

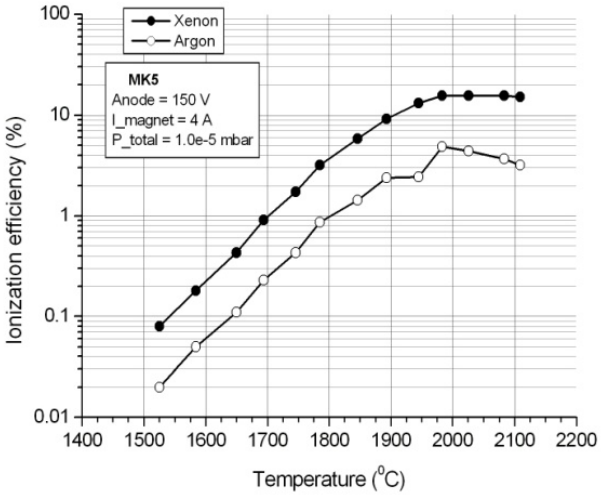

Figure 5.14. Temperature dependence of the MK5 ionization efficiency for Ar and Xe.

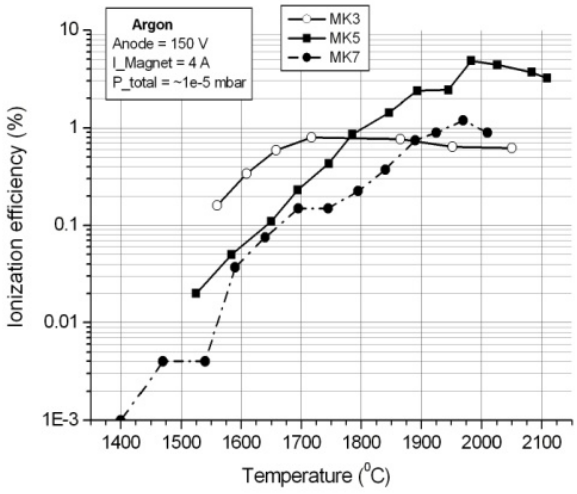

Figure 5.15. Temperature dependence of the Ar ionization efficiency for all the FEBIAD sub-types.

The general temperature dependence for an MK5 ion source is presented in figure 5.14. All the measurements that are not having the anode potential or the magnetic field as parameters have been done using the constant values of 150V for the anode and 4A for the magnet.

It can be seen that the variation is the same for both Argon and Xenon (and for all the other noble gases); there is only a shift in the efficiency value at the same temperature, given by the difference in ionization cross section and mass, as predicted by eq. (4.26).

It can be seen that the source is operating in the same regime up to about 1900°C. After ~1950°C, the ionization efficiency reaches its maximum and eventually will start to fall. The

reason of this saturation is not clear from this set of measurements. It may be interpreted as a limitation of the ionization inside the source, but additional investigation and analysis showed that this is an effect given by the increase of the impurity partial pressures (see section 5.6)

As the Tantalum cathode is the same for all the FEBIAD sub-types, this behavior is generally valid for all ISOLDE sources, but it is of interest to directly compare their performances for the same operation parameters. Figure 5.15 presents the comparison between the measured Argon ionization efficiencies for the three FEBIAD sub-types. All the measurements were done using the same values for the magnet (4A), the same operating pressure ($\sim 1 \cdot 10^{-5}$mbar) and electron energy (150 eV). The MK3 ion source was operated with a ΔV=10V between the two anodes (but with Anode1=150V, for obtaining the same electron energy).

Below ~1700°C, the temperature variation follows the same slope for the three source types, but the MK3 efficiency is significantly higher than for the other two sub-types. This behavior is probably related to the higher extraction field seen by the ions due to the potential difference between the anodes, but could not be fully understood, due to the opposite behavior at higher temperatures. There can be several explanations that could not be differentiated through the investigations done within this work:

- The "impurity type" of limitation (observed only above ~2000°C for MK5 and MK7 sources) is appearing at lower temperatures in the MK3 ion source, due to the different nature of component materials and consequently of the occurring impurities;
- The electrical field distribution inside the source is becoming inefficient at high electron densities (any accelerating field for ions is acting as a decelerating field for electrons and at higher electron densities for the same anode polarizations, space charge limitation can appear in the process of electron transport from the emitting cathode to the active volume).

The unexpected conclusion of this comparison is that, even though the use of a ΔV between the anode potentials is increasing a few times the ionization efficiency, the maximum ionization efficiency achievable with the MK3 ion sources is below (with almost one order of magnitude) the maximum ionization efficiencies of the MK5 sub-type.

Another important information visible in figure 5.15 is that, compared to the MK5 behavior, the MK7 source yields a lower efficiency all over the temperature range. This difference between the two source types was consistent for all the measurements done during this work and was also observed elsewhere [90]. The origin of this difference is not clear only from this kind of measurement, as the two source types are having the same cathode, the same volume, the same component materials and the same surface of the extraction hole. The generally accepted explanations for the difference were either the lower temperature in the MK7 ion source volume, due to the presence of the water cooled transfer line, either the higher background pressure coming from the target container in the MK5 source and leading to a higher density plasma. Nevertheless, from the results presented in this work, another hypothesis was advanced and successfully confirmed (see section 8.1 for details): the outlet side of the MK5 source is providing a better extraction factor, f_{extr}, by creating a larger penetration on the extraction field gradient in the ion source volume.

The confinement-extraction factor, $f=f_{elec} \cdot f_{extr}$, can be calculated for the data presented in figures 5.14-15, using eq. (4.26). The result is presented in figures 5.16 and 5.17. The difference between f_Argon and f_Xenon (fig.5.16) could not be predicted by the model comprised in eq. (4.26), as the two curves have been measured for the same operating conditions of the ion source, therefore for the same distribution of electron density inside the ion source.

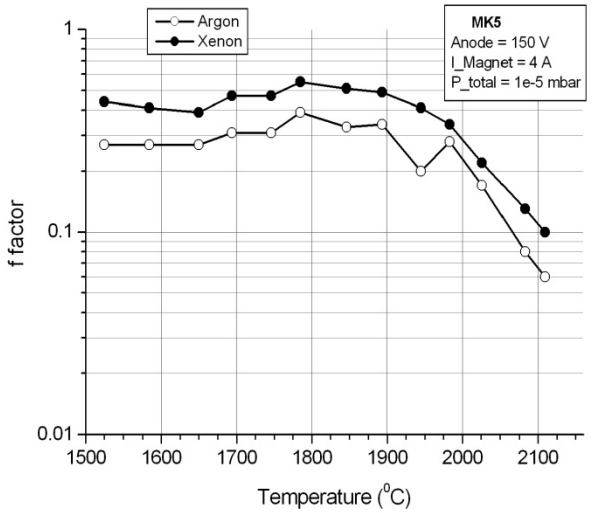

Figure 5.16. The confinement-extraction factor, f, for the measurement in fig.5.14.

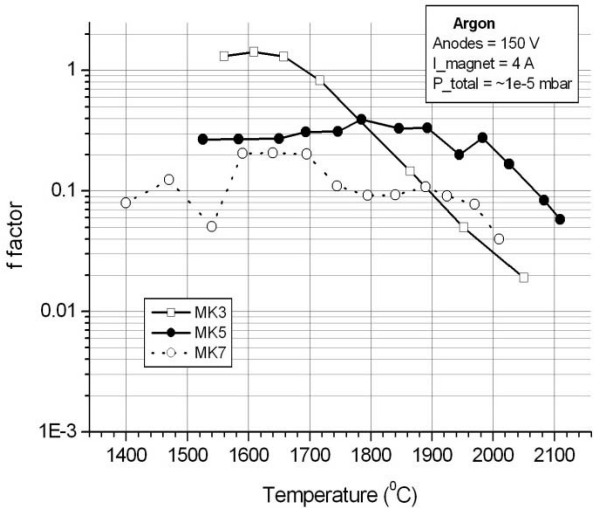

Figure 5.17. The confinement-extraction factor, f, for the measurement in fig.5.15.

This difference can have several origins:

- A different active volume for the two species, due to different energies of the ions of the different species. No evidence was found within the present work to confirm this hypothesis and it was therefore neglected in the following.
- A selective loss rate through the plasma sheath for the different species, as a consequence of the Bohm's stability criterion [61], stating that only the ions having a velocity above a given threshold (defined by the electron temperature) can pass through the plasma sheath. For the same energy of the different ion species (as it is the case for the FEBIAD sources), that would mean that a higher fraction of the light ions will be lost through the plasma sheath compared to the heavier species, due to their higher velocity distribution. This behavior is consistent with the experimental behavior from figure 5.16, but the experimental difference between Argon and Xenon is too high for being justified by this effect.
- A different confinement time in the source volume for the neutral atoms of the different species (longer times for the heavier elements, with lower velocities), making possible more cycles of ionization-recombination for the heavy elements before leaving the ion source volume. This way, the heavier elements have a greater change of leaving the source as ions than as neutral. This effect can justify the observed difference between the f factors of the different elements (see section 7.1.4).

Coming back at figure 5.17, the MK7 is a more complex case. The source presents the same degrading of f at high temperatures as the MK5 source, but on top of that, it also often presents oscillations of f, as those presented in figure 5.17. These oscillations are produced by variations of the charged particle density in the extracting volume (leading to variations of f_{elec} and/or f_{extr}). They are most probably having a bigger amplitude for the MK7 source compared to the MK5 due to the bigger MK5 extracting volume, which makes the extracted current less sensitive to local variations (that can be produced by the evaporation of different impurities or simply due to magnetic modulation of the electron density as a function of temperature – see figure 5.8 b).

On average, it can be seen that the difference between the f factors of the MK5 and MK7 sources (and consequently between their ionization efficiencies) is of about a factor 3.

5.5. Dependence of the ionization efficiency on the internal pressure

The dependence on the internal pressure is the critical one for the ion source versatility. The source has to support the consequences of a coupling with targets of different materials and geometries and operated at different temperatures. For the ISOLDE case, the geometry remains constant, but the target operating temperatures are varying from ~1100°C for CaO to ~2200°C for UC, and the evaporated material effusing to the ion source can raise the background pressure up to 10^{-4} mbar.

If implemented at a different facility, this value can be different, either due to different target geometry, to different transfer conductance from the target to the ion source or to different implementation of the gas pumping system. For this, but especially for beam power upgrades, the ion source has to be able to withstand a higher operation pressure.

It is important to underline that the FEBIAD sources will not have any problems in operating towards lower pressures. As was pointed out earlier in this section, the source does not need any buffer gas for operation; therefore there is no threshold on the minimum pressure required for obtaining the maximum ionization efficiency.

On the other side, there is a change of performance towards the higher (total) operation pressures. We present here the experimental evidence of these pressure limitations, which will be further analyzed in section 7.2.

The total operating pressure is the sum of:

a) the pressure of the radioactive products, p_r;

b) the tracer/buffer gas pressure, p_t;

c) the background pressure, p_b, generated by the evaporation of the unit materials and of the impurities in the system.

The typical values for these contributions have been presented in table 2.1.

In this section, we only investigate the effect of the tracer/buffer gas pressure. The effect of the background pressure will be presented in the next section. Considering that for all present facilities $p_r << p_t$, as long as the sum of p_t and p_b is not generating an ionization limitation, the pressure p_r will not have any influence on this study. For the next facilities where p_r is expected to increase strongly, the source behavior can be extrapolated from the current investigations on the total pressure considered as the sum of p_t and p_b.

The figures 5.18 and 5.19 are presenting the measured dependence of the Argon and Xenon ionization efficiencies for a MK5 ion source. The employed tracer gas is constituted of 95% Argon and 5% Xenon. The Anode was operated at a constant value of 150V and the Magnet at 4A. The amount of injected gas is known to a precision of 1%, but the pressure mentioned in parentheses is not measured directly, being estimated from the injected gas amount by using eq. (4.26).

From figure 5.18 a), it can be seen that the Argon efficiency (for an MK5 source) is affected by its own partial pressure, a significant decrease appearing above a partial pressure of about 4e-5 mbar. Figure 5.19 a) offers the explanation of this decrease, which is the limitation of the extracted Argon current. In the analyzed case, the Argon partial pressure represents more than 90% of the total operation pressure and consequently the Argon current can be identified (within a ~10% error) with the total current extracted from the ion source.

It is very interesting to note that the limitation is not appearing only towards the high currents, but it is present all along the temperature range when the operation pressure goes above a threshold value (of around 4e-5mbar, as resulting from the figure 5.19 a). The origin of this

threshold pressure is not straightforward from this set of measurements and is investigated separately in the section 7.2.

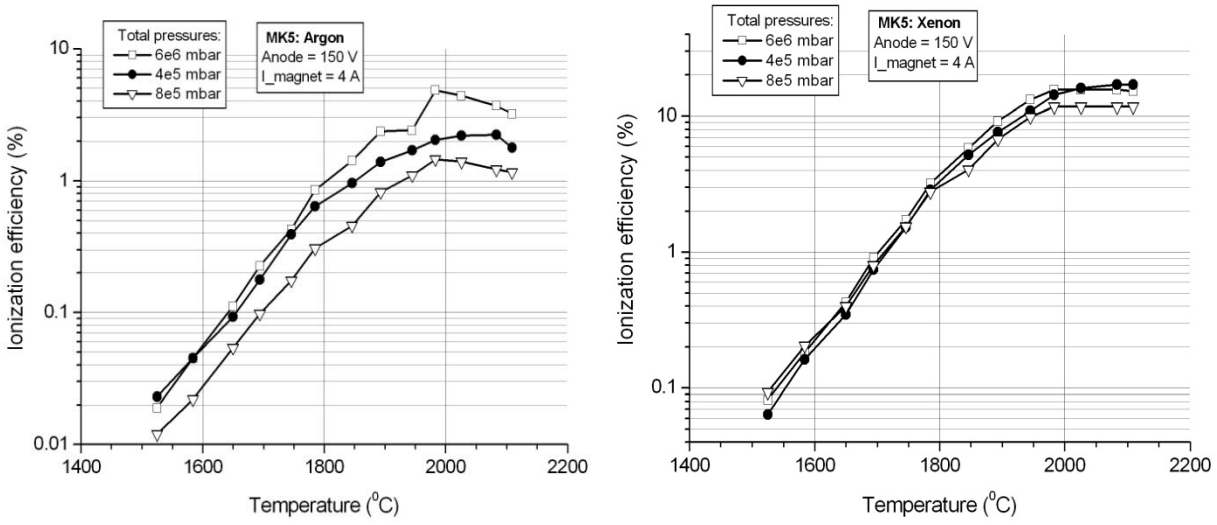

a) b)

Figure 5.18. Pressure & temperature dependence of MK5 ionization efficiencies. **a)** Argon; **b)** Xenon.

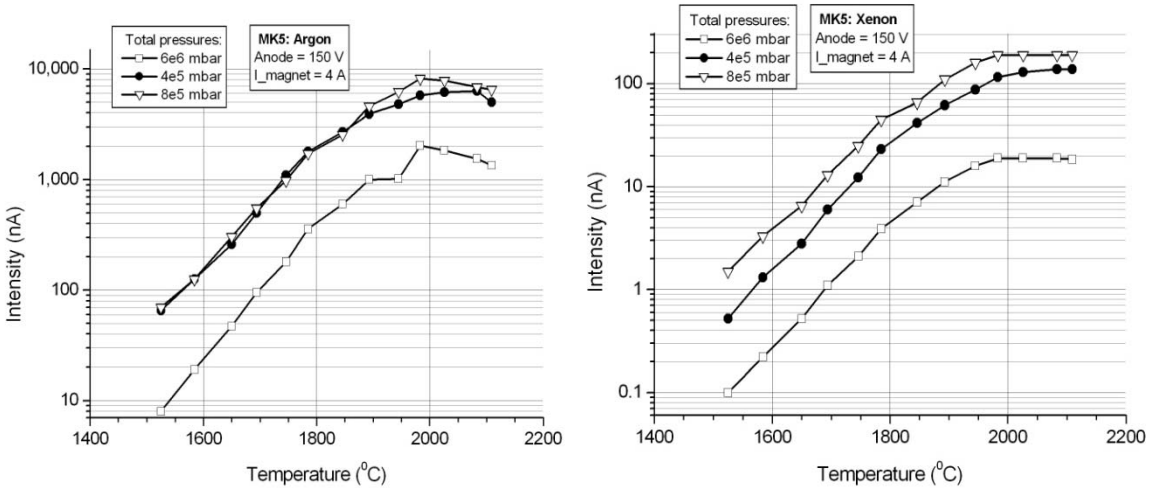

a) b)

Figure 5.19. Pressure & temperature dependence of MK5 beam intensities. **a)** Argon; **b)** Xenon.

The behavior is slightly different for Xenon, whose ionization efficiency is not saturated for the considered operating pressures. This may appear to be justified here by the important difference between the partial pressures of the two gases, but similar results were obtained for total pressures constituted entirely out of Xenon. The origin of this kind of limitation will be investigated in section 7.2.

The particular design of the MK3 sources is offering more information on the evolution of the plasma properties towards the pressure variation. At lower pressures (on the order of 10^{-6} mbar), the source is more efficient (by up to a factor 2) when operated with the two anodes at a different potential, as can be seen in figure 5.20 a). But, when the pressure is increased (towards 10^{-4} mbar), the highest efficiency is obtained by applying the same potential to the two anodes (figure 5.20 b).

This can be explained by the fact that at low pressures, the externally applied electrical fields are dominating the electrical field distribution inside the source. The plasma density is not sufficient to shield the anodes potentials and therefore the produced ions will be directed towards the outlet plate, polarized at a lower potential compared to the rest of the plasma chamber. With the increase of the operating pressure, the plasma density will increasingly shield the anodes potentials and the advantage of operating the outlet plate at a lower potential is being lost. More than that, it can be seen that the efficiency is even decreasing below the value corresponding to equal anodes potential. This is occurring because the outlet plate (Anode2) is representing in this case an important loss source for the plasma: as it represents a full end cap of the plasma chamber, even though the plasma Debye length is becoming small enough for shielding the anode potentials in most of the ion source volume, the ionic loss current from the plasma to the outlet plate will be higher compared to the case with both anodes at the same potential.

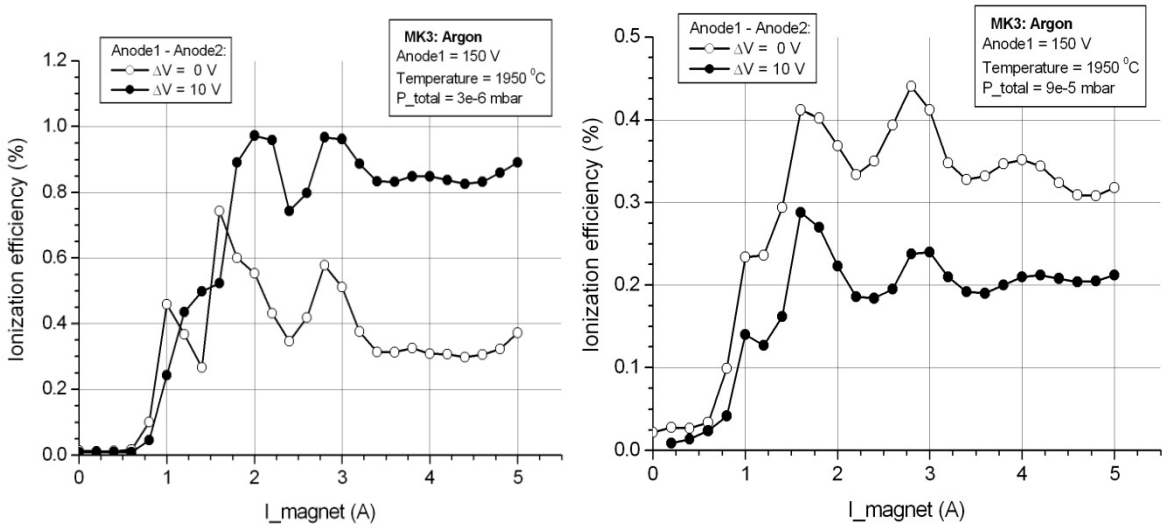

Figure 5.20. Pressure variation of the magnetic and anode dependence of MK3 ionization efficiencies. **a)** Total pressure: 3e-6 mbar; **b)** Total pressure: 9e-5 mbar.

The full dependence on the operation pressure of the ionization efficiency for the two operation modes described above is presented in figure 5.21. It can be seen that the ionization efficiency for the ΔV=10V mode is constantly decreasing above ~5e-5 mbar, while for the ΔV=0 mode the efficiency is remaining constant up to 1e-4 mbar. This is because when ΔV=0, the active volume of the MK3 source is only determined by the puller potential (and this influence is limited due to the small diameter of the source aperture), therefore not very sensitive to the plasma density.

For allowing this broad pressure range, the presented measurements were obtained in three measurement sessions (marked in the figure with I, II and III), each one characterized by a different fixed calibrated leak feeding the ion source with the buffer gas (4.0e-6 mbarl/s for I, 2.0e-5 mbarl/s for II and 6e-3 mbarl/s for III). The variation of the effective leak rate was insured by the variation of the pressure applied on the fixed calibrated leak. It is important to notice the reproducibility of the ion source performances, proven by the superposition of the curves I and II for both of the operation modes.

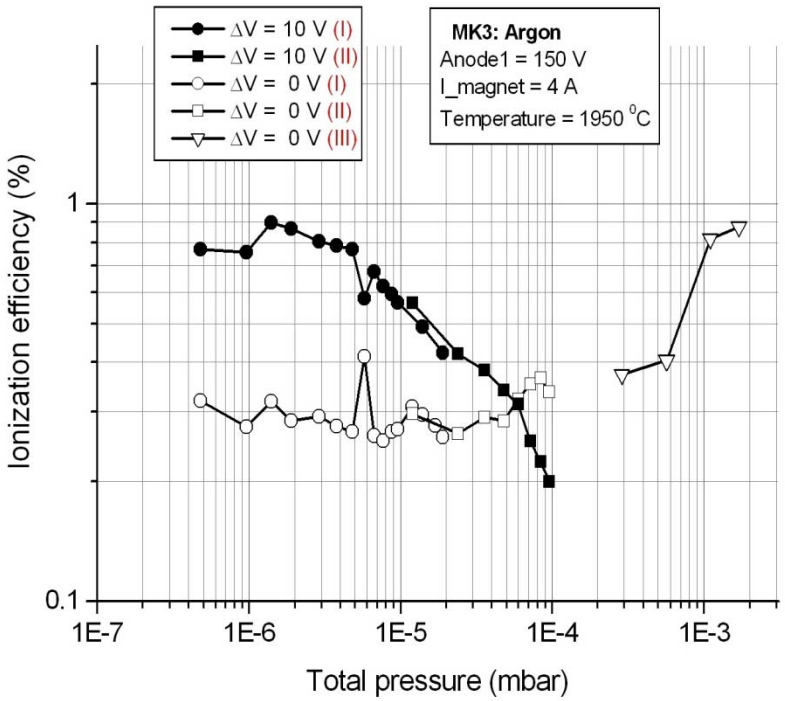

Figure 5.21. Pressure dependence of the ionization efficiency for two operation modes of an MK3 ion source: with the anodes at the same potential (ΔV=0) and with the Anode2 (outlet plate) at a lower potential than Anode1 (the plasma chamber cylinder) (ΔV=10V). Results obtained in 3 measurement sessions (marked with I, II and III), characterized by different values of the employed calibrated leak. For the session III, the points are confounded for the operation modes with ΔV=0 and ΔV=10V.

Useful information is brought by the measurement session III, where the ionization efficiency is rising again for high operation pressures (on the order of 10^{-3} mbar). More than that, there is no notable difference between the efficiencies obtained for ΔV=10V and for ΔV=0; this could be expected from the behavior recorded in figure 5.13, where it is shown that the plasma potential is becoming less sensible to anode potential variations for high operation pressures.

To understand better the behavior at high operation pressures, we detail the ion source behavior for this case in figure 5.22, a) and b). The typical ion source behavior below 10^{-4} mbar is similar to the curves obtained at 2.9e-4 mbar in this figure: the ionization efficiency is uniformly increasing up to a limit temperature (which here is of about 1800°C, but it can be higher depending on the individual source unit), where it saturates and eventually falls down for temperatures above this threshold.

In figure b), one can see that this efficiency limitation is equivalent with the limitation of the extracted Argon current to about 3μA. Before the investigations presented in this work, it was thought that this is a limit given by the source geometry and materials (space charge limitation of the extracted beam or limited electron emission from the source cathode), but the operation of the ion source at pressures on the order of 10^{-3} mbar (figure 5.22) showed that the source can generate ion currents of up to 60 μAe (for the presented measurement at 1.7e-3 mbar), continuing the same trend of intensity increase up to 2000°C.

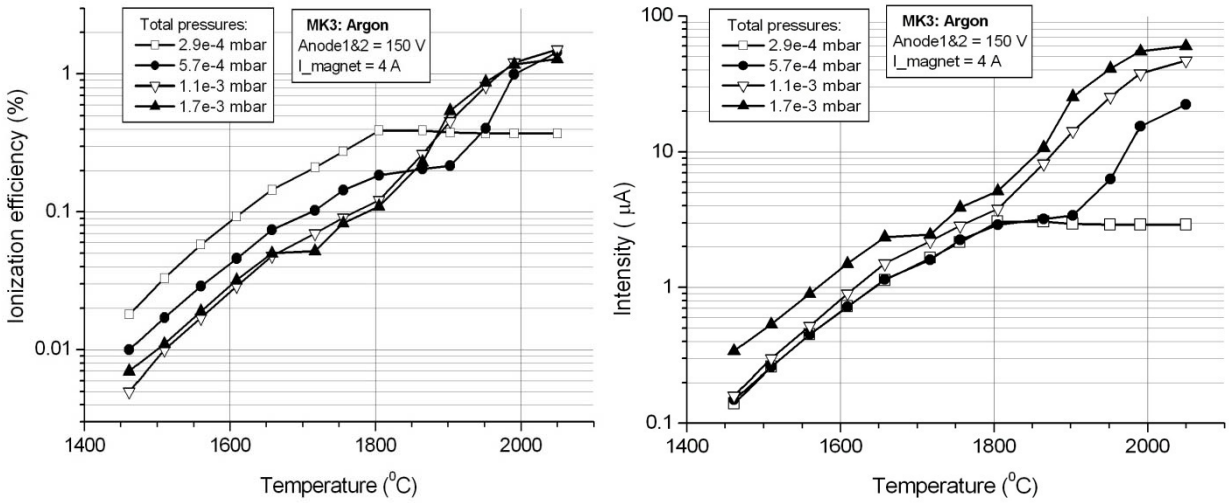

Fig 5.22. Pressure and temperature dependence of the Argon ionization efficiency **(a)** and current intensity **(b).**

These measurements are proving several things:

- There is no limit on the cathode emitted current (at least not up to 2000°C). The limitation of the Argon current for the MK3 ion source operated at low pressures is appearing due to the change of the background pressure, as will be detailed in section 5.6;
- The source is operating below the space charge limited emission (which is of about 60 µAe, in accord with the Child-Langmuir formula, applied for the employed extraction system – see also section 7.2.4);
- The source is normally being operated at a low plasma density, which permits the application of the ionization model described in chapter 4;
- If the proper operation mode is employed, the FEBIAD ion sources can operate at pressures of up to 10^{-3} mbar, with similar values for the ionization efficiency;

For completing the picture of the pressure dependence, it has to be mentioned that the behavior described in figure 5.21 is also dependent on temperature. In figures 5.23 a) and b), it can be seen that even for a constant pressure (5.5e-6 mbar in this case), the noted difference between the operation modes with $\Delta V=0$ and $\Delta V=10V$ can be reversed by the change of the operation temperature.

When decreasing the temperature (towards 1500°C), the ionization efficiency for the operation mode with a difference between the anodes potentials is decreasing more rapidly than for the operation with $\Delta V=0$ (see figure a).

The phenomenon behind this inversion is very likely to be the increase of the electron beam losses towards the Anode1 (the plasma chamber cylinder) for $\Delta V=10V$ at low plasma density (for constant pressure, a lower cathode emission is directly translating into a lower ion density), due to the repulsive potential of the Anode2.

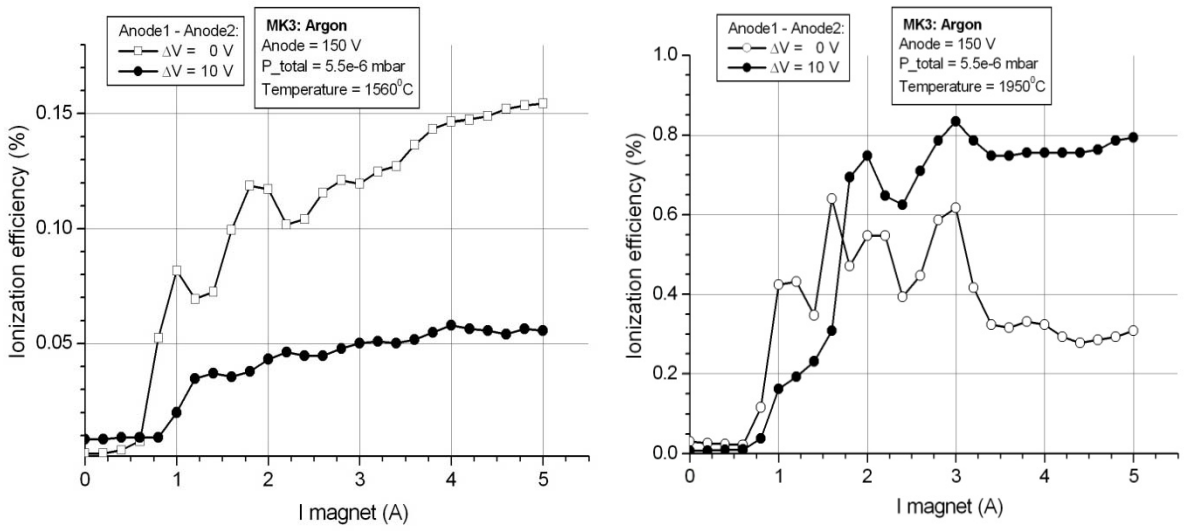

a) b)

Fig 5.23. Temperature variation of the magnetic and anode dependence of MK3 ionization efficiencies. **a)** Temperature=1560°C; **b)** Temperature=1950°C.

5.6. Dependence of the ionization efficiency on the gas composition and on impurities

The complex gas composition inside a FEBIAD ion source makes the total extracted beam a cocktail of many elements, the mass separated spectrum presenting practically a peak at every mass (only with different intensities). A typical mass scan for a MK5 ion source is presented in figure 5.25.

As explained before, the only controlled pressure component is given by the buffer gas (Argon and Xenon in this case) and any modeling of the ion source behavior is valid as long as the p_b component remains the dominant one inside the source.

When knowing the ionization efficiency for the buffer gas components and the mass scan components and intensities, one can estimate the partial pressures of all the elements present in the extracted beam, by using the presented formula for the ionization efficiency (4.26) and the measured intensity for each element.

It can be seen in figure 5.25 that in this case the buffer gas is no longer dominant in the extracted beam, therefore its partial pressure is also surpassed by the background pressure given by the evaporation of the unit materials. This is typically the case for temperatures above 1900°C, when the partial pressure of the source materials is strongly increasing and eventually limiting the ionization of the elements of interest, as it can be seen in figure 5.26.

If looking only at the Krypton ionization curve, one can think that the source ionization ability is limited above ~2000°C, but the total current presents a continuous intensity increase, confirming that the ion source can further increase its ionization at higher operation temperatures, if the limitations appearing in this case can be well understood.

If the total pressure inside the source would be constant, the evolution of the total current would be controlled only by the increase of the density of the primary electrons (which means a linear increase on a semi-log scale). The total current in figure 5.26 starts to surpass this linear

dependence above ~1950°C, due to the fact that the background pressure starts to increase. This doesn't mean that the proposed ionization model is no longer valid in this case, but only that the considered neutral density has to be updated in accord with the increase of partial pressure for some components of the background pressure.

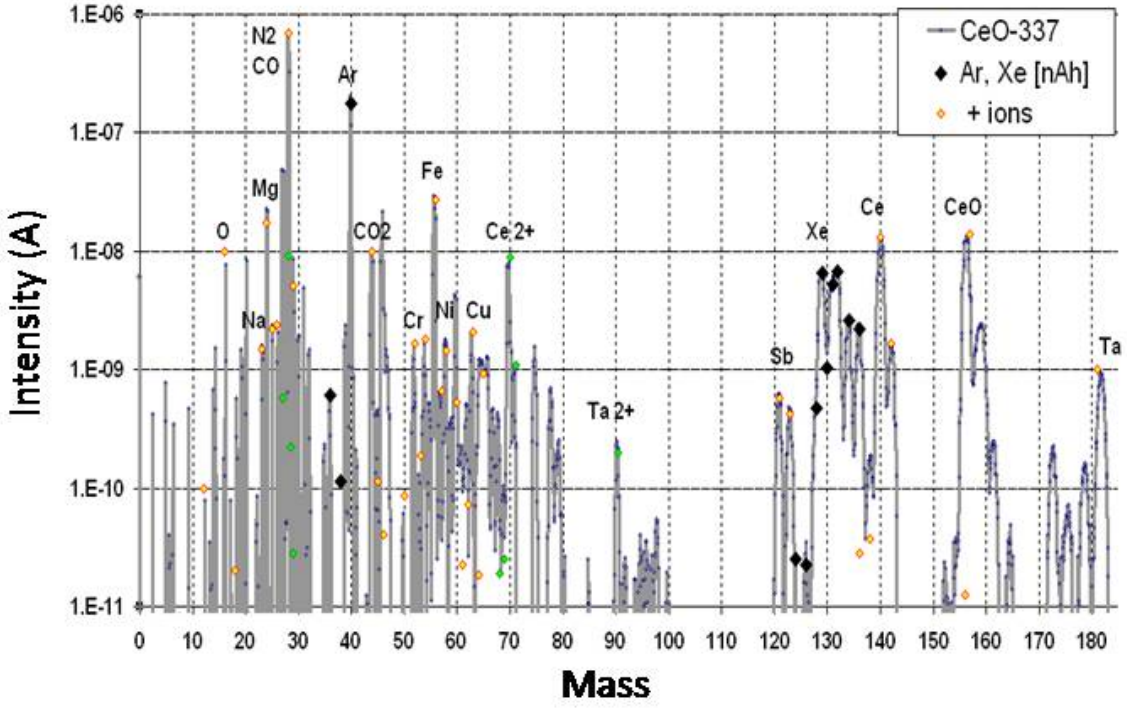

Figure 5.25. A typical mass scan for an MK5 ISOLDE FEBIAD ion source. In this case, the buffer gas was composed of 95%Ar and 5%Xe. The source was coupled to a target made of CeO.

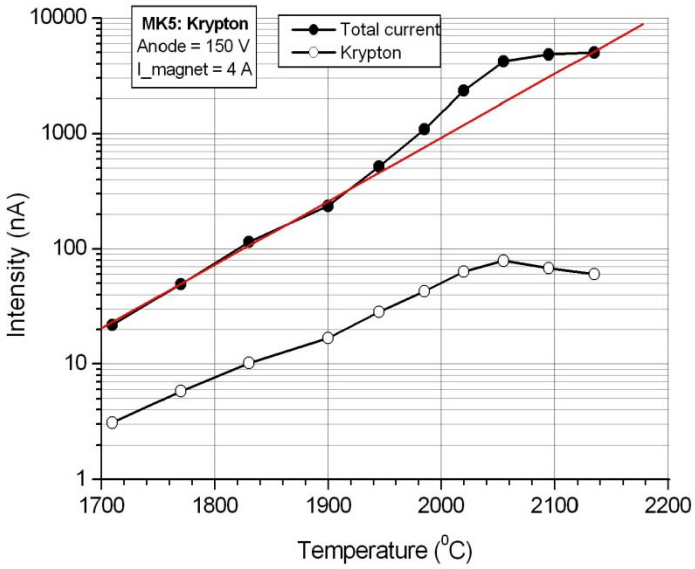

Figure 5.26. Temperature dependence of the Krypton intensity versus the total current (see text).

The most significant impurities increasing the background pressure in the ISOLDE FEBIADs are Sodium, Potassium and Carbon Monoxide. The big difference between these impurities is

that Na and K are appearing in limited amount, therefore they can be outgassed after some operation time at sufficiently high temperature, while CO is generated practically in "unlimited" amount (due to the ion source materials) and its partial pressure constantly increases towards the high operation temperatures. The comparison between the expected linear dependence and the real evolution of the total current in figure 5.26 is showing that the impurity is outgassing in this case and the source can be operated at higher temperatures after some outgassing time

If the curve of the total current was continuously growing compared to the linear fit, the only solution would be to operate the source at a lower temperature, which would also reduce the available Krypton current.

But still, even with the total current fitting the linear curve, it is not clear from these measurements why is the Krypton intensity decreasing when the total current increases; this will be further investigated in section 7.2.

One can better understand now the measurements in figure 5.22, where the reason of the limitation of the Argon ionization at 2.9e-4 mbar is the strong relative increase of the background pressure. When more Argon is added (up to 1.7e-3 mbar), its partial pressure is becoming again dominant and its ionization representative for the ion source performance. Therefore, from this available data, the background pressure for that unit can be estimated to be on the order of 10^{-3} mbar at 2000°C.

It is now evident that the best characterization of the overall performance of the ion source requires the knowledge of the evolution of the total beam, not only of the ionization efficiency of any of the beam components.

For a given unit, the background pressure is only depending on the source and target temperatures. Therefore, the dependence of the ionization efficiency for a given element on the gas composition was studied by keeping the unit at a constant temperature.

The ionization efficiency of the Xenon, Argon and Helium were studied this way for the same total buffer pressures of different compositions, but no difference in efficiency was observed.

In conclusion, the influence of the gas composition on the ionization efficiency of a given element is only appearing when the partial pressure of the other elements is high enough for changing the plasma properties inside the source, to an operation regime which would not be established by the partial pressure of the gas of interest alone. The limitations leading to changes in the operation regime are described in section 7.1.1.

5.7. Overview

The detailed investigations presented in this section allowed the better comprehension of the FEBIAD behavior and are representing the main support of the ionization model presented in chapter 4. This model was proven to fit the normal operation conditions of the ISOLDE FEBIADs, it was employed for the improvement of the ionization efficiency of these sources (as will be detailed in chapter 8) and can serve to future improvements and source customizations (as will be detailed in chapter 9).

CHAPTER 6

BEAM ENERGY MEASUREMENTS.

The beam energy is a measure which is not completely fixed by the external parameters applied to the ion source, but also depending on the properties of the ion source plasma for a given operation regime. Therefore, when precise values are needed, this parameter has to be measured apart.

The knowledge of the beam energy is important for several aspects:

a) The setting up of the optical elements (dipole, quadrupoles, etc.) for an efficient beam transport;
b) The matching of the beam energy for injection into different systems (RFQ, charge booster, LINAC);
c) The characterization of the ion source performance.

The total energy of the beam is always given by the sum of the contributions given by the accelerating potential, by the potential of the plasma where the ions are being extracted from, and by the ion temperature in the plasma:

$$E_{beam} = (eQ)V_{acceleration} + (eQ)V_{plasma} + kT_{ion} \qquad (6.1)$$

In the FEBIAD case, considering the low plasma density, it is more accurate to use the term of "**volume potential**" instead of "plasma potential", as the FEBIAD plasma density and potential is highly non uniform. Also, for the equation above, Q=1 for all the analyzed ions and we can neglect the ion temperature (as they only have the thermal energy, of ~0.2eV, much below the volume potential).

As in this study we are only interested in characterizing the ion source performance (point c above), the acceleration potential is already subtracted from the measured beam energy, therefore what is called "beam energy" in the following discussion and figures refers directly to the volume potential of the ion starting point inside the ion source.

The measurements have been done on the ISOLDE Offline Separator for an MK5 ("hot plasma") ion source, using the device described in section 3.1.4. The beam intensity is measured on the collector plate of the device, while the potential of the middle plate of the device, V_{device}, is ramped from the value of the extraction potential V_{extr} up to a maximum value of V_{extr}+300V, by using an additional power supply.

When $V_{device} = V_{extr}$, the integrality of the beam will pass this potential barrier. When V_{device} reaches and goes beyond the energy of the beam, the beam intensity measured on the collector plate will be progressively reduced, until the beam will be completely stopped by the device.

The typical result of such a measurement is presented in figure 6.1. The beam energy distribution peak is obtained through the differentiation of the raw measurement data.

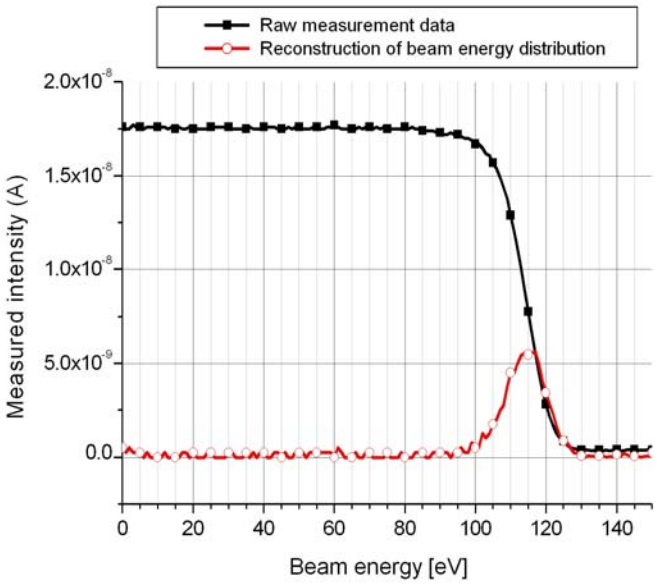

Figure 6.1. Reconstruction of the beam energy distribution through the differentiation of the raw measurement data

The measurement step for all the presented measurements is 1V; for a better visibility though, not all the experimental points are marked with symbols on the graphs (only one point over 3 is represented).

In the following, it is presented a detailed investigation of the influence of the ion source parameters on the extracted beam energy. All the measurements have been done using an operation gas composed of 40% Helium, 20% Neon, 20% Krypton and 20% Xenon.

6.1. Dependence of the beam energy on the separator parameters.

Among the first investigations done (especially during the commissioning of the experimental device), a special attention was accorded to the possible influence of the beam transport elements on the measured beam energy. In this context, the following results have been obtained:

- The settings of the **Einzel Lens** are not affecting the beam energy (as long as the beam size is maintained within reasonable limits for not hitting any restriction aperture).
- The **dipole magnet** is not affecting the beam energy (within the available precision). This investigation has been done by comparing the results of the lightest and heaviest stable isotopes of Krypton and Xenon for which the intensity could be made sufficiently high for allowing a beam energy measurement (>1nA): ^{80}Kr, ^{86}Kr, ^{128}Xe and ^{136}Xe.

- The **extraction voltage** is <u>not</u> affecting the beam energy, for voltages between 15kV and 30kV (all the presented results have been obtained at 20kV, for minimizing the risk of sparking).
  This behavior is an effect of the rarefied plasma inside the FEBIAD ion source, the plasma sheath being defined preponderantly by the internal electrical field distribution and not by the extraction field applied externally.
- The length of the **extraction gap** is <u>not</u> affecting the beam energy (as long as the resulting beam divergence can still be compensated by the Einzel Lens, for maintaining the integrality of the beam in the beam pipe).

6.2. Dependence of the beam energy on the operation pressure.

One of the main parameters defining the volume potential inside a FEBIAD ion source is the operation pressure.

The results presented below have been obtained for the following ion source parameters: Anode = 150 V; Source magnet = 3.5A; Temperature = 1950°C. The pressures marked on the figures are the total operation pressures.

It can be seen below that the variation range induced by this parameter is significant and affecting all the beam components.

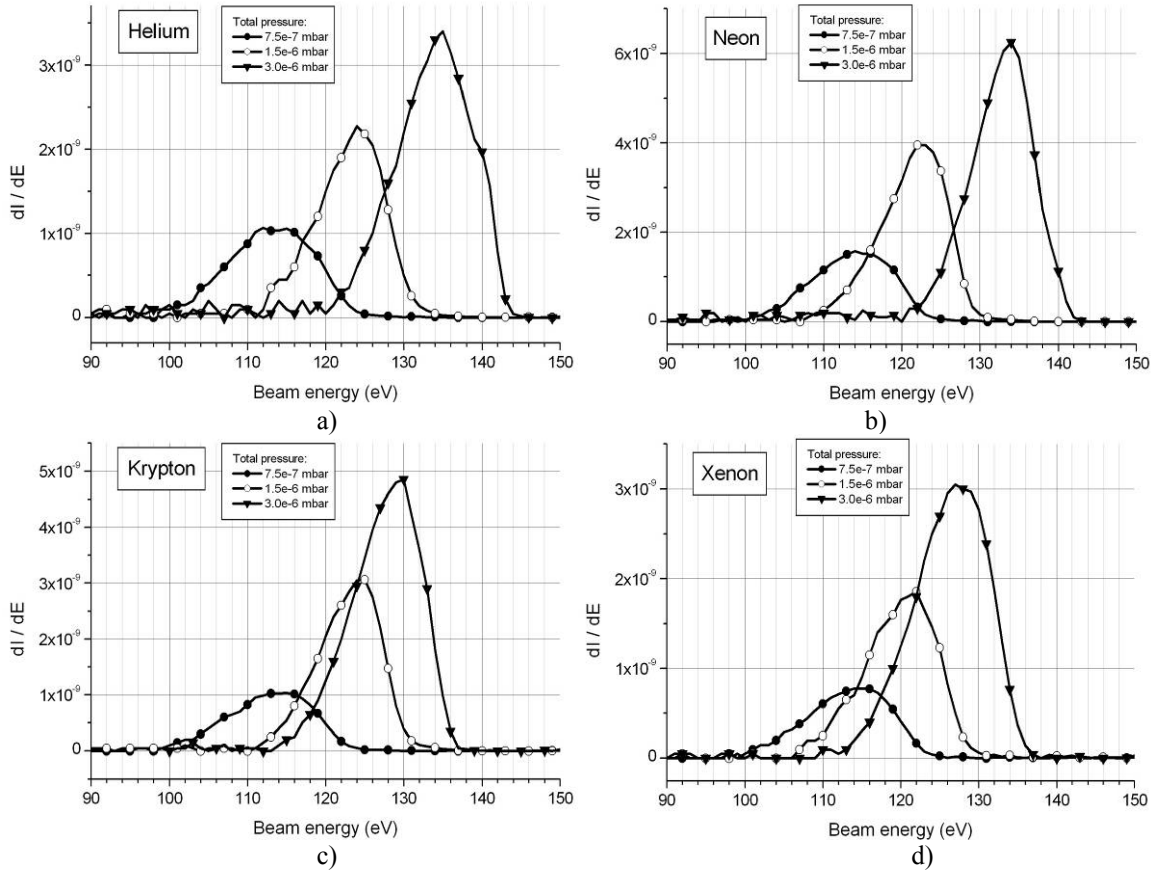

Figure 6.2. Pressure dependence of the beam energy, for all the beam components

6.3. Dependence of the beam energy on the ionized element.

The results presented in the previous section showed that the energy distribution of the extracted ions is slightly different for the different species composing the total current, even during stable operation.

Figure 6.3 (a and b) presents the same data as figure 6.2, but this time grouped with respect to the total operation pressure.

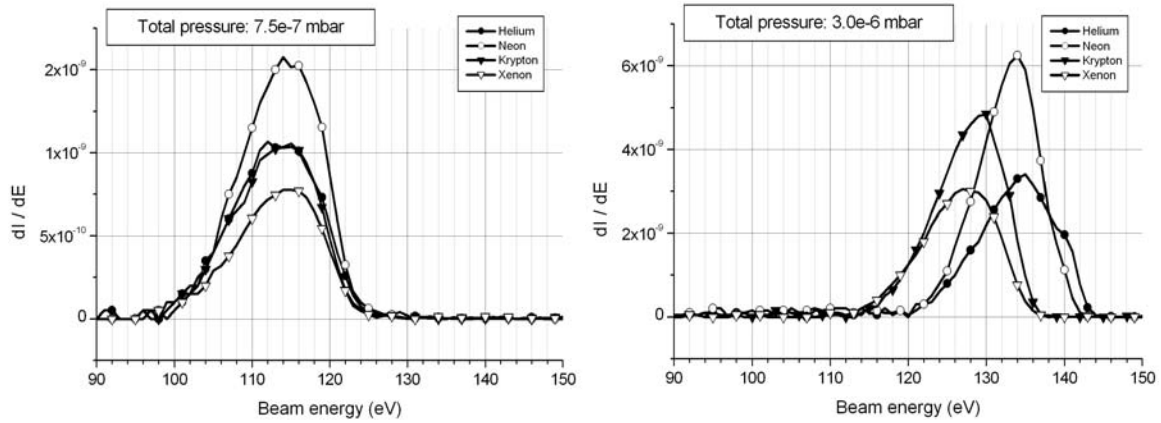

a) b)

Figure 6.3. Dependence of the beam energy on the ionized element, for two operation pressures

It can be seen that the difference between the elements is not noticeable at very low operation pressures, but it increases with the increase of the operation pressure.

This effect can be explained by the fact that the ions of different species are extracted from slightly different regions inside the ion source. For identifying the corresponding regions, we have to consider the boundary conditions imposed by the source electrodes: the anode cylindrical body (including the grid facing the cathode) is at 150V, while the central part of the outlet plate is grounded.

Therefore, the general behavior is that the heavier elements are extracted preponderantly from the region closer to the extraction plate, while the lighter elements are extracted from a more internal region. A more detailed investigation of the internal potential distribution was done using the simulation program CPO and is presented in chapter 8 (section 8.1.2).

As this element differentiation is only appearing towards the higher operation pressures, it is an effect of the saturation of the ion density inside a FEBIAD. When the operation pressure (and consequently the ion density) is approaching the threshold value, a more important part of the generated ions will be evacuated from the plasma towards the ion source walls. The data presented in figure 6.3 b) is showing that this evacuation process is selective; therefore the decrease of the extraction fraction, f_{extr}, will not be the same for all the elements. As all the ions are supposed to have the same energy (the thermal energy of the gas), it is not clear if this selectivity is given by the transition through the plasma sheath or by a slightly different trapping time of the different ion species in the plasma (which would indeed lead to a difference in energy for the different species).

6.4. Dependence of the beam energy on the operation temperature.

The operation temperature affects the volume potential through the space charge of the electrons generated by the cathode. For a constant operation pressure, a temperature increase will lead to a higher electron density inside the source, thus reducing the volume potential and the beam energy.

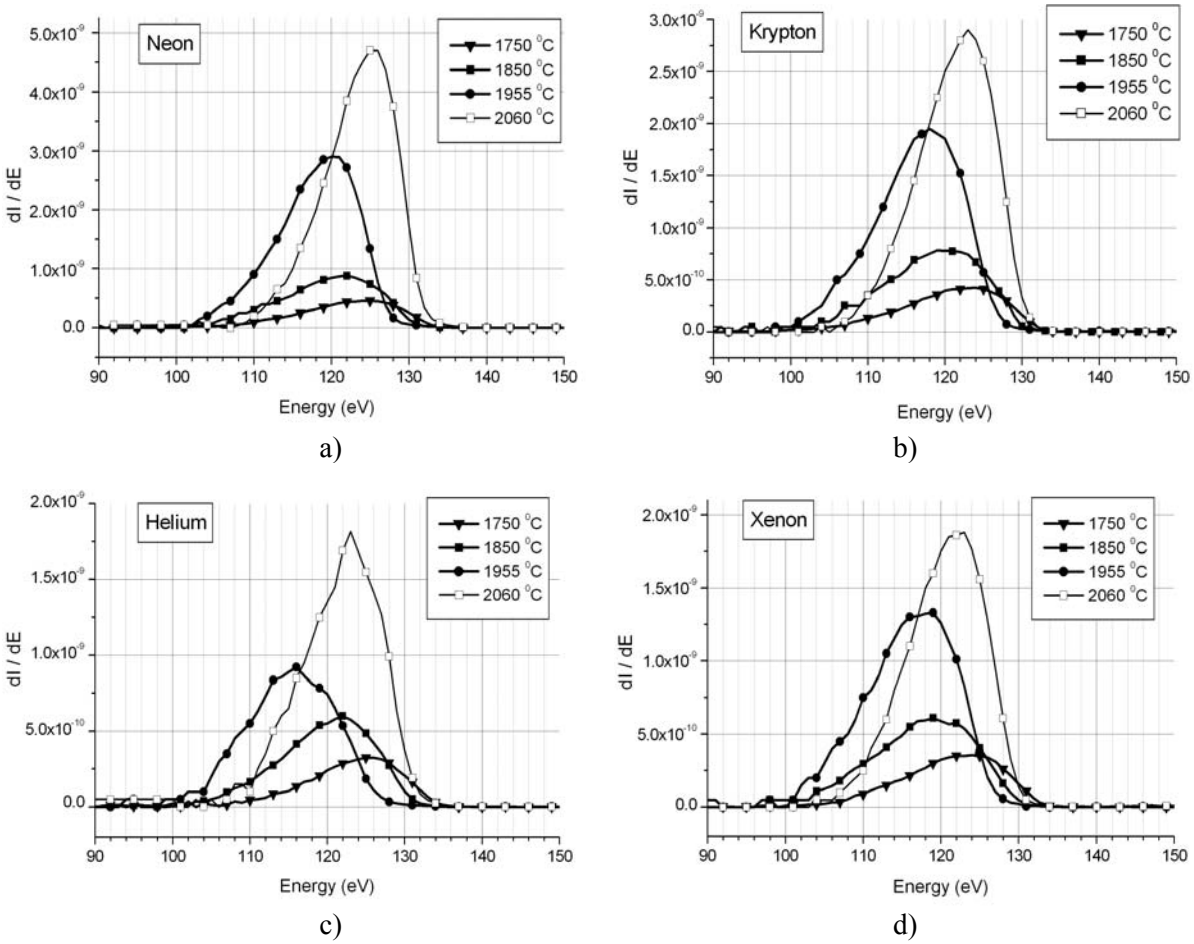

Figure 6.4. Temperature dependence of the beam energy, for all the beam components

The ion source operation parameters used for these measurements are: Anode = 150V; Source magnet = 3.5A; Pressure = 1.5e-6 mbar.

A notable effect is the change from the expected dependence for the measurement point at 2060°C. The explanation is not emerging from the presented graphs and can only be found when considering the overall source performance: at high temperatures, the total pressure is no longer dominated by the buffer gas, but by the partial pressure of the component materials of the ion source (as was also confirmed for this case, by the complete mass scan). Therefore, at 2060°C the ion density is increasing significantly due to the impurities, thus increasing the resulting volume potential inside the ion source.

6.5. Dependence of the beam energy on the anode potential.

It had been shown that the volume potential of a FEBIAD for the standard operation conditions at ISOLDE is below the anode potential. But the difference between the volume potential and the anode potential will not remain constant when the anode potential will be changed.

The figure 6.5 is presenting the measured dependence of the volume potential where the Neon and Krypton is being extracted from, for anode values between 90V and 170V. The other operation parameters are: Temperature = 1950C; Source magnet = 3.5A; Total pressure = 1.5e-6mbar.

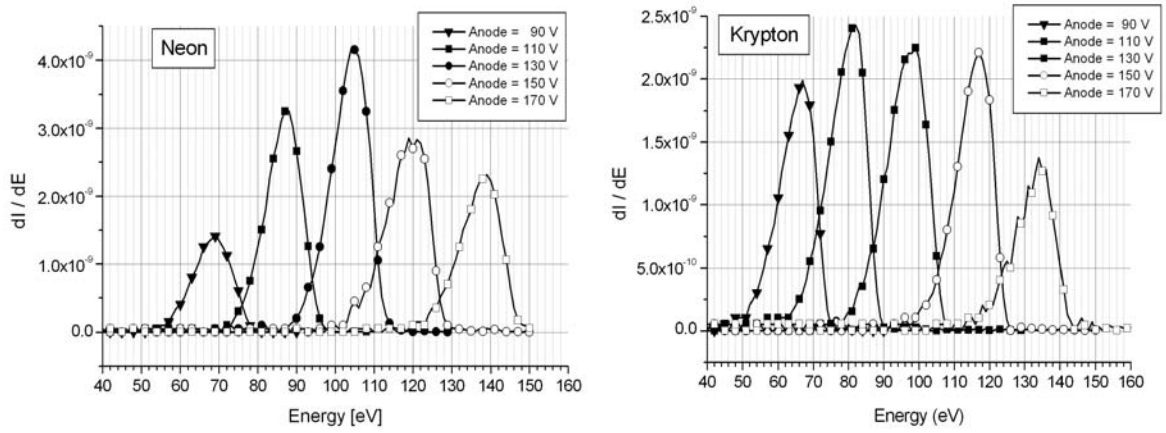

a) b)

Figure 6.5. Dependence of the beam energy on the anode potential, for Neon and Krypton

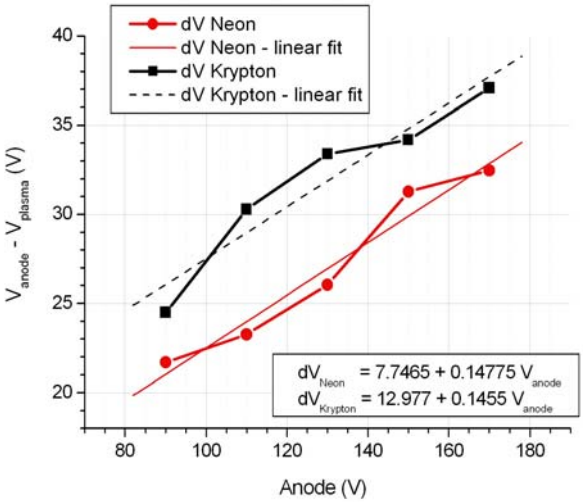

Figure 6.6. Dependence of the beam energy on the anode potential. Extrapolation.

The figure 6.6 presents the evolution of the potential difference $dV = V_{anode} - V_{plasma}$ with respect to the anode potential. The experimental points are representing the central point of the Gaussian fit for the energy distributions presented in figure 6.5.

For the analyzed range, the data can be fitted linearly. The principal use of such a fit is for extrapolations during the ion source operation, when the ion source tuning might require the modification of the anode potential and the extraction potential has to be corrected (according to

equation 6.1) for maintaining the same total energy of the beam (for not affecting the transport efficiency along the separator).

6.6. Dependence of the beam energy on the source magnet.

The low strength and quasi-uniform configuration of the magnetic field inside the FEBIAD is limiting its action only to the electrons. An increase of the magnetic field is modulating the electron density in the central zone of the ion source, with a general trend of increasing the total electron density (see figure 5.8 d). Therefore, the volume potential will be decreased by the increase of the magnetic field inside the source, as can also be seen in figure 6.7, as measured for Krypton.

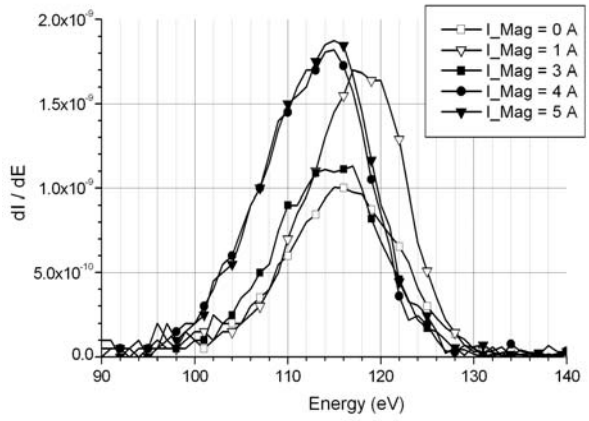

Figure 6.7. Dependence of the beam energy on source magnet (measured for Krypton).

The other source operation parameters during these measurements were: Temperature = 1950°C; Anode = 150V; Pressure = 1.5e-6mbar.

6.7. Dependence of the beam energy on the ionization mechanism.

An interesting observation was made in a different measurement session (without employing the beam energy meter), when the use of a smaller diameter of the outlet plate (0.5mm instead of 1.5mm) increased the mass resolution provided from the source: the separated peaks were having a waist of only ~2mm at the position of the scanner from the offline separator (details on the separator and diagnostics position are given in section 3.1.2). The waist at that position for the standard outlet is ~5mm.

This way, the fine structure of the FEBIAD peaks could be observed.

The figure 6.8 presents the evolution of the X positions of the separated beams of Kr^{2+} and K^{+}, for different potentials applied to the source anode. As was presented in figure 6.5, it is normal for FEBIAD to have a direct influence of the anode potential on the beam energy (and consequently on the position of the separated beam for a constant dipole strength, like it is the case here). The Kr^{2+} peaks are following this standard behavior, which is not the case for the K^{+} peak.

When $V_{anode} \neq 0$, the potassium peak presents two components: one due to the surface ionization and one due to the electron beam ionization. The surface ionized fraction can be identified for the case $V_{anode}=0$, when it represents the only peak remaining in the spectrum.

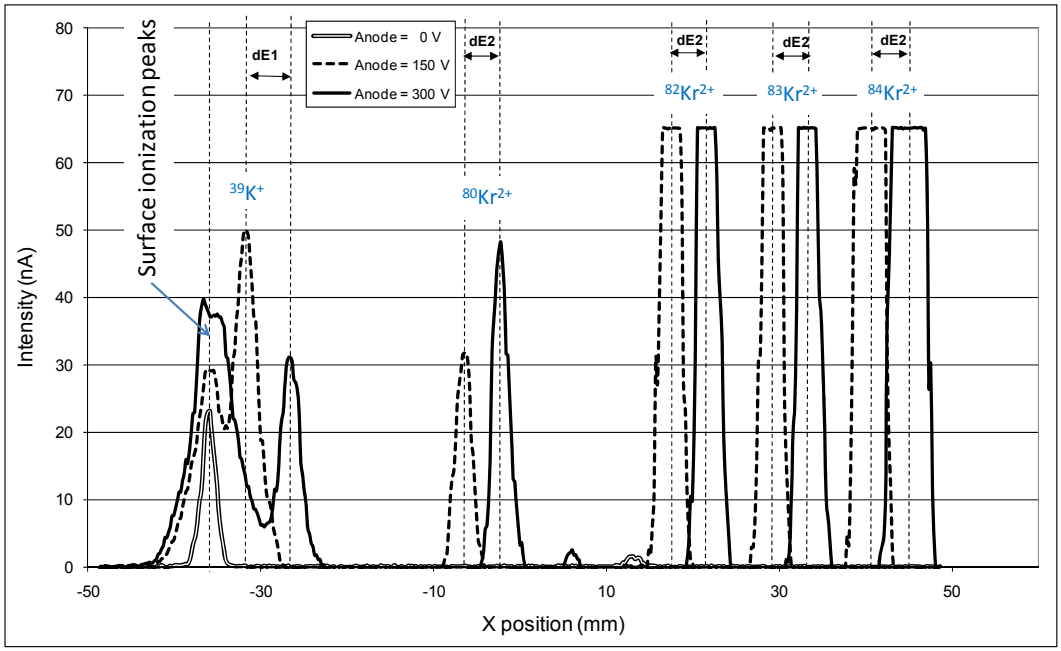

Figure 6.8. Energy difference between surface ionized and volume ionized ions.

There are two important pieces of information provided by this measurement:

- There is a difference between the beam energy of the ions generated through surface ionization and through electron beam impact. This can be justified by the fact that the two types of ions are starting from different positions inside the ion source, corresponding to different potentials.
- The energy of the surface ionized component is independent on the anode potential. This can only be justified by the fact that the ions are produced on a part of the source wall remaining at the same potential. Out of the possible options (cathode, insulators, thermal screens on the outlet side), the thermal screens are the most probable candidate.

The general information extracted from this measurement is that the beam energy of the ions produced through electron impact is given by the volume potential at the place where they are produced, while the beam energy of the ions produced through surface ionization is given by the potential of the surface where they have been generated (it may not always be a surface with a constant potential, like in the case presented in fig.6.8).

6.8. Overview and conclusions.

The measurement of the beam energy allows the characterization of the ion source performance, by providing information on the electrical field distribution inside the ion source. By using the knowledge on the ion source behavior (acquired also through other investigation methods), this primary information can be derived for obtaining other ion source internal parameters:

- The **electron** and **ion densities** inside the ion source;
- The **f factor** (from formula 4.26) and the geometry of the corresponding "active" volume;
- The **operation regime** (dominated by the cathode electrons or by the plasma ions; saturated by impurities or controlled by the buffer gas);
- The **saturation pressure**, where the saturation of the ion density inside the ion source is leading to the apparition of selective ion losses from the plasma.

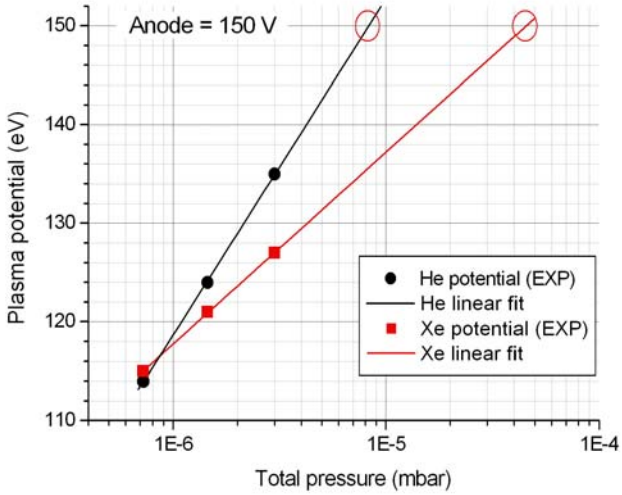

Figure 6.9. Deduction of the saturation pressure from BEM measurements.

As an example, for the ion source investigated in this chapter, the saturation pressure at 1950°C can be obtained from the measurements presented in figure 6.2. The figure 6.9 is showing that the dependence of the volume potential on the total pressure can be fitted linearly on a semi-log scale and the saturation pressure will be given by the intersection of the linear fit with the ordinate of the anode potential (150V here).

It can be seen that the lighter elements will reach the saturation at lower operation pressures, which means, for example, that the increase of the pressure of impurities inside the ion source, the lighter elements will be the first ones to have their ionization efficiency reduced.

The value of the saturation pressure can be increased (for all the elements) by the increase of the primary electron density (by increasing the operation temperature while maintaining a low impurity pressure or by using a different cathode material).

CHAPTER 7

LIMITATIONS ACTING ON THE IONIZATION EFFICIENCY

Any model has a limited domain of applicability with respect to the variation of the employed parameters, due to the change of the assumed ratio between the dominant and competing phenomena.

Any ion source has a limited range of variation of the operation parameters, due to different physical limitations (physical and chemical properties of the employed materials, particular operation conditions, power supply performances).

The superposition of these limitations will restrict the applicability of a model outside a well defined domain.

In this chapter we will detail the applicability restrictions generated both by the analytical model and by the real physical system serving as ion source.

In section 7.1 we will make the summary of the limitations observed for the ionization efficiency of the noble gases during the experimental investigations presented in chapters 5 and 6. The analysis of the neglected phenomena and of the sources of errors of the employed model will justify the introduction of a correction term to the model, which will allow the consideration of the limited confinement time of the neutral atoms in the ion source volume.

This correction is proved to be sufficient for the standard operation conditions of the ISOLDE FEBIADs. For applying the model outside the domain for which is has been deduced and checked experimentally, one has to investigate the evolution of the ratio between the dominant and the secondary phenomena, as well as the new phenomena possible to appear and limit the ion source performance. This investigation is presented in section 7.2.

7.1. Model limitations. Correction for the gas pumping.

7.1.1. **Experimentally observed limitations of the ionization efficiency.**

Even though the model developed for the ionization efficiency of the FEBIAD sources showed a good global concordance with the experimental data, several unexpected behaviors were recorded during the experimental investigations presented in chapters 5 and 6.

As these particular behaviors are important keys to the understanding of the phenomena limiting the ion source performances, we will review them in the following.

a) *Different f factors for different species.*

By applying the developed model (formula 4.26) to the experimentally measured ionization efficiencies (figure 5.14), it was observed that the corresponding f factors are consistently different for Argon compared to Xenon (namely, $f_{Xe} > f_{Ar}$). This can suggest that different active volumes are corresponding to the different elements, but a closer analytical investigation (section 7.1.4) will show that this is an effect of considering the f factor globally (for the whole residence time of the investigated atom). The heavier elements will have a higher ionization cross section and a longer residence time, and therefore will be ionized more times before leaving the ion source volume.

This means that the real f factor that is linked to the active volume through the formula $f = V_{active} / V_{total}$ is the f_0 factor, characterizing only one ionization process. The difference between the two can be significant and therefore requires a model correction, especially when needing to access the geometrical active volume or the time dependence of the particle density inside the ion source.

The dependence of the global f factor on f_0 and the resulting model correction is presented in section 7.1.4 and is found to be dependent on element, operation temperature and ion source geometry.

b) *Element selectivity at high operation pressures.*

Extensive measurements of the energy of the extracted beam (chapter 6) showed that the beam energy of the different elements starts to differentiate at the increase of the operation pressure (see figure 6.3). This is suggesting that the different elements will be extracted from slightly different positions inside the ion source (according to the potential distribution inside the source). The correspondence between the beam energy and the start position of the ion inside the source can be approximated using the simulated electrical potential distribution inside the source (obtained with CPO and presented in section 8.1.2)

The origin of this effect could not be cleared up in the present work.

c) *High temperature limitation.*

A limitation of the ionization efficiency was systematically observed towards high operation temperatures (roughly above 2000°). This can be observed for example in figure 5.14.

Additional investigations (see figures 5.22 and 5.26) showed that this behavior is only appearing for separated beam components at constant partial pressure (which is the case for the

buffer gas or for the produced radioactive products), but not for the total beam extracted from the ion source. The limitation of the ion current of the species of interest is therefore appearing due to a strong increase of the vapor pressure of the component materials (or of unwanted impurities) at high temperature, which will then dominate the total extracted beam.

This limitation provided information that the ion source can be efficiently operated at temperatures higher than 2000°C if the background pressure can be maintained sufficiently low. This was the basis of the development that will be presented in section 8.2.

Therefore, this limitation is linked to another listed limitation: the pressure limitation.

d) *Pressure limitation.*

A significant change in the plasma properties (and therefore in the ionizing mode) is appearing at the increase of the operation pressure above 1e-4 mbar (see figure 5.21). Through extensive investigations of the beam energy (chapter 6), it was found that this transition is characterized by the shift of the plasma potential from a negative to a positive value with respect to the potential of the plasma chamber (i.e. anode) walls.

At low pressures, the plasma is dominated by the negative space charge of the primary electron beam, while at high pressures the buildup of the generated ions will be able to maintain a positive plasma potential towards the center of the ion source.

The compilation of the results from chapter 6 showed that the transition is characterized by the total pressure (independent on the gas composition) and is not occurring at the same total pressure for all the elements (see figure 6.9): the lighter elements are having a lower transition pressure. This means that at the increase of the operation pressure (due to impurities becoming volatile at high temperature, for example), the first elements to be affected will be the light ones, while the heaviest will still maintain their high ionization efficiency up to higher pressures.

This was also confirmed by the results that will be presented in section 8.2.4 (see figure 8.18).

The above mentioned pressure values are linked to a specific input gas flow through the source geometry. This means that the input gas flow can be increased without reaching the transition pressure value, if the source geometry is adapted for reducing the residence time of the neutral atoms. Of course, for maintaining a high ionization efficiency this has to be done together with the increase of the primary electron density.

An important remark is that the FEBIAD sources can also be operated above this threshold pressure with similar ionization efficiencies (like confirmed by the measurements at high pressure from figure 5.21). The drawbacks would be:

- The presented model will no longer be accurate (at least it is not confirmed by the present work);
- The heavy elements (compared to the main component of the generated plasma) can be trapped inside the plasma and therefore their ionization efficiency significantly reduced. This was observed during the measurements at high pressure presented in figure 5.21. The use of Xenon as buffer gas can allow the efficient extraction from the plasma of the lighter gases, but considering the interest for heavier ISOL beams, this solution would not be satisfactory. The use of a heavier molecular gas as buffer gas would lead to the formation of several molecules of the gas of interest and therefore to the splitting of the useful current at different masses;
- Higher beam intensity and emittance (not covered by this work).

e) *Ion current limitation all along the temperature range.*

It was observed during the experimental investigations presented in chapter 5 that when increasing the FEBIAD operation pressure above ~10^{-4} mbar, the extracted ion current is reaching a saturation value (see figure 5.19).

The particularity of this kind of limitation is that it is appearing all along the temperature variation range, therefore for a wide range of plasma densities and of background pressures (only increasing towards high temperatures)

This behavior was believed to be linked to the charge exchange in the source, but it will be shown in section 7.2.1 that the change exchange cannot generate this kind of figure. An alternate explanation is proposed in section 7.2.5, where it is showed that this difference can appear both due to the limitation of the ion density inside the ion source or to the space charge limitation of the ion transport from the source volume to the source outlet plate.

Like it is the case also for the pressure limitation, this kind of saturation occurs first for the lighter ions, which are leaving the source volume in a shorter time and are having a smaller ionization cross section.

f) *Dependence on ion source subtype.*

The ionization efficiency for the same element and for the same operation conditions (total and partial pressures, temperature, anode potential, magnetic field) was found to be consistently different for each of the ion source subtypes used at ISOLDE (MK3, MK5 and MK7). This difference was presented in figure 5.15. In section 8.1 will be confirmed experimentally that this difference is generated by differences in the outlet plate geometry. By modifying this geometry, the high ionization efficiencies characterizing the MK5 subtype could be extended to the MK7 subtype.

For the presented model, this difference translates directly into a difference of the f factor, due to a maximization of the active volume. This result is specific to the ion source operation at low plasma density (where the plasma potential is negative with respect to the plasma chamber potential and the externally applied potential is dominating the internal field distribution). At high plasma densities (positive plasma potential), the geometry of the outlet plate will no longer have a strong influence on the extracted beam intensity (but the source can still provide high ionization efficiencies).

7.1.2. **Phenomena neglected in the employed model. Model approximations**

As it was described in section 4.2.1, the proposed model is neglecting some of the phenomena presented in section 2.3, due to their limited influence on the 1+ ionization over the standard variation range of the FEBIAD operation parameters (approach justified in the same section 4.2.1). The list of these neglected phenomena is:

a) The ionization produced by secondary electrons;
b) The multiple ionization (only 1+ ions are analyzed);
c) The charge exchange from the produced ions to the neutral atoms;
d) The surface ionization on the ion source walls;
e) The thermal electronic emission of the ion source walls;
f) The elastic collisions of the charged particles in the ion source volume.

Additionally, during the inference of the model, the following assumptions have been used:

a) *There are no charge accumulations inside the source volume.*

Each charged particle (electron or ion), once generated, will only have one passage through the ion source volume. This assumption is justified by the fact that the FEBIAD plasma is not dense enough for shielding the externally applied electrical fields (confirmed by experimental measurements: see figures 5.11, 5.21 and 6.2 and the corresponding explanations in the text).

b) *The neutral gas pressure is not affected by the extracted ion current.*

This is justified by the fact that the input gas flow is continuously supplying enough gas for maintaining the same pressure. As it will be presented in section 7.1.4, the ionization time for the atoms of the input gas is comparable to the total time spent in the ion source as neutrals (in the absence of any ionization), therefore from the pressure point of view, there is no difference if the atoms are leaving the source as neutrals or as ions, as long as they spend a comparable time inside the source.

If required, the model can be corrected for this effect; this was not included in the present work as this would require a self-consistent solution obtained through several iterations, which would make the parameter dependence of the model difficult to follow analytically.

c) *The f factor is including all the successive ionizations.*

The formula (4.26) was developed by taking into account only one ionization process. In reality, depending on the ion source operation parameters, some elements will spend more or less time into the ion source, compared to this reference ionization time. The effect of this is that the f factor will not characterize directly the geometrical active volume, but it will characterize globally the total number of ionizations before pumping. This approximation led to the observed difference between the f factors of different elements (Argon and Xenon in figure 5.16) and will be corrected for in section 7.1.4.

d) *Negligible sticking time.*

The sticking time of the neutral atoms on the ion source walls is considered to be negligible compared to their flight time between two wall collisions. This is an accurate assumption for the noble gases (the experimentally investigated cases from this work), but it will require an additional correction for all the other elements, which will have a sticking time strongly depending on the operation temperature. This correction will be presented in section 9.1.2.

e) *No radioactive decay losses.*

The model was deduced and tested for the stable isotopes of the noble gases, therefore no correction is needed for the data already presented. This is not the case for the production of radioactive ion beams, therefore a correction for this effect will be introduced in section 9.1.3.

7.1.3. **Sources of errors (affecting the calculation of the f factor)**

The principal sources of errors for the data presented in this work are listed below:

a) *Estimation of the neutral gas pressure.*

The neutral gas pressure inside the ion source is not measured directly. It is only estimated from the input gas flow (known with a precision of 1%), by using the formula 4.24. The error induced by this approximation is not affecting the announced values of the ionization efficiency, but only the corresponding f factors and the values for the threshold pressures (with up to 50%).

Also, the formula 4.24 assumes that the flow through the source outlet is in the molecular regime.

b) *Estimation of the electron emission from the cathode.*

The electron beam current considered in the ionization formula is not measured experimentally, but calculated using the Richardson-Dushman equation, employing the standard emission parameters for the cathode material. The real emission parameters (A,W) can be slightly different for the real cathode material. Also, the temperature of the cathode emissive surface was considered to the uniform and identical to the temperature measured during the heating calibration. Still, it was observed in some cases that after a full cooling of the unit, the calibration can shift with up to 50-100°C. When occurring, this can affect the estimation of the f factors with up to a factor 2.

c) *Estimation of the energy of the primary electrons.*

The assumptions concerning the energy of the primary electrons are:

- The passage through the accelerating grid introduces no energy spread or divergence;
- The grid transparence to the electron beam is equal to its geometrical transparence;
- The electrons are not losing energy during their passage through the ion source volume (the ratio of the electrons producing ionizations to the total number of electrons was shown in section 4.2.1 to be negligible).

d) *Estimation of the temperature of the plasma chamber*

It is assumed to be identical to the cathode temperature, due to the small source dimensions and direct visibility of the cathode to the full plasma chamber volume. Still, it is possible that the temperature in the outlet plate region is lower with 100 to 200°C. This can have an influence of the following calculations:

- a small influence of the estimation of the atom velocities;
- a significant influence on the estimation of the sticking times of some atoms on this surface;
- a significant influence on the estimation of the impurity partial pressures (when the impurities are originating in the extraction side).

7.1.4. **Correction of the model for the gas pumping.**

The formula developed in chapter 4 (equation 4.26) is assuming a global f factor:

- Out of any selection N_0 of neutral atoms, all are ionized in a time equal to the ionization time;
- Out of the produced ions, only a fraction ($f \cdot N_0$) is extracted as beam;
- The rest of the ions, $(1-f) \cdot N_0$, are lost through pumping.

This assumption is not accurate, especially not for atoms that will spend into the source significantly less or more time compared to the ionization time.

We will now correct the model for this effect by taking into account that an atom may suffer several ionizations before being lost as neutral through the outlet hole of the source. In this case, the difference compared to the initial assumption is that the step described above is repeated i times, until:

$$i \cdot t_{ioniz} = t_{pump} \tag{7.1}$$

The time required for ionization can be obtained from the same formalism used in section 4.2.3, as being the inverse of the ionization frequency:

$$t_{ioniz} = \frac{1}{\nu_{ioniz}} = \frac{1}{n_e \cdot \sigma_i \cdot v_{rel}} \tag{7.2}$$

It is now evident that the ionization rate expressed by the formula (4.13) refers only to one ionization process:

$$R_{ioniz} = n_n \cdot n_e \cdot \sigma_i \cdot v_{rel} = n_n \cdot \nu_{ioniz} = \frac{n_n}{t_{ioniz}} \tag{7.3}$$

This model correction can be done in several manners, according to the desired precision. In a first approximation (see figure 7.1) one can consider a global pumping, where the atoms are suffering several ionizations until their residence time equals the average pumping time (when all the remaining atoms from the initial population are considered to be pumped). In a second approximation (see figure 7.2), the pumping can be considered as continuous, occurring until all the initial population is extracted, either as ions or neutrals.

The pumping times for these two approaches are computed in the following way:

a) For the first approximation (average pumping):

$$\left\langle t_{pump} \right\rangle = \frac{L}{v_n} \tag{7.4}$$

Where v_n is the thermal velocity of the atoms (4.15) and L is the length of the full atom trajectory into the ion source (before pumping), defined as the product between the average number of collisions with the ion source walls, N_{pump}, and the average flight length between two collisions, l_{avg}:

$$L = N_{pump} \cdot l_{avg} \tag{7.5}$$

The average number of collisions before leaving the ion source volume, N_{pump}, is defined geometrically, as the inverse of the probability to leave the source after one collision, p_{pump}:

$$p_{pump} = \frac{S_{out}}{S_{total}}; \qquad N_{pump} = \frac{1}{p_{pump}} = \frac{S_{total}}{S_{out}} \tag{7.6}$$

b) For the second approximation (continuous pumping)

Out of any selection N_0 of neutral atoms at an initial moment t_0, the number of remaining particles inside the ion source at a moment $t>t_0$ can be expressed as:

$$N = N_0 \cdot \exp\left[-\frac{t}{t_c}\right] \tag{7.7}$$

where the pumping constant, t_c, is depending on the source volume and on the conductance of the outlet aperture, C (given by formula 4.22):

$$t_c = \frac{V}{C} \tag{7.8}$$

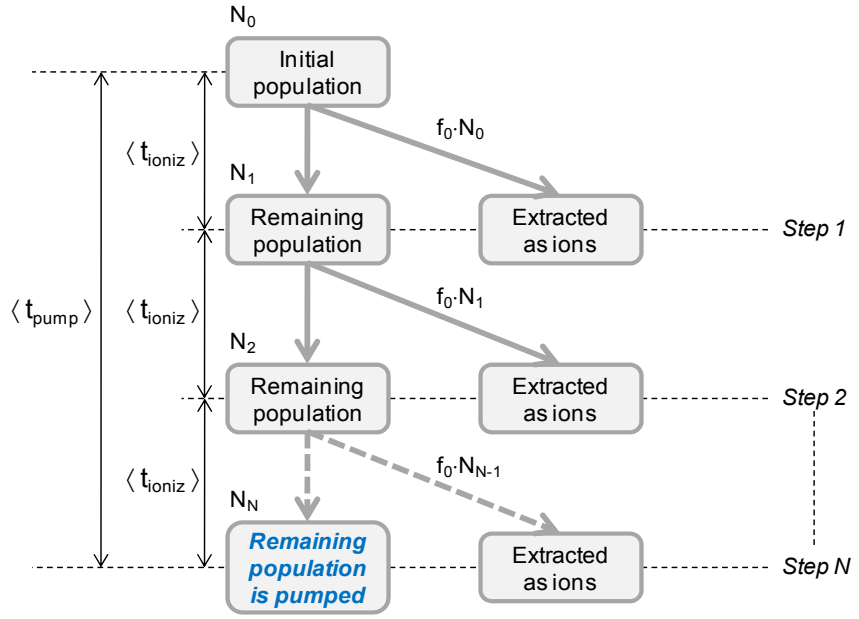

Figure 7.1. Effect of succesive ionizations. **First aprroximation**: average times for the ionization and pumping.

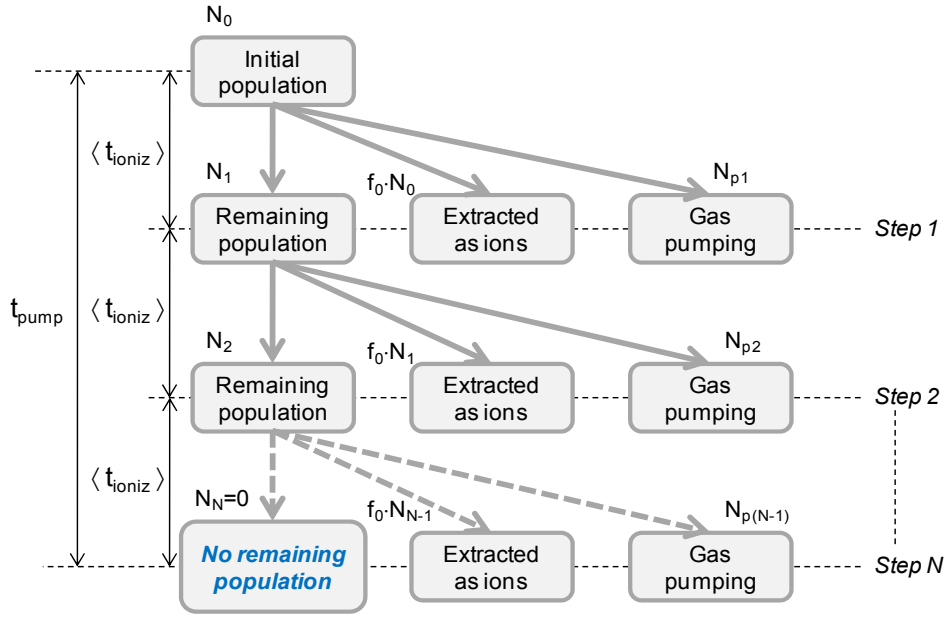

Figure 7.2. Effect of succesive ionizations. **Second aprroximation**: average ionization time, distributed pumping.

In the present study we will only employ the first approximation. The second approximation would make very complex the resulting analytical expressions and the gain in precision is not significant here; if needed, it can be easily implemented using numerical solving.

From figure 7.1, it can be seen that the ion populations generated at different steps can be expressed as:

$$\begin{aligned} N_1 &= N_0 - N_0 \cdot f_0 = N_0 \cdot (1 - f_0) \\ N_2 &= N_1 - N_1 \cdot f_0 = N_0 \cdot (1 - f_0)^2 \\ &\cdots\cdots\cdots\cdots\cdots\cdots\cdots\cdots\cdots\cdots \\ N_i &= N_{i-1} - N_{i-1} \cdot f_0 = N_0 \cdot (1 - f_0)^i \end{aligned} \qquad (7.9)$$

The total number of extracted ions will be:

$$N_{extracted} = \sum_{i=0}^{N-1} f_0 N_i = (f_0 N_0) \cdot \sum_{i=0}^{N-1} (1 - f_0)^i \qquad (7.10)$$

Therefore the correction factor is $\sum_{i=0}^{N-1} (1 - f_0)^i$ and can be used for linking the global extraction factor f to the "one-ionization" extraction factor, f_0:

$$f = f_0 \cdot \sum_{i=0}^{N-1} (1 - f_0)^i \qquad (7.11)$$

The extraction factor for one ionization, f_0, is only depending on the plasma parameters, while the global f factor will depend on element, as long as they will suffer a different number of ionizations.

If successive ionizations are possible for an element, the resulting ionization efficiency will be higher compared to the one predicted by the formula 4.26. The relative gain compared to the efficiency for one ionization is presented in figure 7.3.a and the evolution of the global f factor on N is presented in figure 7.3.b. The curves are obtained using the formula (7.11).

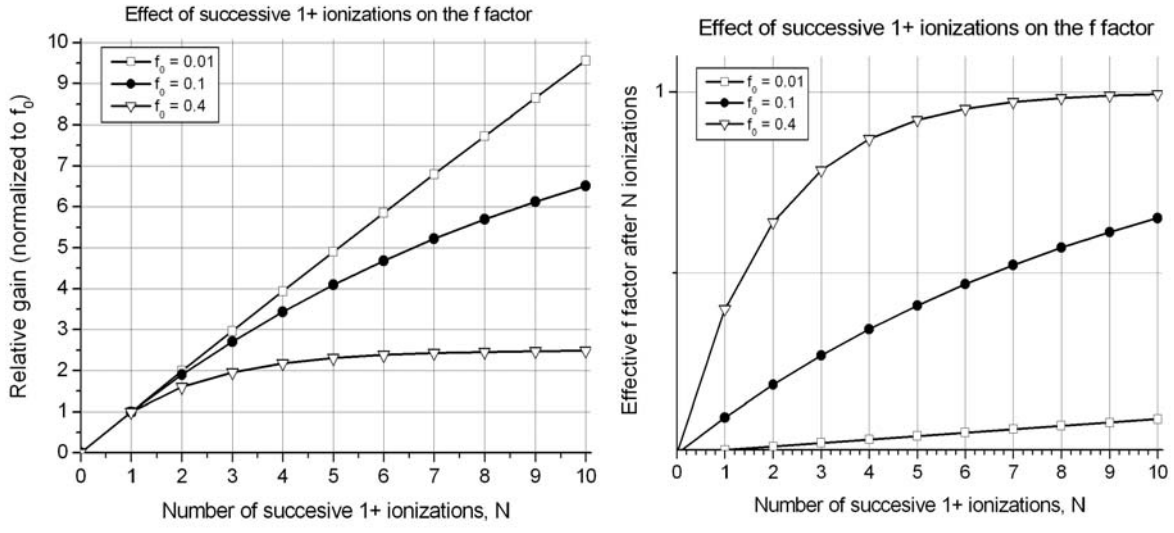

a) b)

Figure 7.3. Relative gain in ionization efficiency (compared to one ionization) as a function of the number of ionizations (**a**) and the corresponding global f values (**b**).The influence of f_0 is also shown.

It can be seen that:

- For small f_0 values ($f_0<0.01$), the global f is obtained by simple multiplication, $f=N\cdot f_0$;
- For big f_0 values ($f_0>0.4$), no significant gain is obtained for more than ~3 ionizations.

Therefore (considering also that f_0 is constant for all the elements) the global f factor will present a significant dependence on the element especially for small N and small f_0 values (if N is high enough for both elements, even when $f=N\cdot f_0$, the ratio of the relative gains can be lower than 10%). For an ion source, small N is equivalent with short residence time and/or low primary electron density. Small f_0 means a low efficiency of the extraction system. If these situations are avoided, similar (and high) ionization efficiencies can be achieved for all the elements.

Still, a stepwise approach as employed above can introduce significant errors if the ionization number N is not considered as being a fractional number (especially for N close to 1). Therefore, the most practical way to integrate this result into the formula 4.26 is to express N as the ratio of two characteristic lengths:

$$N = \frac{L}{\lambda_n} \qquad (7.12)$$

where L = the length of the full atom trajectory into the ion source (formula 7.5);
λ_n = the neutral free path (formula 4.10).

L is determined only by the source geometry and is directly linked to the pumping time ($L = t_{pump} \cdot v_n$). The formula (7.12) presents therefore the advantage of having only one parameter depending on the ion source operation conditions.

Considering that for the cases investigated in this work, N is small (N<5), we will consider in the following the approximation:

$$f \approx f_0 \cdot N = \frac{f_0 \cdot L}{\lambda_n} \qquad (7.13)$$

The figure 7.3.a is showing the range of application of this approximation. When needed, the formula (7.11) will have to be employed or even the algorithm from the figure 7.2.

A side effect of this model correction is that the observed temperature invariance of the global f factor (figure 5.16) is no longer evident (considering that λ_n is not temperature invariant). But this can still be explained, considering that the f_0 term is also expected to vary on the temperature:

- f_0 is expected to directly depend on the Debye length, $f_0=\text{const}\cdot\lambda_D$; at the increase of the temperature, λ_D will decrease, but the resulting effect on the f_0 factor cannot be quantified using the present data. In any case, f_0 cannot profit of the increase of the λ_D above the source dimensions (in the best case, it will increase asymptotically towards 1).
- At the increase of the temperature, λ_n will decrease (due to the increase of the primary electron density).

Therefore, the ratio (f_0/λ_n) can still be observed as temperature invariant, considering the present uncertainties (model and measurement).

We can now explain the results from figure 5.16, where we saw a difference between the global f factors of Argon and Xenon, all along the temperature variation range:

a) *Confirmation of the element dependence of the f factor ($f_{Xe} / f_{Ar} > 1$)*

From the figure 5.16, we take the average values for the interval [1500; 2000]°C:

$$f_{Ar} \approx 0.25; \qquad f_{Xe} \approx 0.45 \tag{7.14}$$
$$\Rightarrow f_{Xe} / f_{Ar} \approx 1.8$$

From the equation (7.13) we can see that

$$\frac{f_{Ar}}{f_{Xe}} = \frac{\lambda_{Xe}}{\lambda_{Ar}} \tag{7.15}$$

From equation (4.10), we have (independent on temperature):

$$\frac{\lambda_{Ar}}{\lambda_{Xe}} = 2.64 \tag{7.16}$$

This model correction is indeed predicting that the heavier elements will have a higher f value (like it was observed experimentally), but for the more precise estimation of the f_0 factor, we will have to apply the correction for the ion extraction, using the formula (7.11).

b) *Calculation of the one-ionization factor, f_0.*

We will consider the case of Argon and Xenon at 1900°C.

- From the experimental measurements (fig 5.16), we have $f_{Ar} \approx 0.35$ and $f_{Xe} \approx 0.50$.
- We calculate the ionization lengths for the two elements using the formula (4.10):

$$\lambda_{Ar} = 861 \text{ cm} \tag{7.17}$$
$$\lambda_{Xe} = 326 \text{ cm}$$

- We calculate the ionization numbers for the two elements, N_{Ar} and N_{Xe}:

$$L = N_{pump} \cdot l_{avg} \;\Rightarrow\; L = 550 \cdot 1.5 = 825cm \tag{7.18}$$

where N_{pump} = the average number of atom-wall collisions before pumping (7.6);
l_{avg} = the average dimension of the plasma chamber.

Therefore we have:

$$N_{Ar} = L / \lambda_{Ar} = 825 / 861 = 0.96 \tag{7.19}$$
$$N_{Xe} = L / \lambda_{Xe} = 825 / 326 = 2.53$$

- We obtain the value of f_0 as the parameter of the curve given by the equation (7.11), that can fit (like in figure 7.3.b) our particular set of parameters (f_{Ar}, f_{Xe}, N_{Ar} and N_{Xe}):

In the current case, we have $f_0 \approx 0.36$.

This factor represents the probability for an ion (of any element!) to be extracted after one ionization, when the source is operating at 1900°C. For the present case, the Argon ionization occurs in average after $\lambda_{Ar}/l_{avg} \approx 861/1.5 = 574$ wall collisions of the neutral atom, and the Xenon ionization after $\lambda_{Xe}/l_{avg} \approx 326/1.5 = 217$ wall collisions.

The direct application of this method (employing fractional N numbers) for $N \ll 1$ is not giving accurate results for the f_0, as neither the ionization nor the gas pumping are not linear phenomena. In the present work, this is not a problem, as we are mainly interested in the high temperature range where N becomes superior to 1. Otherwise, one will have to consider:

- a more accurate distribution of ionization probability for flight paths smaller than the ionization lengths;
- a more accurate time evolution of the number of particles pumped (or not pumped) from the ion source.

7.2. Analysis of the limiting phenomena.

The developed ionization efficiency model assumes that no saturation or concurrent phenomena occurs during the transport of the charged particles from the place where they are generated (cathode surface for the primary electrons and ion source volume for the ions) to the place where they are useful to the ion source operation (ion source volume for the primary electrons and the extracted beam for the ions). The appearance of any such phenomena would lower the densities of the affected populations, compared to the estimated values. We will detail in this section all the limiting phenomena that can occur for FEBIAD sources, depending on the operation parameters.

For the primary electrons, the main limiting phenomena that can occur is the space charge limitation at the passage through the accelerating grid.

For the generated ions, the possible limitations can be generated by:

- the charge exchange to the neutral atoms in the source volume;
- the minimum extraction time;
- the maximum ion density into the ion source volume;
- the maximum ionization rate for a given density of the primary electrons;
- the space charge limitation at the extraction puller;
- the space-charge limitation at the outlet plate.

7.2.1. **The charge exchange from 1+ ions to the neutral atoms.**

The charge exchange rate can be calculated using the same type of formula as for the direct ionization (4.13):

$$R_{ch-exc} = n_{1+} \cdot n_n \cdot \sigma_{ch-exc} \cdot v_{rel} \qquad (7.20)$$

where $$\sigma_{ch-exc} = 1.43 \cdot 10^{-12} \cdot Z_q^{1.17} \cdot E_i^{-2.76} \qquad (7.21)$$

Considering that n_q and v_{rel} (between the ions and the neutral atoms) are not directly available and would consequently introduce considerable errors, $R_{ch\text{-}exc}$ can also be expressed as:

$$R_{ch-exc} = R_{ioniz} \cdot p_{\text{int}\,eract} \qquad (7.22)$$

The interaction probability between a 1+ ion and the background neutral atoms, $p_{interact}$, is given by:

$$p_{\text{int}\,eract} = 1 - \exp\left(-n_n \cdot \sigma_{ch-exc} \cdot l_{\text{int}\,eract}\right) \qquad (7.23)$$

This interaction probability is referring to their full lifetime, characterized here by their full trajectory length, $l_{interact}$.

Consequently, the percentage ion loss through change exchange will only depend on the composition and pressure of the background gas (for a fixed ion source geometry):

$$\frac{R_{ch-exc}}{R_{ioniz}} = 1 - \exp\left(-n_n \cdot \sigma_{ch-exc} \cdot l_{\text{int}\,eract}\right) \qquad (7.24)$$

The figure 7.4 is showing the evolution of this percentage loss as a function of the background pressure, for three typical background gases:

- **Argon**, which is the most employed buffer gas and therefore having a partial pressure inside the source of a few orders of magnitude higher than the radioactive products.

- **Potassium**, a contaminant present in FEBIAD sources at the intermediate temperatures, between 1500 and 1800°C (as below ~1500°C it is not volatile and ionized, and above ~1800°C will be completely vaporized and purged from the system);
- **Carbon monoxide**, which is produced in the FEBIAD ion sources especially towards the high temperatures (>1800°C) due to the release of the oxygen from the Tantalum oxide layers on the cathode surface;

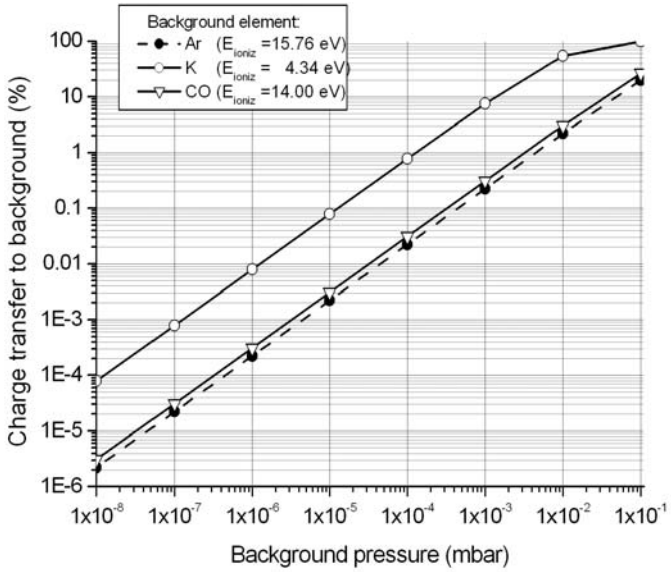

Figure 7.4. Influence of the charge exchange on the useful ionization in a FEBIAD

It can be seen that the strongest effect is given by a background gas having a low ionization potential (Potassium, in this analysis) but, even like this, it would only affect the ionization of another gas by less than 10% for partial pressures below 10^{-3} mbar (the case for the present use of FEBIAD ion sources). The situation is even less restrictive for the most important contaminant, CO, which would reach a 10% ionization influence through charge exchange only at a partial pressure of $\sim 5 \cdot 10^{2}$ mbar, much above the values possible to occur in practice (as a parenthesis, at this pressure the direct ionization of CO would generate a current of about 50mA, which is far above the ion currents of ISOLDE FEBIADS).

This low influence of charge exchange is a particularity of small arc discharge ion sources without ion trapping, where $l_{interact}$ is very small. As an example, for an ion source with trapping properties, the probability of charge exchange is increasing linearly with the number of ion oscillations in the plasma (compared to the graphs in figure 7.4).

Considering that the background pressures in the FEBIAD sources are generated by the material evaporation, the charge exchange limitation would only occur towards the high temperatures; therefore, a limitation occurring all along the temperature domain (like in figure 5.19) cannot be generated by charge exchange.

More than that, a particularity linked to the 1+ ion sources is that there is no external effect of self charge exchange for any set of operation parameters; for two species entering the ion source, the total resulting currents following direct ionization and charge exchange will be:

$$\begin{cases} I_1 = I_{1\_direct} - I_{12} + I_{21} \\ I_2 = I_{2\_direct} - I_{21} + I_{12} \end{cases} \tag{7.25}$$

where I_{1_direct}, I_{2_direct} = the ion currents produced through direct ionization (electron impact) for the species 1, respectively 2;
I_{12}, I_{21} = the ion currents produced through charge-exchange from species 1 to 2 and, respectively, 2 to 1.

When 1 and 2 refers to the same gas, $I_{12}=I_{21}$ and therefore the extracted Argon current cannot be limited due to the charge-exchange (regardless of the ion source operation conditions), considering that the only parameter in figure 5.19 is its own partial pressure.

7.2.2. **The minimum extraction time.**

For an efficient ion source operation, the relation between the important time parameters of the source has to be the following:

$$t_{extr} < t_{ioniz} < t_{pump} \tag{7.26}$$

If the ionization time is not sufficiently short compared to the pumping time, the ionization efficiency will be limited due to effusion losses from the ion source volume.

If the extraction time of the ion from the source volume is not sufficiently short compared to the ionization time, the continuous generation of new ions can lead to the accumulation of the positive space charge in the center of the ion source, which will repel more of the created ions towards the ion source walls (compared to the estimation of the presented model).

We will investigate in this section the evolution of these specific times, for identifying if any limitation can appear over the range of variation of the FEBIAD parameters. The extracted current can be further limited by the extraction time through the limitation of the maximum ion density in the FEBIAD sources; this aspect will be presented in the next section (7.2.4).

The ionization time was already introduced through the formula (7.2) and the pumping time through the formula (7.4).

We will deduce here the expression for the ion extraction time. For the electrical fields acting on the ion we will make the assumptions presented in figure 7.5: 150V for the anode cylinder, 0V for the outlet plate (which is grounded) and U_i = 130V for the volume potential where the ion is being extracted from (based on the measurements from chapter 6). The distance d will be proportional with the Debye length (formula 4.11); we will consider here a factor of proportionality of 1 (in reality, it can be of up to ~3.5 – see section 4.2.1). Of course, d cannot follow the increase of λ_D to a value higher than the source length (22mm).

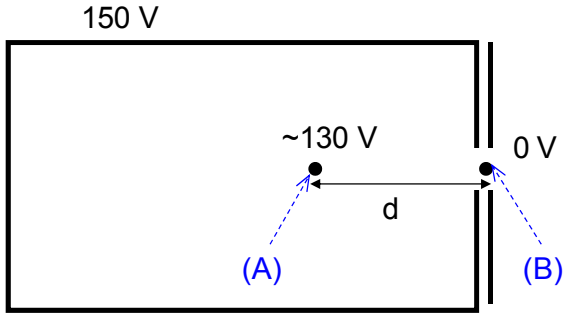

Figure 7.5. Assumptions used for the calculation of the extraction time

The generated ion will have an accelerated motion between the points A and B, therefore:

$$t_{extr} = \frac{v_B}{a_i} \tag{7.27}$$

The final ion velocity (when the ion leaves the ion source volume in point B) is given by the acceleration in the electrical potential:

$$E_{ion} = q \cdot U_i = \frac{M_i \cdot v_B^2}{2} \tag{7.28}$$

$$\Rightarrow v_B = \sqrt{\frac{2QU_i}{M}} \tag{7.29}$$

Assuming a constant acceleration, a_i is given by:

$$a_i = \frac{q \cdot \frac{U_i}{d}}{M_i} \tag{7.30}$$

Therefore, the ion extraction time will be:

$$t_{extr} = d\sqrt{\frac{2M_i}{qU_i}} \tag{7.31}$$

As the main parameter for all the specific times from the relation (7.26) is the operation temperature, we present in figure 7.6 their evolution as a function of ion source temperature.

The specific times (pumping, ionization, extraction) are computed according to the formulas (7.4), (7.2) and (7.31), respectively. In the formula (7.31), d was considered to be equal to the Debye length. Considering that in reality $d \leq \sim 3.5\lambda_D$ (as was detailed in section 4.2.1), the real extraction time can also be up to ~3.5 times higher than the calculated value.

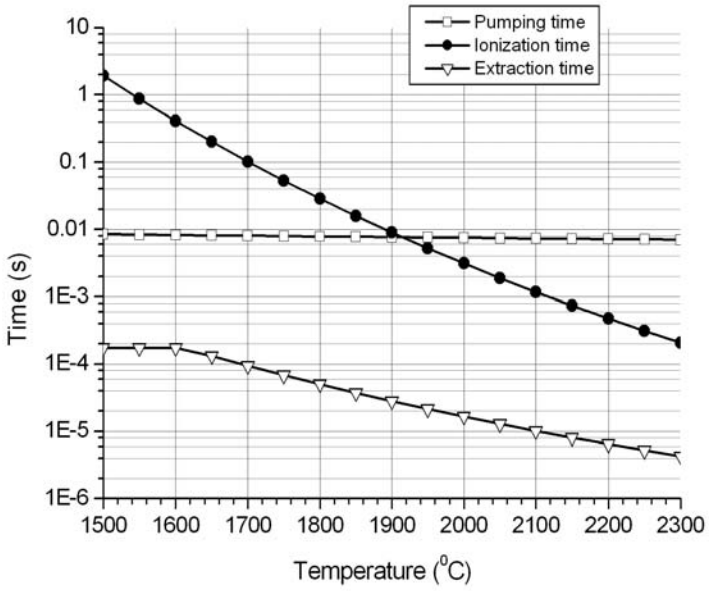

Figure 7.6. Temperature evolution of the FEBIAD specific times (ionization, extraction, pumping).

We can see that the relation 7.26 is fulfilled above 1900°C. Below this temperature, the main limitation acting on the ionization efficiency is the long ionization time compared to the pumping time. Above this temperature, most of the atoms reaching the ion source volume will be ionized at least once, but still for an efficient operation, the active extraction volume (and the corresponding f_0 factor) will have to be made as high as possible. A quality factor describing the ion source ionization performance can be therefore defined as:

$$Q_{ioniz} = f_0 \cdot \frac{t_{ioniz}}{t_{pump}} \qquad (7.32)$$

$$Q_{ioniz} < 1$$

The f_0 factor will only lose its importance for the ionization efficiency when the ionization time will be much smaller compared to the pumping time (which is not the case for FEBIAD sources, as can be seen in figure 7.6).

Towards the high temperatures, the difference between the ionization time and the extraction time is continuously decreasing; therefore a limitation due to the accumulated space charge will appear, at a temperature depending on the trap capacity of the ion source (investigated in the next section, 7.2.3).

7.2.3. **The maximum ion and electron densities into the ion source volume.**

As the FEBIAD sources are not having a magnetic or electrical field configuration that can trap the generated ions, the only mechanism controlling the ion losses is the electrical field distribution generated by the primary electron beam…

The qualitative description of the resulting electrical field distribution inside a FEBIAD ion source is presented in figure 7.7. A more accurate field distribution (obtained through CPO simulations) will be presented in section 8.2.2.

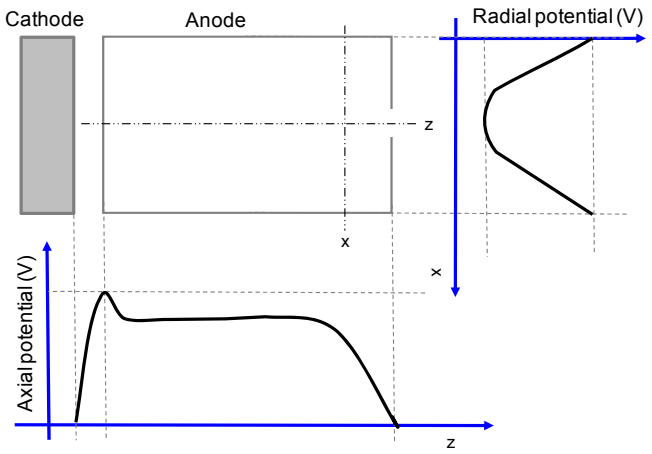

Figure 7.7. Electrical field distribution in FEBIAD ion sources (qualitative)

Beam energy measurements (presented in chapter 6) have shown that the potential in the ion source volume ("plasma potential") is below the Anode potential, therefore inside a FEBIAD there is an excess of electrons. The produced ions will be trapped in this radial potential well and the amount of total positive charge in the ion source volume will be limited by the density of primary electrons. The ions produced in excess (when the pressure exceeds a certain limit) will be lost on the ion source walls. As this excess of electrons is produced by the cathode emission, the electron density (and consequently the "trap capacity" of the ion source) will be temperature dependent. The resulting ion density limitation is presented in figure 7.8.

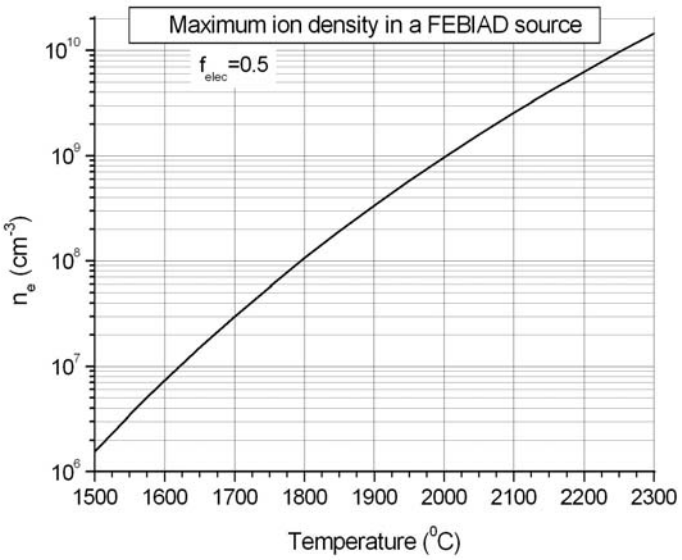

Figure 7.8. Temperature dependence of the maximum ion density sustained by the primary electron beam.

The radial potential gap can be estimated through an electrostatic approach. This way, the measured beam energies presented in chapter 6 can be linked to the electron density in excess inside the ion source.

Considering the assumptions presented in figure 7.9, we write the Gauss Law for the marked volume:

$$\Phi_{E,S} = \frac{Q_V}{\varepsilon_0} \tag{7.33}$$

$\Phi_{E,S}$ = electric flux through the surface S

Q_V = the electrical (surplus) charge in the volume V, closed by surface S

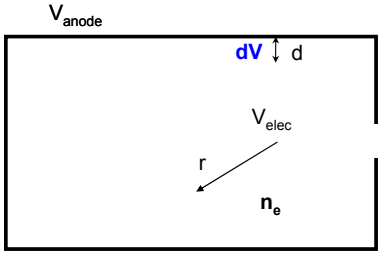

Figure 7.9. Assumptions used for the calculation of the trap capacity.

Considering V a sphere and E uniform over S:

$$\Phi_{E,S} = \oint_S E dS \overset{E=ct}{\equiv} E \cdot S = \frac{V_{elec}}{d} \cdot S \tag{7.34}$$

Therefore:

$$\frac{V_{elec} \cdot S}{d} = \frac{n_e \cdot V_{olume} \cdot e}{\varepsilon_0} \tag{7.35}$$

And the potential drop can be expressed as depending of the electron density:

$$V_{elec} = \frac{n_e \cdot e \cdot r \cdot d}{3\varepsilon_0} \tag{7.36}$$

We make the assumption

$$d \equiv 0.1 \cdot r = 0.5mm \tag{7.37}$$

For T=2000°C we have $n_e \approx 2 \cdot 10^9$ cm^{-3} and therefore we obtain V_{elec} = -30V, which is compatible with the experimental values presented in chapter 6: the measured internal potential ranges from 110V to 140V for anode potentials of 150V (therefore V_{elec} varies from -40V to -10V, respectively).

It is now possible to express the FEBIAD plasma potential (with respect to the anode, which constitutes the ion source walls) as a function of the excess electron density (figure 7.10).

It can now be seen that if the excess of electron density is increasing above a threshold value (which we will note in the following with n_{e_max}), the plasma potential will become negative with respect to the ground too (not only with respect to the source walls). As the central part of the outlet plate is grounded, in this case the produced ions will be at a negative potential with respect to the extraction and therefore the ion extraction will be strongly reduced. In addition, a decreasing plasma potential will progressively slow the primary ions and consequently reducing the ionization rate; for a plasma potential equal to the cathode potential (a few volts), the primary electrons will be fully decelerated in the source volume.

For example, for the standard value for the anode potential (150V), this limitation can occur above 2100°C; the temperature (and electron density) can be further increased if the anode potential is increased to a higher value (at 300V, the temperature can be increased up to ~2250°C without reaching the limitation) or if the operation pressure is increased for compensating the negative space charge.

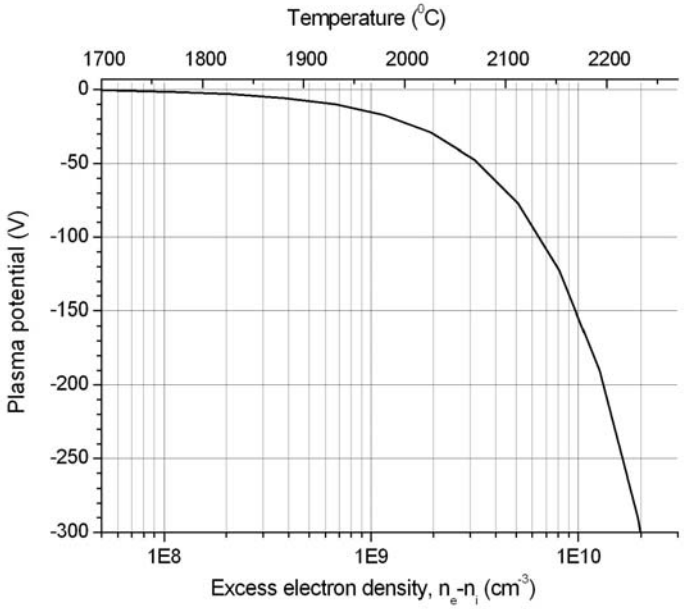

Figure 7.10. Dependence of the plasma potential (with respect to the plasma chamber) on the non-compensated electron density, as predicted by formula (7.36). The temperature scale is only estimative, valid only for $n_i << n_e$.

The maximum electron density not compensated by ions will therefore depend linearly on the anode potential. For the dimension assumption (7.37), the dependence is shown in figure 7.11.

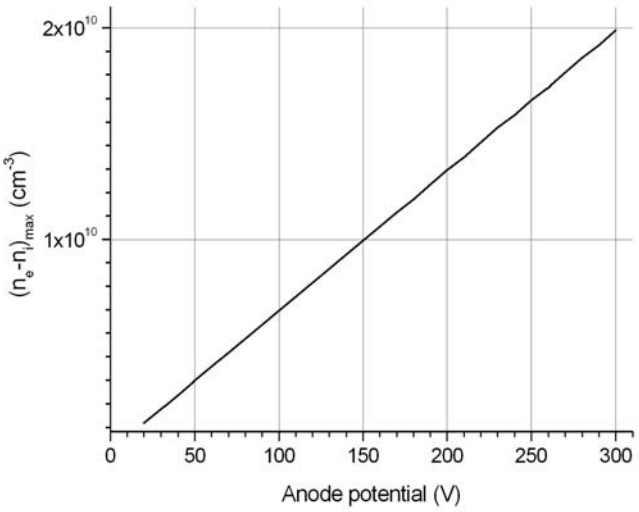

Figure 7.11.The maximum uncompensated electron density in a FEBIAD source.

For the standard value of the anode potential (150V), the maximum non-compensated electron density is ~10^{10} cm^{-3} and can be reached at temperatures above ~2150°C (increasing proportionally with the operation pressure). We can therefore express the required ion densities for allowing the ion source operation at higher temperatures (equivalent with higher plasma densities).

The figure 7.12 is putting together the listed limitations acting on the ion density:

- for electron densities smaller than n_{e_max}, the ion density can have any value inferior to the electron density, $n_i \leq n_e$ (depending on the operation pressure);
- for electron densities above n_{e_max}, the ion density will have to fulfill the relation:

$$n_e \geq n_i \geq n_e - n_{e\_\max} \quad (7.38)$$

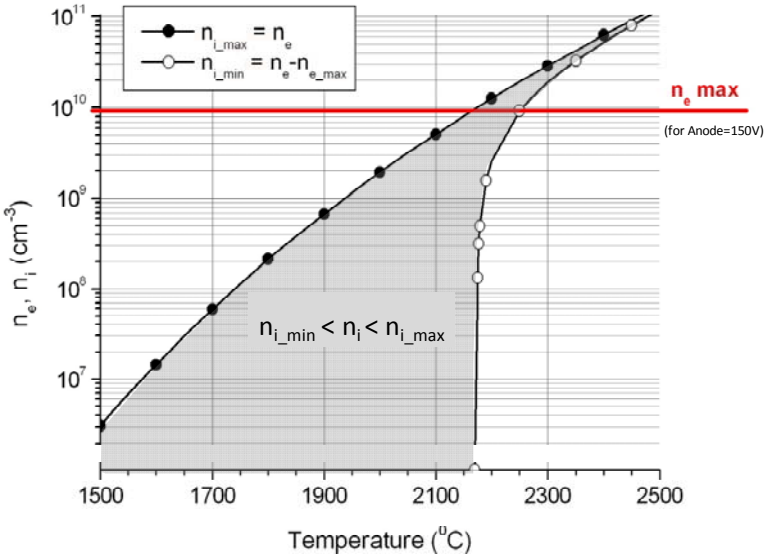

Figure 7.12. The variation range of the ion density inside a FEBIAD source.

It can be seen that the FEBIAD sources can operate without support gas for temperatures below ~2150°C (when $n_{i\_min}=0$), while above this value both the ionization and the ion extraction

will be strongly reduced if the operation pressure is not increased sufficiently for producing at least n_{i_min} ions. A consequence of this is that at high temperatures, the electron and ion densities will have very close values.

It is important to note that the ion source can still operate at higher pressures than the pressure required for producing an ion density $n_i=n_{i\_max}$ (the ions produced in excess will be rapidly lost from the plasma), while if the pressure is insufficient for producing the minimum ion density $n_i=n_{i\_min}$, the extracted current will rapidly fall to zero. This makes the ion source tuning easier for the high temperatures, as the variation range of the operation pressure will not be as narrow as the one of the ion density.

In conclusion, in a FEBIAD ion source the maximum ion density is limited by the electron beam density and the maximum excess of electron density (with respect to the ion density) is limited by the potential of the anodes.

7.2.4. **The ion space charge limitation at the extraction puller.**

According to the Child-Langmuir law [91][92], the maximum current density that can be accelerated by an electrical field is obtained under space-charge limited conditions and follows the relation:

$$j = \frac{4}{9}\varepsilon_0 \cdot \sqrt{\frac{2q}{m_i}} \cdot \frac{U^{3/2}}{d^2} \tag{7.39}$$

where j = the current density;
q = the ion charge;
m_i = the ion mass;
U = the applied voltage;
d = the extraction gap width.

Therefore, the maximum current extracted through a round aperture of radius a can be obtained using the relation:

$$I[\mu A] = 1.71 \cdot 10^{-7} \cdot \sqrt{\frac{Q}{M}} \cdot \left(\frac{a}{d}\right)^2 \cdot U^{3/2}[V] \tag{7.40}$$

where Q is the ion charge state and M is the ion mass in amu.

For the ISOLDE FEBIAD sources, the minimum applied voltage is 30kV, the standard extraction gap is of 60 mm and the standard aperture radius is 0.75mm.

It can be seen that for the standard FEBIAD geometry (a=0.75mm), currents of more than 50μA can be extracted at 30kV (typically, the extraction gap can be reduced down to ~35mm without electrical sparking). But, if going for a smaller aperture (the measurements from section 6.7, requiring a very good mass resolution, have been done employing a source aperture of 0.25mm), the maximum currents can decrease significantly.

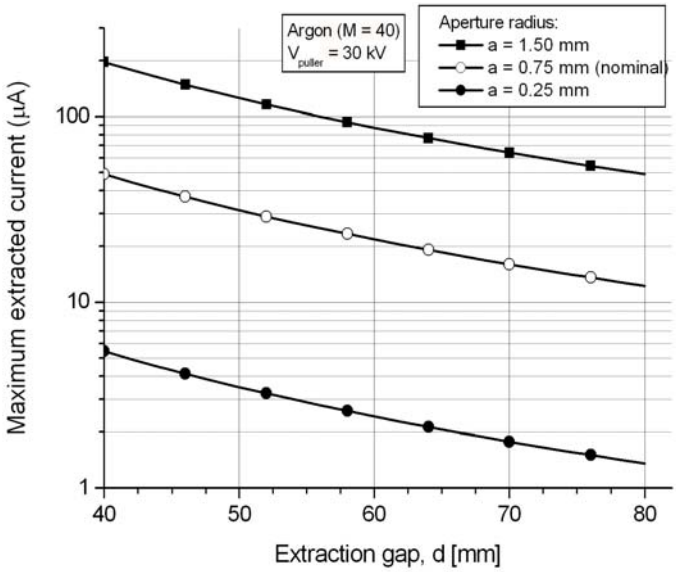

Figure 7.14. The space-charge limited current (theoretical) extracted from a FEBIAD by the puller at 30kV.

7.2.5. **The ion space charge limitation at the plasma boundary.**

The same approach as for the external puller can be applied for the interior side of the outlet plate (see figure 7.5): the extraction of the ions from the ion source plasma may be space charge limited if the extraction gap d (now of the order of the Debye length) is not sufficiently short compared to the potential difference between the plasma and the outlet plate.

The theoretical variation of the space-charge limited current as a function of the extraction gap and of the outlet plate radius is presented in figure 7.15. The plasma potential is considered to be 130V.

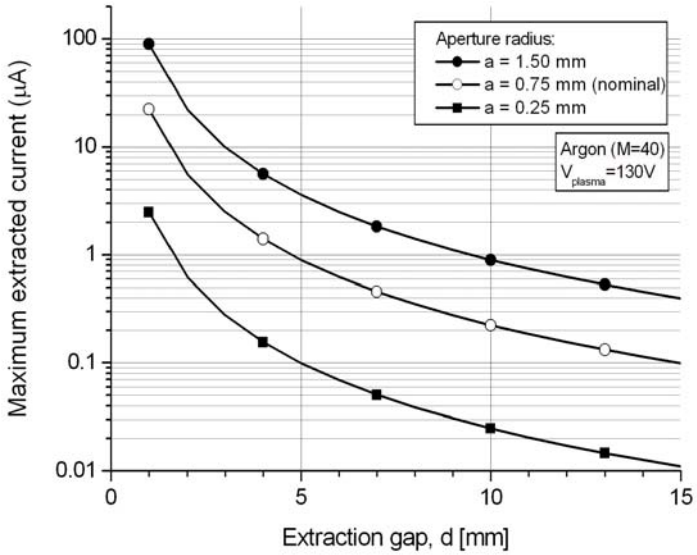

Figure 7.15. The space-charge limited current (theoretical) extracted from a FEBIAD plasma at a potential of 130V.

This type of limitation can justify the experimentally observed limitation of the maximum extracted current, all along the temperature range (figure 5.19), as the extraction gap is temperature dependent (decreasing towards the high temperatures, the same as the Debye length). Figure 7.15 is showing the best fit of the experimental data using the formula (7.40), where U=130V and $d_{effective}=(1/2.8)*\lambda_D$ (considering that not all the ions are having the same d).

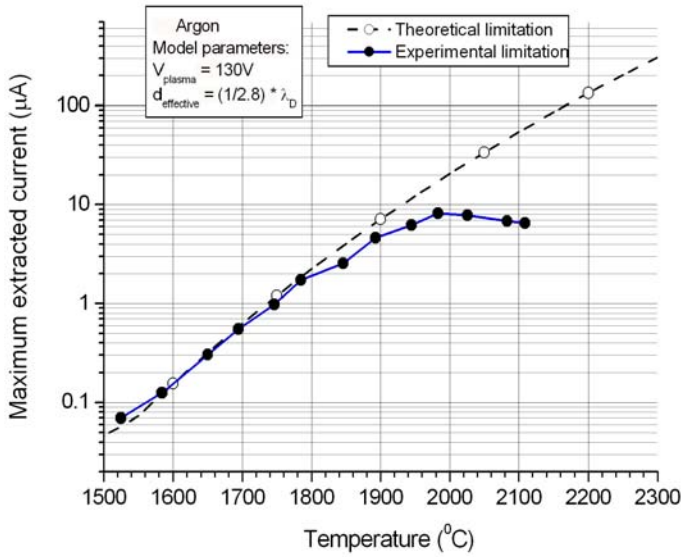

Figure 7.16. Theoretical justification of the experimentally observed limitation (figure 5.19) of the extracted current.

Therefore, the space charge limitation at the plasma boundary is an issue for FEBIAD sources when higher currents (compared to the theoretical curve in figure 7.16) are to be extracted. This limitation can be surpassed if the source can be efficiently operated at sufficiently high temperatures or if the extraction system is modified for producing a higher ΔV between the plasma and the outlet plate (either by increasing the anode potential and keeping the outlet plate grounded, either by keeping the same values for the anode potential and putting the outlet plate at a negative potential).

It has to be also considered that the higher will be the excess of electron density, the smaller will be the plasma potential (see figure 7.10) and consequently the space-charge limited current. This is therefore adding an additional condition on the minimum ion density (even for electron densities below n_{e_max}), depending on the required extracted current from the source.

When the source is reaching the space-charge limited mode, the ion density inside the source will increase towards its saturation value, n_{i_max} (see figure 7.12), thus increasing the plasma potential and the space-charge limited current. When $n_i = n_{i\_max}$, the plasma potential will be equal to the anode potential.

7.2.6. **The electron space charge limitation at the accelerating grid.**

The accelerating grid placed in front of the cathode is a component specific to the design of FEBIAD sources. It was introduced by Kirchner and Roeckl [47] for allowing the source operation at low pressures, where the thermal cathode emission can be space charge limited due to an insufficient compensating ion density.

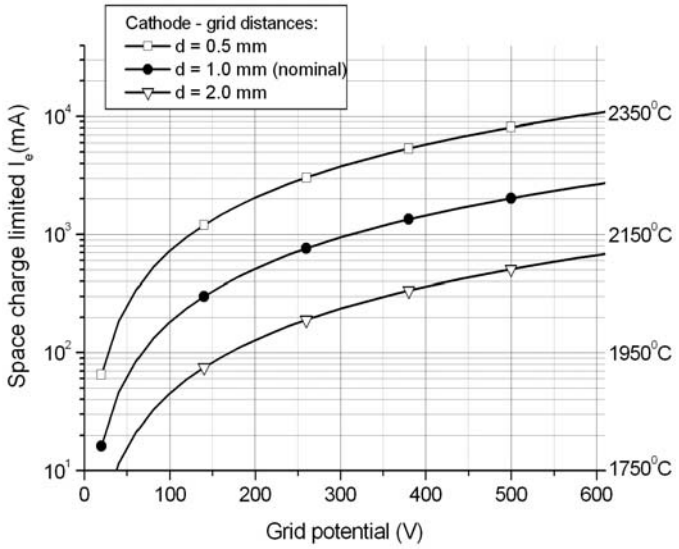

Figure 7.17. The space-charge limited cathode at the accelerating grid (theoretical). The real values will be higher due to compensating ion density and cathode/grid deformation at high temperature. On the right axis, the cathode temperatures corresponding to the emitted electron currents.

Even so, the presence of the grid is not solving all the space charge limitations, without a careful dimensioning. The figure 7.17 is showing the evolution of the maximum electron current drawn by the grid from the cathode, for different values of the accelerating potential and of the cathode-grid distances (according to the same formula 7.40, where M is now equal to m_e/1amu). On the right axis, there are indicated the temperature values where the corresponding electron currents are reached for a Tantalum cathode (standard at ISOLDE).

It can be seen that for the standard cathode-grid distance (1 mm), if the anode is operated at 150V, the electron current is becoming space-charge limited at ~2025°C if no ions are compensating for the negative electron space charge. This will not be the case in reality, as at high temperatures there is always an increasing background pressure, even if no buffer gas is injected. But still, there is not a large tolerance with respect to this possible limitation, therefore if one wants to significantly increase the electron currents (either by reaching temperatures higher than 2200°C, either by using a cathode in a different material that can emit more electrons at a lower temperature), the following options are available:

- Increasing the grid potential to a higher value (at the expense of decreasing the ionization cross section and of complicating the source design);
- Decreasing the cathode-grid distance (at the expense of risking an electrical shortcut between the two components, as both of them will deform at high temperature);
- Increasing the operation pressure for compensating the negative space-charge between the cathode and the grid (with the risk of reaching in the process another limitation).

CHAPTER 8

FEBIAD PROTOTYPES BASED ON THE DEVELOPED ION SOURCE MODEL

The detailed investigations presented in the preceding chapters are allowing the optimization of the FEBIAD performances through the elimination of the observed limitations. The exhaustive list of the source customizations enabled by the current comprehension will be presented in chapter 9 and represents the basis of the VADIS concept of optimizing the source design for specific requirements. In this chapter are presented the first two examples of performance improvement, already implemented at ISOLDE.

Two ion source prototypes have been constructed and tested:

a) The first one eliminated the observed difference in ionization efficiency between the MK5 and MK7 sources (figure 5.15), thus confirming the proposed physical justification of this difference (details in 8.1.1) and increasing the noble gas ionization efficiencies for all the ISOLDE experiments;

b) The second one (details in 8.2) modified the observed limitation of the ionization efficiency at high temperatures (see section 7.1.1.c), by increasing the temperature where the ionization efficiency saturates and therefore reaching higher efficiencies for all the elements produced at ISOLDE.

This latter design constitutes the basis of the VD ion source series, which replaced the MK series starting from 2009 (VD5 instead of MK5 and VD7 instead of MK7; the VD3 design optimization is not included in the present thesis).

8.1. Optimization of the ion source extraction. Improvement of the FEBIAD ionization efficiency for the noble gases.

8.1.1. **Motivation.**

By comparing the performances of the different source subtypes, for the same set of operation parameters (temperature, pressure, gas composition, anode potential, magnetic field), it has been observed that the ionization efficiency of the MK7 source is systematically lower (by up to a factor 3), compared to the MK5 source. The measurements done for Argon have already been presented in chapter 5 (figure 5.15); the same type of dependence was obtained for the other noble gases (Xenon results presented in figure 8.1), for all the employed sets of operation parameters (I_magnet from 0A to 6A, Anode from 50V to 300V, pressure from 10^{-7} mbar to 10^{-4} mbar) and for all the ion source units investigated during this project.

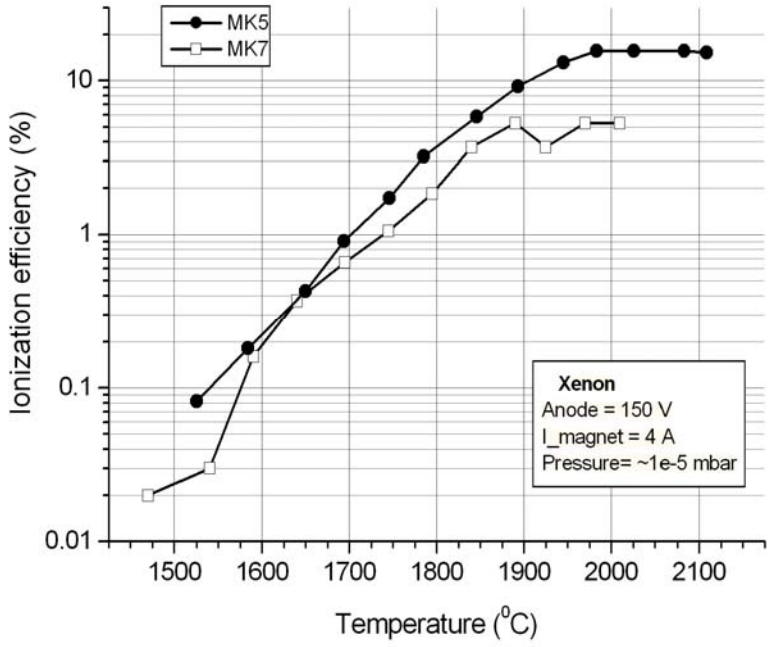

Figure 8.1. Difference between the ionization efficiencies of the MK5 and MK7 subtypes

This behavior was previously observed [90], but the origin was not clear until now. Several hypotheses have been advanced, but none of them could be confirmed:

- Difference due to the (presumable) difference in pressure (and impurity composition) inside the two source subtypes: as the MK7 source is coupled to the target through a water-cooled transfer line, all the condensable elements are not reaching the ion source volume, opposite to the MK5 source, presenting a hot transfer line allowing most of the radioactive products to reach the ion source;
- Difference in the neutral gas flow through the target-source unit: the injection positions of both the buffer gas and radioactive products into the source volume are different for the two source subtypes (see figures 5.2 and 5.3). Additionally, the gas conductance of the connection between the target and the source are different for the two sources (due to the different geometry and volume of the transfer line)

- Difference in the temperature distribution inside the unit, due to the water cooling of the transfer line.

The consequence of this difference was that the production of exotic noble gases was not able to profit of the best FEBIAD ionization efficiencies available at ISOLDE, as only the MK7 type can be used for this application, for the elimination of the condensable contaminants (an important requirement for the ISOL beams).

Also, when not fully understood, this kind of difference is one of the most important obstacles towards the implementation of the source design to other facilities, or even for updating or developing other components of the target-ion source unit (due to its compactness).

8.1.2. **Original approach.**

Useful information has been put together during the present work. The ionization efficiency was found to be **independent** (or presenting a very small dependence) on the following factors:

- The operation pressure and composition (at least around the nominal parameter values – see sections 5.5 and 5.6);
- The target temperature and material;
- The effusion volume coupled to the ion source (several units were tested with and without target material filling the target cylinder);
- The position of the buffer gas injection (non-standard injection has been tested for the MK7 type during the study of the merging of several transfer lines into the ion source [93].

This information eliminated the hypotheses presented in section 8.1.1, proving that the difference between the MK5 and MK7 types is not originating in the flow of the neutral gas through the target-ion source unit.

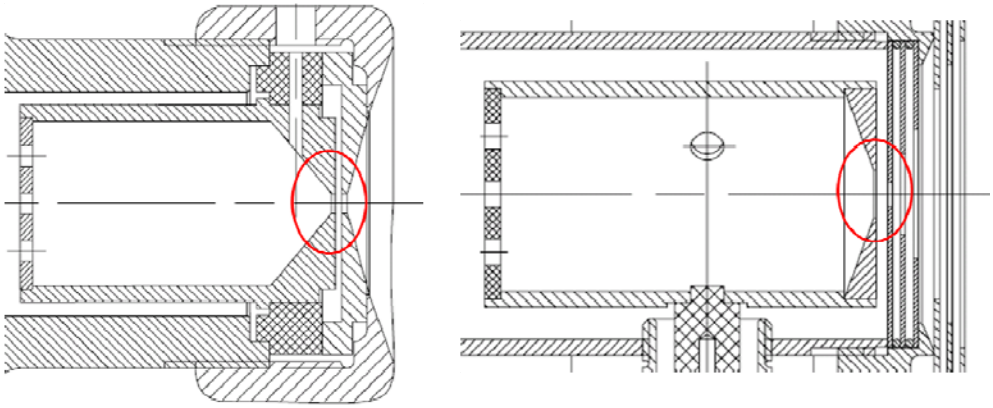

Figure 8.2. Difference in the extraction geometry between the MK7 **(left)** and MK5 **(right)** subtypes.

Therefore, by taking a closer look at the dynamics of the charged particles inside the source, a new hypothesis has been advanced to justify the difference in efficiency: the small difference in the extraction geometry between MK5 and MK7 (figure 8.2) can lead to significantly different electrical field penetration inside the source volume and consequently to different f factors (see figure 5.17). Namely, the bigger outlet hole diameter of the MK5 anode (polarized typically at 150V) allows the penetration of the low potential lines (the thermal screens facing the anode are

at the ground potential) inside the source volume, compared to the MK7 where both the anode and the thermal screens are having the same diameter (while the electrical polarization is the same as for MK5).

This idea is primarily justified by the fact that the FEBIAD sources are having a low density plasma (from ~10^6 cm^{-3} at 1500°C up to 10^{10} cm^{-3} at 2200°C, figure 7.12), insufficient for shielding the externally applied electrical fields due to the small dimensions, comparable to the plasma Debye length (ranging from 10 cm at 1400°C down to 1 mm at 2200°C, figure 4.4). Additionally, the source behavior was observed to fit the same model for the temperature domain between 1400°C and 2000°C.

A possible disturbing factor for this approach could have been the influence of the main extraction potential on the internal electrical field distribution. The puller is typically polarized at 60 kV and positioned at 60 mm from the thermal screens of the source. The effect of the extraction voltage, V_{extr}, and of the puller position, d_{extr}, was investigated both for the plasma potential (see section 6.1) and for the ionization efficiency of the noble gases (for all the subtypes) and no significant influence has been observed for a wide variation range ($d_{extr} \in [3.5; 8]$ cm and $V_{extr} \in [15;30]$ kV). This is due to the small aperture diameter (1.5 mm) of the thermal screens mounted at the source extraction. Therefore, the extraction field generated by the puller is not sufficient for extracting the ions from the source volume, but only to guide those reaching the extraction aperture due to the internal field distribution.

The influence of the extraction geometry on the internal electrical field was investigated using the CPO simulation program (introduced in section 3.3.2).

In a first step, the distribution of the internal electrical field was investigated for the case where the space charge of the ions and electrons is negligible compared to the electrical field generated by the source electrodes.

The figure 8.3 presents the employed MK7 geometry (axially symmetric), with the resulting potential lines around the extraction aperture for the case when the anode cylinder is polarized at 150V (the thermal screens being always at the ground potential).

Considering that the average energy of the ions is 0.17eV at 2000°C (the thermal energy), any ion generated at a position where the volume potential is below 149.8V will not have enough energy to reach the anode walls (at 150V) and will be accelerated towards the source extraction. Therefore the active volume of the source is comprised between the potential surfaces at 0V (surface touching the thermal screens) and at 149.8V; in figure 8.3, the potential lines are drawn from 145V to 149.9V, with a step of 0.1V. Considering the position details given on the right side of the same figure, we can estimate the active volume to be ~0.036 cm^3, which gives an f factor of 0.014.

The figure 8.4 presents the electrical field distribution obtained for the MK5 source. For this case, we obtain an active volume of ~0.56 cm^3 and an f factor of 0.22.

Consequently, this first approximation would predict a difference between the ionization efficiencies of the two subtypes of up to 15 times (as the ratio of the two f factors, 0.22 and 0.014)! This is not the case, as both the simulated f factors are underestimated (compared to the experimental values from figure 5.17); therefore, we will have to also consider the space charge of the generated ions and electrons. As a general qualitative behavior (see figure 8.5), it is expected that the surfaces limiting the active volume (having the potential of 149.8V) will penetrate more into the ion source volume (for both source types) in the presence of the charged particles, due to the fact that the FEBIAD plasma is having an excess of electrons.

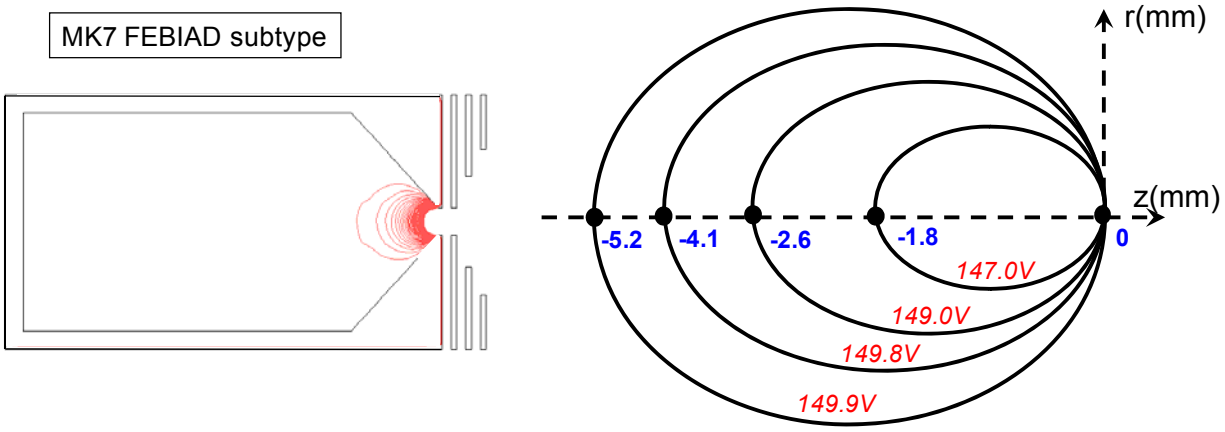

Figure 8.3. Electrical field distribution for the MK7 source, for the case where the charged particle distribution is negligible inside the source. On the left, the equipotential lines are drawn from 145V to 149.9V, with a step of 0.1V. On the right, details are given on the z position of some of the potential lines.

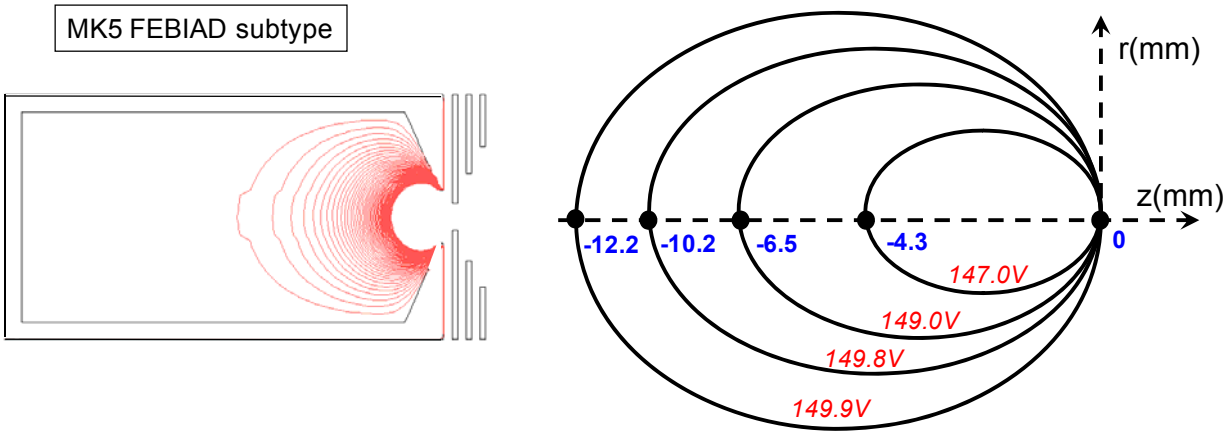

Figure 8.4. Electrical field distribution for the MK5 source, for the case where the charged particle distribution is negligible inside the source. On the left, the equipotential lines are drawn from 145V to 149.9V, with a step of 0.1V. On the right, details are given on the z position of some of the potential lines.

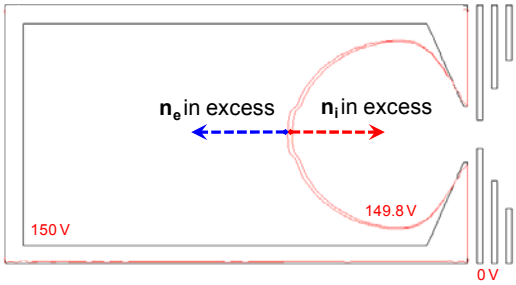

Figure 8.5. Influence of the electron and ion density on the electrical field lines presented in figures 8.1 and 8.2 (qualitative). Considering the FEBIAD ion energies (<0.2eV), the active volume is delimited by the potential line of 149.8 V (for the standard value of the anode potential of 150 V).

More details on the expected evolution of the internal potential distribution in the presence of the space charge of the particles have been obtained employing the same CPO code.

We underline that the code was not developed for accurately simulating the plasma meniscus, but can treat very well the particle trajectories in a superposition of electrical and magnetic

fields, which is sufficient for the FEBIAD sources, considering their low density plasma properties, where the electrical neutrality only appears far from the extraction aperture.

In a first stage, the qualitative influence of the intensity of the primary electron beam on the potential distribution was studied.

For all the tests below, the electrons were launched from the anode side facing the grid (z=0), with the kinetic energy of 150 eV. The anode potential was kept constant at 150 V.

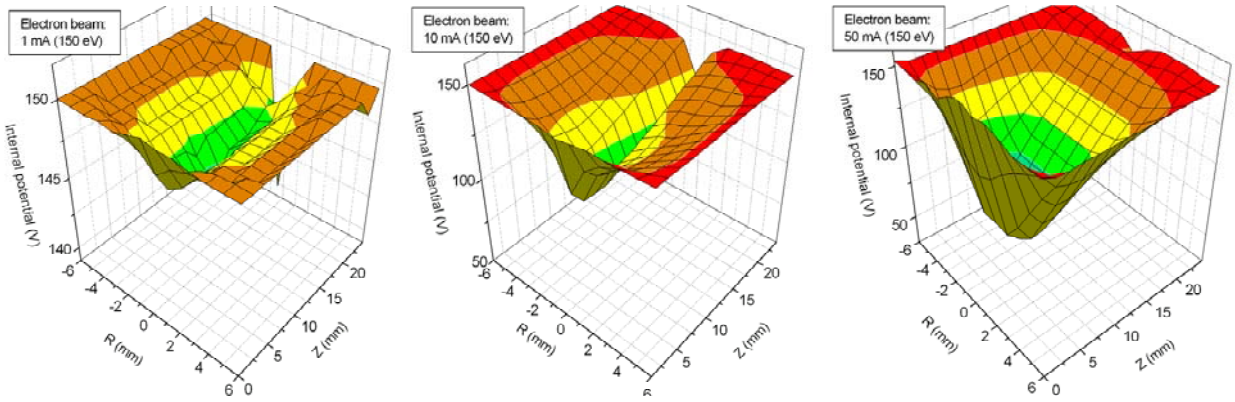

Figure 8.6. The evolution of the potential distribution (MK7) at the increase of the intensity of the primary electron beam: 1mA, 10mA and 50mA, corresponding respectively to 1600, 1750 and 1900 °C.

It can be seen in figure 8.6 that the potential drop in the middle of the plasma chamber is compatible with the values predicted by formula (7.36) (as shown in figure 7.10). The additional information that could not be predicted by that formula is that the region with the lowest potential is not always connected through equipotential lines with the source outlet plate. At the increase of the electron beam intensity, a lower potential region appears in front of the anode grid, while towards the extraction side the potential remains higher, due to the expansion (leading to losses) of the electron beam due to its own space charge.

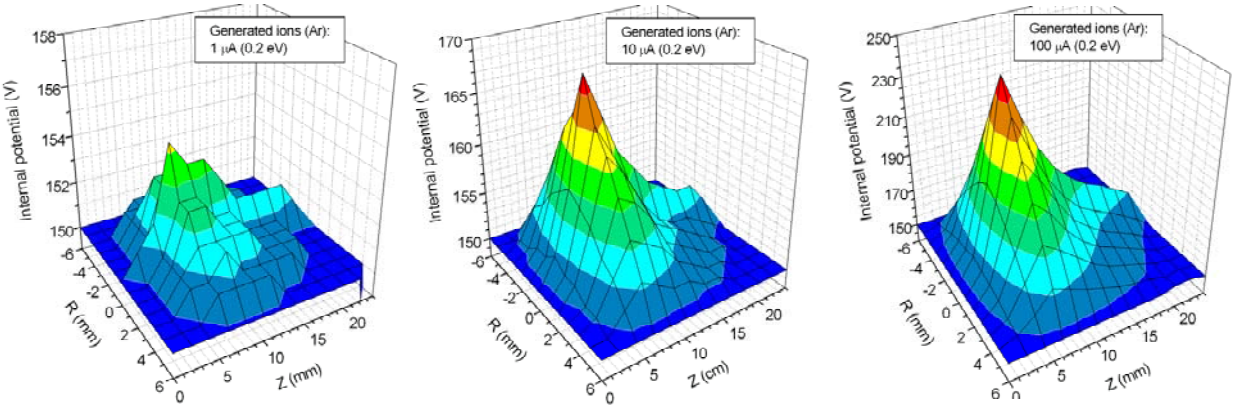

Figure 8.7. The evolution of the potential distribution (MK7) at the increase of the intensity of the generated ions. The electron contribution is neglected.

This potential distribution is characteristic to the source operation when the ion density is negligible compared to the electron density. At the increase of the operation pressure, the ion density will increase and partially compensate the negative space charge of the electrons. The extent of this compensation is presented in figure 8.7. These potential distributions have been

obtained through the superposition of the background potential produced by the anode polarization (figure 8.6) and the potential generated by the space charge of the generated ions; the electrons are neglected. Ion intensities of 1, 10 and 100 μA have been launched at one side of the ion source with the energy of 0.2 eV and let to make only one passage through the source volume. For a source operation with an f factor of 0.1, this corresponds to extracted currents of 0.1, 1 and 10 μA, respectively.

It can be seen that the typical intensities of generated ions (~10 μA) cannot fully compensate the potential well generated by the primary electrons (for >50mA of electron beams, which is the case above 1900°C), therefore the main aspect to concentrate on is the connection of the outlet aperture with a fraction as high as possible of the source volume.

By putting together the electrons and ions in the externally applied fields, the difference between the MK5 and MK7 can be better understood. The figure 8.8 is presenting the distribution of the electrical potential inside the MK7 source, in the presence of electrons (total current of 15mA, generated at an energy of 150 eV) and ions (total current of 2.5 μA, generated at 0.2 eV). The figure 8.9 is presenting the potential distribution for the MK5 source, in the same conditions.

It can be seen that the geometry of the MK5 source helps better to the connection of the central potential with the potential of the outlet aperture. A benefic factor in the present case is that the source length (z axis) is short enough for allowing this connection; otherwise, either the diameter of the anode aperture would had to be bigger, either the space charge expansion of the electron beam would had to be limited (for extending the region of minimum potential towards the source extraction).

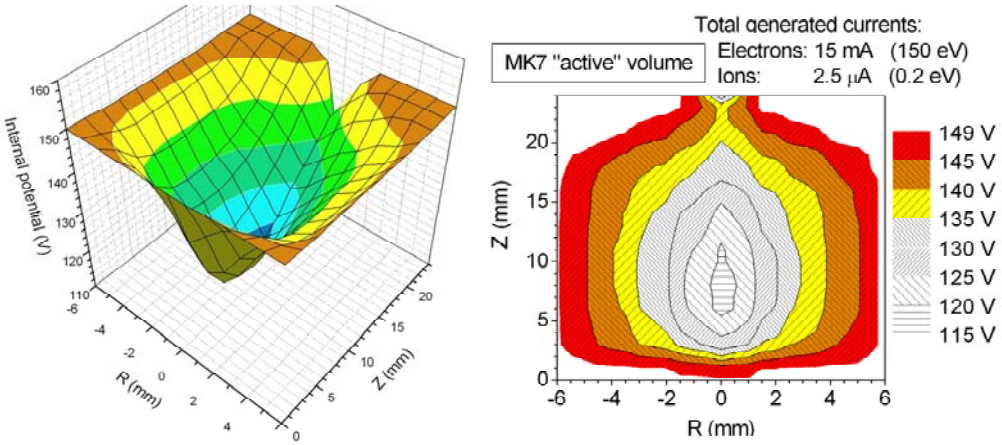

Figure 8.8. Distribution of the electrical potential inside the MK7 source, allowing the estimation of the active volume (see text).

The active volumes of the two sources are delimited by the equipotential surfaces of 149.8V and ~133 V (133V for the MK7 and 131V for the MK5 for the simulations presented in figures 8.8 and 8.9), plus the region just in front of the outlet aperture, where the potential goes down to 0 V but the potential lines are not connected to the central region of the source. We can see that these results are in good agreement with the experimental measurements of the beam energy presented in chapter 6. That also means that the bulk of the extracted ions are originating deeper inside the source (and not in the small region just in front of the outlet aperture).

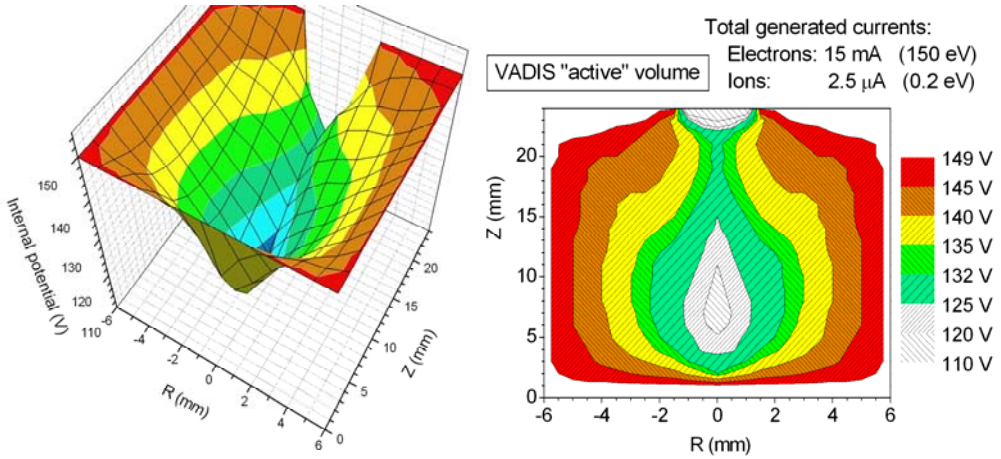

Figure 8.9. Distribution of the electrical potential inside the MK7 source, allowing the estimation of the active volume (see text.)

The difference between these active volumes can justify the higher values of the f factor (and consequently of the ionization efficiency) for the MK5 source compared to the MK7.

8.1.3. **Technical implementation.**

In order to maximize the penetration of the extraction field inside the ion source, the following MK7 components have been modified for the 1st prototype (see figure 8.10):

- The anode cylinder: the diameter of the outlet aperture was increased from 1.5mm to 3.0mm (as for the MK5 sources);
- The thermal screens placed in front of the anode outlet aperture: the internal diameter was kept the same (1.5mm), but the 1-piece design in graphite was replaced with the 3-disk (in Molybdenum) design typical for the MK5 sources.

All the other components were maintained identical to the MK7 sources (including the cold transfer line).

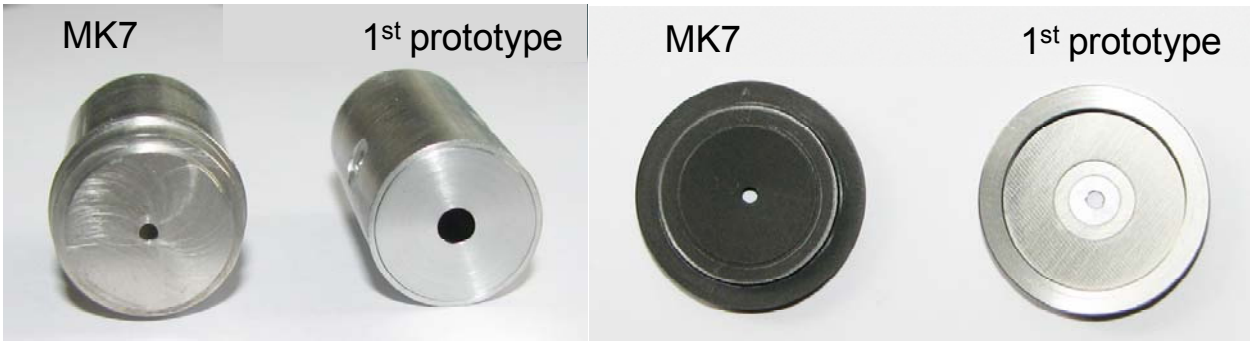

Figure 8.10. Modified components of the MK7 source: anode extraction hole diameter (left) and external thermal screens (right).

This test was only intended to validate the importance of the extraction geometry, and the prototype geometry was maintained identical to the one of the MK5 sources for allowing direct comparisons. Therefore this configuration is not necessarily the optimum one, but this kind of optimization is not treated in the present work (it will be introduced in chapter 9).

8.1.4. **Experimental results.**

The prototype unit was extensively tested on the offline separator and was afterwards employed for the production of radioactive ion beams of Argon, Krypton and Xenon (the yields measured with the developed prototypes are put together in section 8.3).

For all the measurements presented in this section, the anode potential was kept constant at 150V and the magnet current at 3.5A (or 4.0A, where marked on the figures). Two buffer gases have been employed (alternatively):

- A combination of He (40%), Ne (20%), Kr (20%) and Xe (20%) (with natural isotopic distributions);
- 100% Krypton (natural isotopic distribution).

The amounts of injected gas are marked on the figures.

The temperature evolution of the ionization efficiency of the above mentioned gases is presented on the left side of figure 8.11; on the right side, the corresponding f factors calculated for these efficiencies by using the formula 4.26.

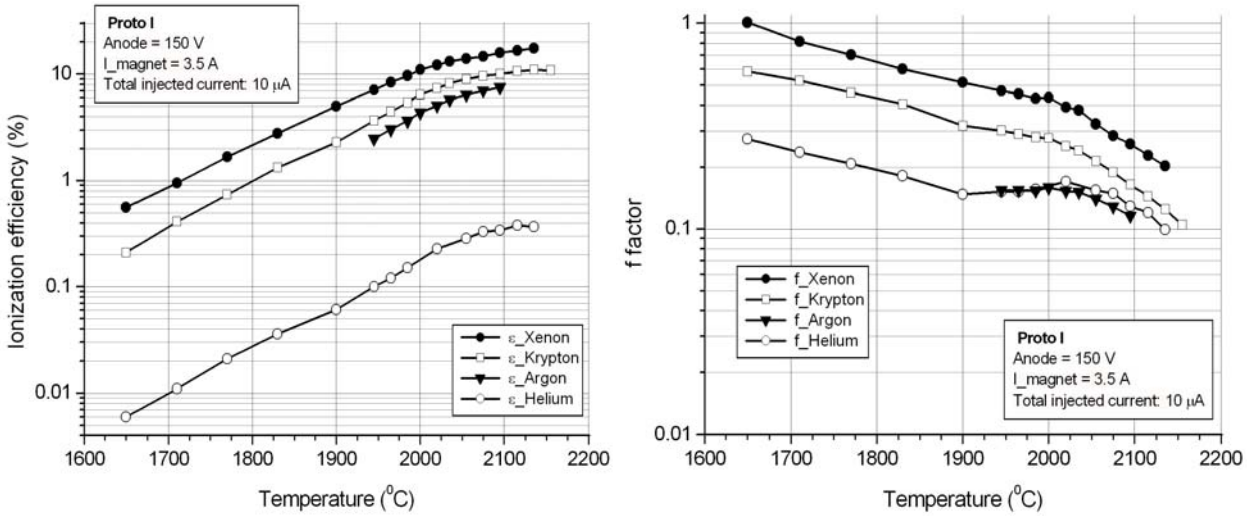

Figure 8.11. Temperature dependence of the ionization efficiency and of the f factor for the 1st prototype.

Compared to the efficiencies presented in figures 5.15 and 8.1, the efficiencies from figure 8.11 are similar to those of the MK5 sources, therefore these results are confirming that the critical factor leading to the performance difference between the MK5 and MK7 sources was the extraction geometry.

Also, an important result is that the f factor is always below unity, which confirms the proposed model assuming only one passage of the primary electrons through the plasma chamber.

The efficiency of the Neon could not be precisely measured due to the presence of a strong contaminant at the same mass.

When looking at the full temperature scale, we can see that the f factor is significantly decreasing towards the high temperatures. The reason for this is that at high temperatures, the gas pressure inside the source is increasing, due to the increase of the background pressure (impurities, material evaporation). The higher pressure will lead to a higher total extracted current which will approach the space charge saturation described in section 7.2.5.

This can be better understood by looking at the figures 8.12-14.

Figure 8.12 presents the time evolution of the source performances at constant operation parameters (2050°C, 150V on anode, 3.5A on magnet, 2.2μA of injected neutral Krypton). It can be seen that the Krypton efficiency was just 3.5% at the source startup, but it increased during the source outgassing up to 12% (corresponding to the measurements presented in figure 8.11), due to the reduction of the partial pressure of the impurities inside the source. In the outgassing process, the total extracted current decreased from ~5 μA down to ~1.5 μA. This is a fortunate case, when the impurities present in the source are mainly due to surface contaminations that can be outgassed in time. The limiting case is when the impurities dominating the beam are appearing from the bulk of the source materials (either contaminations in the volume, either evaporation of the materials themselves); in such case, they will always remain in the beam (more than that, the increase of the temperature can only increase their partial pressure, degrading the source performances).

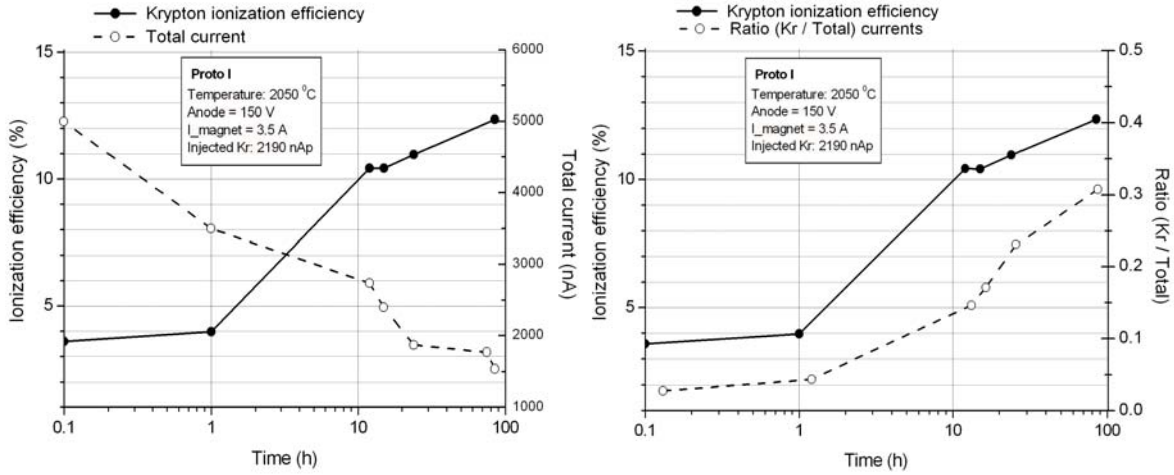

Figure 8.12. Correlation between the decrease of the impurity current in time and the increase of the Krypton ionization efficiency.

Typically, the strongest contaminants appearing in the beam above ~2000°C are the carbon monoxide and some fluoride molecules (especially BF and BF_2). In this case, the contaminants were sodium, potassium and carbon monoxide.

If we define $R_{element}$ as the ratio between the current of a given element from the injected buffer gas (containing only Krypton for the case presented in figure 8.12) and the total current (see formula 8.1), we can observe (figure 8.12, right side) that the best efficiency is obtained for $R_{Kr} = 0.3$, while it the beginning of the measurements, R_{Kr} was only ~0.03.

$$R_{element} = \frac{I_{element}}{I_{total}}$$
$$R_{buffer} = \sum_i R_{element} \qquad (8.1)$$

Figure 8.13 (left) is presenting the detailed temperature dependence of the Kr ionization efficiency versus the ratio to the total current, measured at the source startup (in the first hour of operation). It can be seen that the trend of efficiency increase is changed when R_{Kr} decreases below ~0.04, which is consistent with the values presented in figure 8.12.

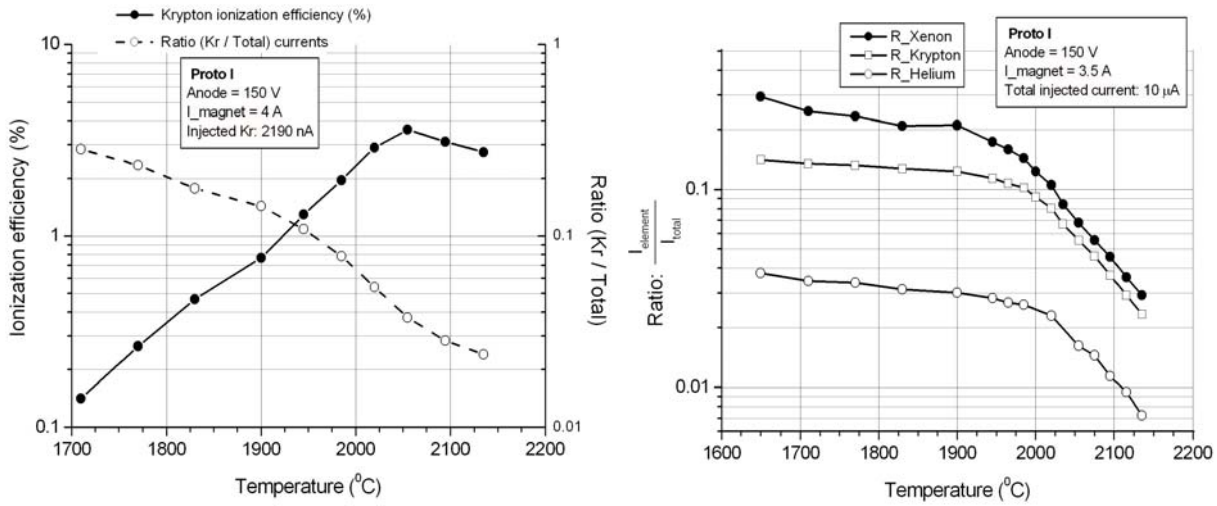

Figure 8.13. Measurements at source startup. **Left**: correlation between the ratio I_{Kr} / I_{total} and ε_{Kr} (buffer gas: Kr). **Right:** temperature dependence of the ratio $R_{element}$ between the current of different buffer gas components and the total extracted current (buffer gas: He-Ne-Kr-Xe).

On the right side of fig 8.13 is presented the temperature evolution of the element ratios measured for the buffer gas He-Ne-Kr-Xe (also at the source startup). At low temperatures, R_{buffer} is close to 50% (therefore the "useful" beam represents 50% of the beam intensity), while at the highest investigated temperature (2140°C), R_{buffer} decreases to ~6.5%. Compared to this, R_{buffer} for the figure on the left is only 2.5%; the main reason for this difference is that the injected amounts of particles were not the same for the two measurements (see the figure legends).

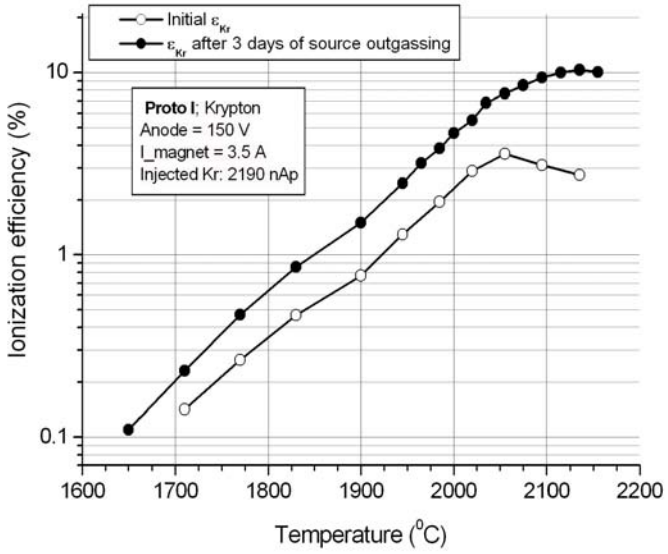

Figure 8.14. Influence of the impurity outgassing on the Krypton ionization efficiency

The detailed comparison between the source performances with and without the bakeable impurities described above is presented in figure 8.14. It can be seen that the ionization efficiency increased considerably after 3 days of source outgassing (described by the figure 8.12, left).

The efficiency values obtained after the full outgassing are reproducing the performances of the MK5 sources, only that this kind of behavior was not observed for any of the standard sources (MK3, MK5 or MK7); here, it appeared due to the presence of an alkaline contamination (Na and K) much above the normal values on the component surfaces, which most probably appeared during the non-standard component machining.

The outgassing procedure had to be repeated after the mounting of the unit on the online separator, but one day of outgassing was enough in that case for reaching the maximum performance.

This result, together with the already observed limitation presented in section 7.2.5, led to the development of a second prototype, where R_{buffer} could be maintained above 0.1 up to more than 2200°C (see section 8.2.4), thus enabling even higher ionization efficiencies.

8.1.5. **Overview.**

This first prototype confirmed the proposed model of the FEBIAD source, where the low plasma density requires a different extraction geometry compared to the classical case of electrically neutral plasmas.

This is a long range result, as the consequent use of the confirmed model can provide other ion source designs optimized for other ranges of operation parameters (higher gas loads, lower temperatures or even more compact sources) or for specific chemical classes of elements (see chapter 9).

Table 8.1. The achieved improvement of the ionization efficiencies of the noble gases.

FEBIAD Ion Source	Ionization efficiency (%)				
	He	Ne	Ar	Kr	Xe
Standard MK7 [94]	0.14	0.36	2.0	4.3	11
1st Prototype	0.37	-	7.8	11	19
Multiplication factor (noble gases)	2.6		3.9	2.6	1.7

The immediate results are presented in table 8.1 and they refer to the increase of the ionization efficiencies for the noble gases produced at ISOLDE by up to a factor 4.

The measured improvements of the radioactive yields are put together for the two designs in section 8.3.

8.2. Optimization of the impurity level inside the source. Improvement of the FEBIAD ionization efficiency for all the elements.

8.2.1. **Motivation.**

As was pointed out in section 8.1.4, the maximum ionization efficiency for a given ion source design are obtained when the contaminants are representing a fraction as low as possible of the total extracted beam. This is a consequence of the limitation of the total current that can be extracted from the ion source volume (for the operation in the “low density” mode, when the plasma potential is negative with respect to the plasma chamber walls; see section 7.2.5).

The goal of this development was to reduce the contamination level at operation temperatures above 2000°C, for maintaining a high fraction $R_{element}$ (as defined by formula 8.1) and consequently a high f and ε.

8.2.2. **Original approach.**

Out of the "list" of the typical contaminants appearing in the beams of the ISOLDE FEBIAD sources, the alkalis are not representing a real problem, as they are only surface contaminants and can be outgassed through a longer operation of the source at (or slightly above) the nominal temperature.

The contaminants posing real problems to the source operation are those that are not possible to be outgassed, due to their presence in a macroscopic amount (as part of the source materials or as an impurity uniformly distributed into the source materials).

The main impurity observed for all the plasma sources at ISOLDE is the carbon monoxide, CO, appearing as 1+ ion at mass 28. It was not clear until the present work if its effect is only negative, as it was also believed that it could enhance the ionization efficiencies of the elements with a lower ionization potential, through charge exchange [95].

The analysis presented in section 7.2.1 showed that this is not the case for the standard variation range of the FEBIAD operation parameters; additionally, the performance limitation analyzed in section 7.2.5 pointed out that the effect of any impurity is only to take a valuable fraction of the extracted current which has a well defined maximum value.

Consequently, the reduction of the CO level was proposed. As CO is a molecular compound, this can be done either through the reduction of the level of carbon, either of oxygen (or of both of them, if possible). The main source of oxygen is the layer of oxide present on the surface of any metallic component of the ion source (especially of the tantalum cathode). As this is a macroscopic quantity, it is not feasible to eliminate it. On the contrary, the carbon present in the ion source enclosure (representing various conducting subparts) is dispensable. After the modifications already implemented for the first prototype, the only remaining graphite component of the old MK5 and MK7 sources was the anode grid facing the cathode.

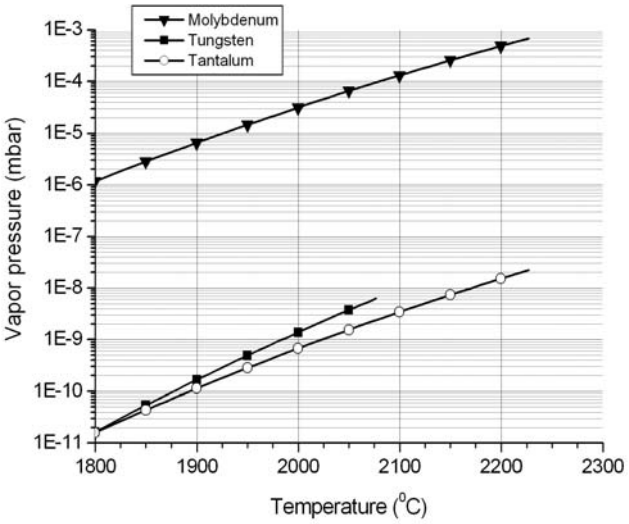

Figure 8.15. Temperature evolution of the vapor pressure for different materials (already employed in the MK series or candidate for better performances)

Therefore, the proposed solution was to change the grid material from graphite to molybdenum. The molybdenum was selected as the most convenient acceptable choice, as it was already present in the source design (as material of the anode), it is easy to machine and its partial pressure below 2200°C is acceptable for achieving an efficient source operation. As can be seen in figure 8.15, the tungsten and tantalum would be better candidates from the partial pressure point of view, but they are more difficult to machine or presenting a higher risk of failure during operation.

8.2.3. **Technical implementation.**

The only change implemented in the design of the second prototype is the material of the accelerating grid (facing the cathode): the graphite was changed to molybdenum (justification in section 8.2.2). The grid geometry was kept the same.

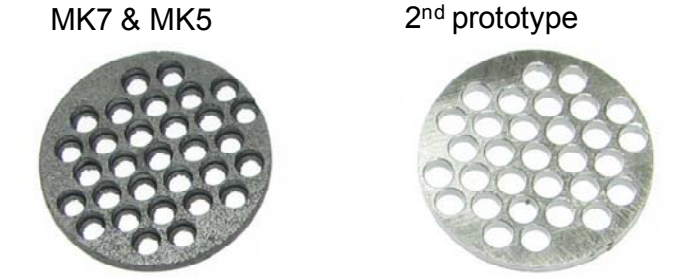

Figure 8.16. Modification of grid material. **Left**: graphite; **right**: molybdenum.

This change was implemented initially to the MK5 type (tests done only offline) and afterwards to the MK7 type too (both offline and online). The achieved efficiencies are practically the same (therefore both source types can profit of this development).

8.2.4. **Experimental results.**

The best performances obtained with the described prototype are presented in figure 8.17. The efficiency curves for Helium, Neon, Krypton and Xenon have been obtained employing the same buffer gas combination as described for the first prototype (He-Ne-Kr-Xe), while the Argon efficiency was measured separately, by using pure Argon as buffer gas. The total injected neutral currents (for all isotopes) for the two cases are indicated on the figure legend.

It can be seen that in this case, the source could be operated up to almost 2300 °C, which represents the record at ISOLDE (after a total operation time – for both offline and online separators – of almost two weeks, the source was still operating at the end of the experiment). Nevertheless, the highest efficiencies are already reached around 1950 °C, but compared to the behavior of the sources from the MK series, the efficiency no longer decreases when increasing the temperature above the value corresponding to the best efficiency (like in figure 8.13, left) – at least not until ~2200°C. This is an indication of the fact that the background pressure is no longer indefinitely increasing towards the high temperatures. Namely, the beam composition at the highest investigated temperature (2285°C) was the following:

- I_{buffer} = 550 nA (summed intensity of all the buffer gas components);
- $I_{impurities}$ = ~4000 nA (summed intensity for all the impurities).

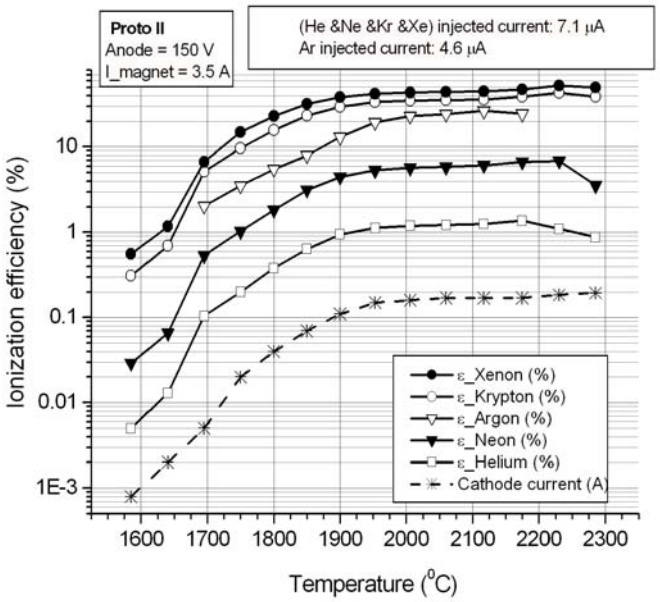

Figure 8.17. Temperature dependence of the ionization efficiency for the 2nd prototype. The dashed curve represents the estimate of the real cathode current (see text).

Therefore, the ratio R_{buffer} was of ~0.12, significantly higher compared to the values observed for the standard MK sources or even for the 1st prototype. This ratio (even higher at lower temperatures) is not justifying the saturation of the efficiency between 1950°C and 2285°C. The origin of the saturation was found when looking at the evolution of the anode drain current, which represents a direct indication of the electron current drawn from the cathode. The evolution of this drain current is presented in figure 8.17 (dashed curve) and is found to follow the same behavior as the measured ionization efficiencies: saturation above ~1950°C and an unusual inflexion (compared to all the other presented temperature dependences of the efficiency) in the temperature dependence between 1600°C and 1800°C. The saturation at high temperatures is appearing due to the space charge limit at the grid (described in section 7.2.6), while the inflexion is due to an imperfect thermal shielding of the unit (which also induced other effects, as it will be described in the following).

A closer look at the performance evolution at the highest temperatures (figure 8.18) is revealing that above 2200°C the efficiencies start to decrease (due to the increase of the background pressure, slower than for the MK series, but always present). The interesting information is that not all the elements are affected the same way: the lighter elements are affected first (He, followed by Ne at a higher temperature/background pressure and so on). This is consistent with the observations from section 6.8, where it was pointed out that the lighter elements are reaching a pressure saturation at lower pressures compared to the heavier elements.

Another remark is that when the background pressure is increasing, the cathode current is also increasing (see the measurement point at 2285°C for the cathode current in figure 8.17). This is due to the consequent increase of the ion density between the cathode and the anode grid, which will partially compensate the negative space charge of the electron beam and will therefore allow a higher electron current to be drawn from the cathode. The consequence of this behavior is that the anode drain current can be used as a monitor of the background pressure inside the source: if this current increases above ~0.4A (compared to the space charge limited value at low ion density of about 0.2A), the background pressure is too high for a reliable source

operation (for the MK series, this was a sign of source degradation, as the increase of the background pressure was linked to CO formation).

When calculating the f factors using the formula 4.26 for the efficiencies in figure 8.17, the results are confusing (figure 8.19 a), as there is no easy to identify tendency (like for all the sources presented before).

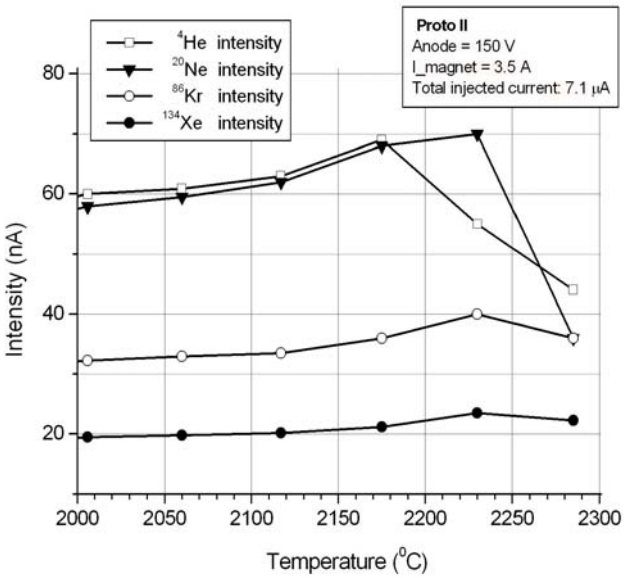

Figure 8.18. Influence of the increase of the background pressure (generated by the temperature increase) on the different elements: the lighter elements are the first affected.

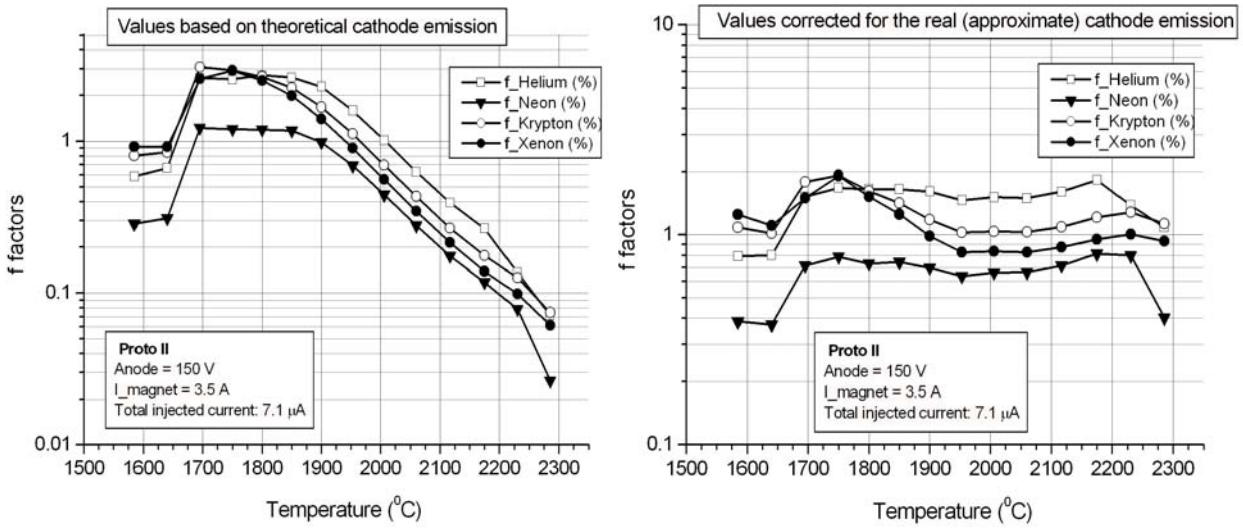

a) b)

Figure 8.19. Temperature evolution of the f factors for the different noble gases: a) values computed using the (4.26) formula, where the cathode emitted current was considered to be given by the Richardson-Dushmann relation (eq.2.2); b) values corrected for the real cathode emission, estimated from the anode drain current (see text).

This is due to the fact that the formula 4.26 is assuming an electron density obtained through the theoretical relation (Richardson-Dushmann, eq. 2.2) for the cathode emission at a given temperature. In reality, this assumption is not correct for this prototype, as it was deduced from the results in fig.8.17 that the cathode emission presents irregularities both at low and at high temperatures. Therefore, meaningful results can only be obtained if the f calculation is corrected for the real cathode currents. The figure 8.19 b is presenting these corrected f values, which are this way becoming quasi-constant and close to unity from 1700°C to 2200°C. Still, these values are subject to errors due to the fact that the cathode current is only approximate (the anode drain is not a precise measure of the cathode current); for this reason, the absolute values of the f factors from figure 8.19 b (especially their value above 1) are not necessarily containing a physical information. This behavior was not investigated further for the present thesis.

The same outgassing effect as for the 1st prototype was observed. Figure 8.20 is presenting the efficiency curves measured during the outgassing process.

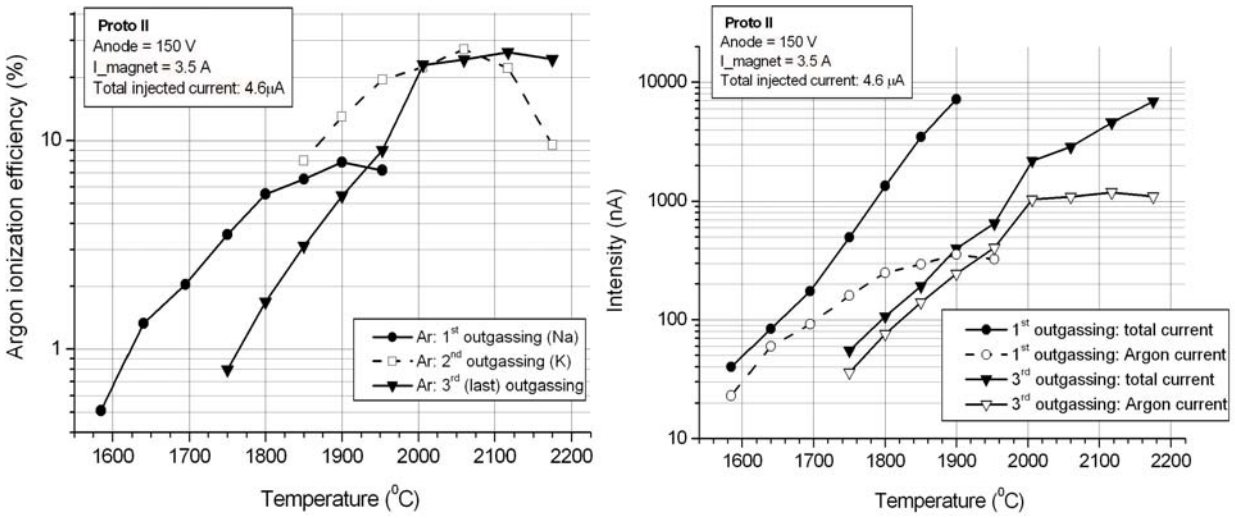

Figure 8.20. Increase of the Argon extracted current (and consequently of the Ar ionization efficiency) at the decrease of the current generated by the background elements. **a)** Due to the reduction of the background pressure, the source temperature could be increased above 2000°C and the Ar current above 1μA; **b)** The evolution of the Ar ionization efficiency due to the source outgassing (see text).

Three curves are presented in figure 8.20 a), as the final efficiencies could only be obtained after two successive heatings of the unit, at increasing temperatures. The first curve ("1st outgassing") was measured at the source startup, when the Argon efficiency got saturated already at 1900°C, due to a strong outgassing of a sodium impurity. The main components of the beam extracted from the source at this moment were the following:

- Ar^+: 350 nA;
- CO^+: 280 nA;
- Na^+: ~6000 nA

The total current was 7200 nA.

After one night of outgassing at 1900°C, the temperature could be further increased up to ~2100°C (the second curve, "2nd outgassing"), when the Argon efficiency started again to decrease due to the increase of the impurity currents, which this time were the following:

- Na^+: 80 nA;
- CO^+: 680 nA;
- K^+: 950 nA;
- Fe^+: 2200 nA.

The Argon current decreased due to these impurities from 1000 nA at 2120°C to 420 nA at 2175°C.

After another night of outgassing at 2100°C, the only strong contaminants remaining in the beam were CO and Fe (at similar intensities compared to those above). At his moment, the 3rd curve from figure 8.20 a) was measured ("3rd outgassing"). It can be seen that the maximum efficiency did not increased from the 2nd to the 3rd curve, but it is no longer decreasing 2100°C, which is a characteristic for the presence of impurities with quasi-constant partial pressures, but that cannot be outgassed from the plasma chamber.

The difference between the ionization efficiencies at lower temperatures between the 3rd and the first two curves is an abnormal behavior and it is a sign that the temperature calibration got shifted, most probably due to a degradation of the thermal shielding around the cathode. This is the reason why the f factors (calculated for efficiencies measured after the 3rd outgassing) had to be corrected all along the temperature range and the efficiency curves from figure 8.17 are presenting the unusual inflexion at low temperatures.

In figure 8.20 b), the total currents are compared to the Argon currents for the 1st and the 3rd outgassing.

8.2.5. **Overview.**

This second prototype achieved two record performances at ISOLDE:

- The highest ionization efficiencies for the noble gases (and theoretically for all the other elements – see section 9.1);
- The highest operation temperatures (without the degradation of the source performance or components).

Additionally, this second prototype added important information for the comprehension of the FEBIAD operation:

- The cathode emission becomes space charge limited around 1950°C;
- The ionization efficiency of the light elements is the first one affected by the increase of the background pressure inside the plasma chamber;
- The calculation of the f factors (using the formula 4.26) should employ, if available, the experimental cathode currents instead of the theoretical values (Richardson-Dushmann), for limiting the errors.

The achieved efficiencies (compared to the standard performances at ISOLDE and to the first prototype) are presented in table 8.2 (where the Radon efficiency is obtained through extrapolation – details in section 9.1).

The design validated by this 2nd prototype allows the further increase of the ionization efficiencies for all the elements produced at ISOLDE.

By using this source design for the production of noble gases (instead of the MK7 sources), the achieved multiplication factor for the ionization efficiency is given by the ratio between the efficiencies of the 2nd prototype and of the standard MK7 sources. For all the other elements (which were until now ionized by the MK5 sources), the multiplication factor is given by the

ratio between the efficiencies of the 2nd prototype and those of the 1st prototype (and is found to be close to 3 for all the elements).

Table 8.1. The achieved improvement of the ionization efficiencies for all the elements produced at ISOLDE.

FEBIAD Ion Source	Ionization Efficiency (%)					
	He	Ne	Ar	Kr	Xe	Rn
Standard MK7 [94]	0.14	0.36	2.0	4.3	11	-
1st Prototype (and MK5)	0.37		7.8	11	19	
2nd Prototype	1.4	6.7	26	38	47	62
Multiplication factor (noble gases)	10	18.6	13	8.8	4.3	
Multiplication factor (all other elements)	~3 (expected)					

8.3. Improvement of the RIB yields. Conclusions.

As any increase of the ionization efficiency acts directly on the total RIB yield, the yields are expected to directly scale with the efficiency gain. The first results are in line with this expectation (table 8.3).

Table 8.3. RIB yields measured with the new ion source design (with the corresponding target materials and element half-lives).

YIELDS	^{31}Ar *(15 ms)*	^{72}Kr *(17 s)*	^{73}Kr *(26 s)*	^{138}Xe *(14.1m)*	^{229}Rn *(~12s)*
Measured (at/μC)	5 [96] *(CaO)*	1.1e4 *(Nb)*	1.2e6 *(Nb)*	2.4e9 *(UC_x)*	200 [97] *(UC_x)*
Database (at/μC)	1.5 *(CaO)*	2.0e3 (Nb)	7.4e4 *(Nb)*	5.7e8 *(UC_x)*	-

The second prototype allowed the determination of the masses of $^{223\text{-}229}$Rn by precision mass spectrometry at ISOLTRAP; the isotope ^{229}Rn was identified for the first time in a laboratory and its half-life could be measured [97].

The excellent results of these ion source designs made them now the new standard ion sources in use at ISOLDE. The VADIS series (“Versatile Arc Discharge Ion Source”; details in chapter 9) replaced the MK series in 2009 and the new units used for RIB production at ISOLDE (VD5, the “hot plasma” version and VD7, the version with water-cooled transfer line) confirmed the efficiencies of the second prototype described in this chapter.

CHAPTER 9

THE VADIS CONCEPT. APPLICABILITY.

The FEBIAD model proposed in chapter 4 is confirmed by experimental results (chapters 5 and 6) for a wide variation range of the operation parameters and could already serve to the improvement of the ionization efficiencies of the noble gases produced at ISOLDE (chapter 8). As will be detailed in section 9.1, the efficiency increase is expected to also apply to all the condensable elements and to any isotope lifetime of the elements produced at ISOLDE.

As was introduced in chapter 2 (and further followed in chapter 7), the ion source performance is limited by the particular design employed: the phenomena driving the ionization are generally occurring (or even enhanced) also outside the available operation range allowed by a fixed design.

The detailed knowledge of the ion source behavior achieved through the presented work allows the customization of the ion source design for eliminating the performance limitations relevant to different specific application (like different chemical classes of elements to be ionized or different range of operation parameters).

A selection of the possible applications of this concept is presented in section 9.3. As these will require detailed investigations before implementation, only the principle description and the critical aspects to optimize are given here, for guiding the following developments.

9.1. Extension of the proposed model.

In the form proposed in section 4.2, the FEBIAD ionization model can predict the ionization efficiency for any element. In the first approach, the element volatility (controlling the time that the element remains sticking on the source walls, at any wall collision) was not included, as it is not affecting the average number of wall collisions suffered by the atoms to be ionized before they leave the ion source volume. For the radioactive isotopes having a limited lifetime, this term becomes important, as part of them will be lost through radioactive decay if they are not ionized and extracted from the source sufficiently fast compared to their lifetime.

Also, it was observed experimentally that the f factor defined by eq. (4.12) depends on the element, due to their different thermal velocity and consequently to the different time they spend in the ionizing electron beam.

We put together in this section all these corrections which will allow the full prediction of the ionization efficiency for any short-lived condensable radioactive isotope.

9.1.1. **Element dependence of the FEBIAD ionization efficiency.**

From equations (4.12) and (4.13), we obtain that the ionization efficiency for a volatile stable isotope:

$$\varepsilon = f \cdot V_{source} \cdot \frac{R_{ioniz} \cdot n_e \cdot n_n \cdot \sigma_{ioniz} \cdot v_{rel}}{n_{n\_in}} \qquad (9.1)$$

where f and σ are the only element dependent factors; the ionization cross section for the investigated isotope is given by the Lotz formula (eq.2.4), while the f factor is given by eq. (7.13). In the latter formula, f_0 can either be estimated through simulation, either can be deduced from the experimental measurement of the ionization efficiency of a trace element (followed by the extrapolation for the investigated element, which can also be done through eq.7.13). Instead of formula (7.13), a higher precision approximation can be used, as presented in section 7.1.4.

9.1.2. **Influence of the element volatility.**

The atoms of different elements reaching a surface at a given temperature T will spend different times sticked to that surface before desorption. This time (called in the following sticking time) depends on the adsorption enthalpy of the specific element on the given surface. The sticking time, t_s, is given by the Frenkel equation [98]:

$$t_{stick} = t_0 \cdot \exp\left(-\frac{\Delta H_a}{kT}\right) \qquad (9.2)$$

where t_0 is the value of the sticking time at infinite temperature and ΔH_a is the partial molar adsorption enthalpy.

The precise knowledge of these two parameters is subject to special experimental investigations [11] and modeling [99][100]. Based on the partial data available at this moment, the adsorption enthalpy can be estimated from the values of the vaporization enthalpy of the elements. The t_0 on a Molybdenum surface was found (in the Targisol project [11]) to be almost the same for all the elements (~1.02e-13 s). Using this data, an estimate for the sticking times t_{stick} on a Molybdenum surface can be obtained for all the elements (fig.9.1).

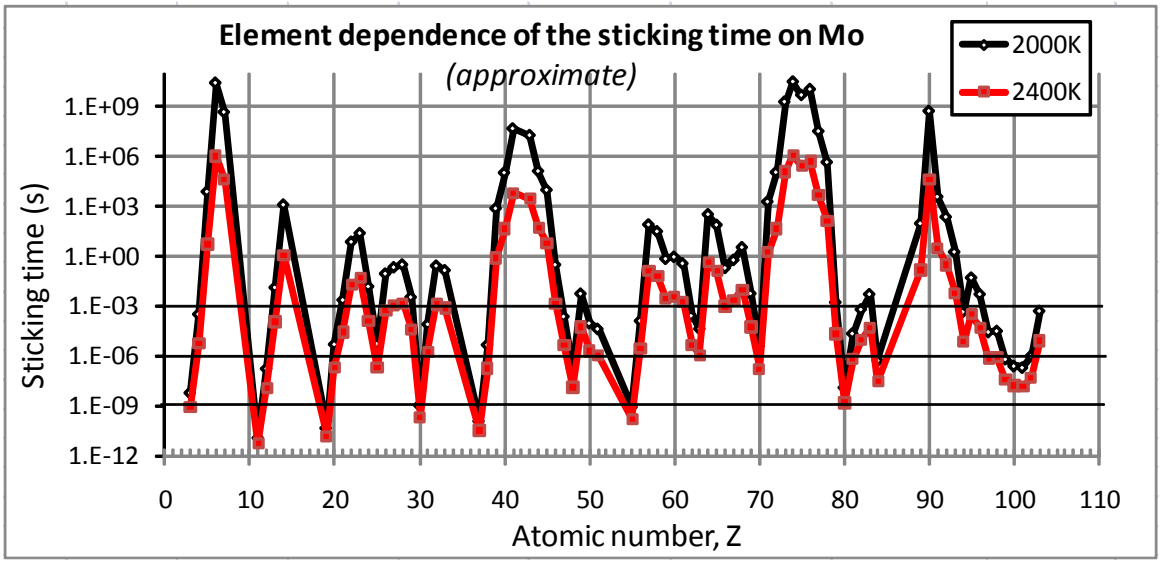

Figure 9.1. Approximation (see text) of the sticking time on a Molybdenum surface (at 2000°K and 2400°K) for the atoms of different elements.

We define the average flight time between two collisions, t_{flight}, as:

$$t_{flight} = \frac{l_{avg}}{v_n} \tag{9.3}$$

where l_{avg} is the average flight length between two collisions (~1.5cm for the standard ISOLDE FEBIADs) and v_n (velocity of the neutral atom) defined by formula (4.15).

We also define the average number of wall collisions before an ionization occurs, N_{col_1ioniz}:

$$N_{col\_1ioniz} = \frac{\lambda_n}{l_{avg}} \tag{9.4}$$

where λ_n (the average free path before ionization) is defined by eq. (4.10).

For the volatile elements (having the sticking time negligible compared to the flight time), the time required for one ionization, t_{ioniz} (expressed in chapter 7 through formula 7.2) can also be expressed as:

$$t_{ioniz}(volatile) = N_{col\_1ioniz} \cdot t_{flight} \tag{9.5}$$

For the condensable elements, this ionization time will be higher:

$$t_{ioniz}(condensable) = N_{col\_1ioniz} \cdot (t_{flight} + t_{stick}) \tag{9.6}$$

The average total time spent by an atom inside the source before pumping, $\langle t_{pump} \rangle$ (eq.7.4), can therefore be expressed as:

$$\langle t_{pump} \rangle (volatile) = N_{pump} \cdot t_{flight} \tag{9.7}$$

$$\langle t_{pump} \rangle (condensable) = N_{pump} \cdot (t_{flight} + t_{stick}) \tag{9.8}$$

The total number of wall collisions before ionization, N_{col_1ioniz}, and before pumping, N_{pump} (eq.7.6), are assumed to be the same (on average) for volatile and condensable elements. With this assumption, for any stable isotope the ionization efficiency should be independent on the element volatility, provided that sufficient measurement time (comparable to the time from

eq.9.8) is possible. This also means that the efficiency improvements achieved for the noble gases (presented in chapter 8) are also applying to the condensable elements.

In reality, this may be slightly different due to several factors:

- The reflection angle at desorption follows a cosine law (no dependence on the incident velocity), while at collisions without sticking, the emission angle depends on the incident angle.
- In the presence of sticking, the element partial pressure inside the source is different compared to the volatile case; this may affect the effusion time.
- Part of the element atoms will be trapped in the cold spots of the TIS unit.
- Not sufficient time can be used for the experiment.
- The radioactive decay of the analyzed isotopes (see section 9.1.3).

For the present work, we did not investigate the dependence of the ionization efficiency on the element volatility. This can be done for example by operating the ion source at different temperatures (sufficiently different for allowing a significant change of the sticking time) and correcting for the typical temperature dependence of the ionization efficiency for a volatile element.

For estimating the effect of the developments presented in chapter 8 on the source response time for the condensable elements produced at ISOLDE, it is sufficient to analyze the relations (9.6) and (9.8). Compared to the previous design, for the source operation at the same temperature, all the terms are remaining constant; the increase of the f factor means that a larger fraction of the generated ions will be extracted after every ionization (see figure 7.3). Therefore, the average response time will be shorter for the new design.

As any increase of the operation temperature reduces t_{ioniz} and N_{col_1ioniz} (due to the higher density of primary electrons), the fact that the development allowed the source operation with high f up to higher temperatures, translates to even shorter response times compared to the old design.

9.1.3. **Influence of the isotope lifetime.**

From a population of N_0 atoms of an isotope with the half-life $T_{1/2}$ entering the ion source volume at the time $t_0=0$, the remaining fraction r of atoms at an ulterior time t is given by the relation:

$$r(t) = \frac{N(t)}{N_0} = \exp\left(-\frac{t \cdot \ln 2}{T_{1/2}}\right) \qquad (9.9)$$

For estimating the ionization efficiency for a given isotope, the curve defined by eq. (9.9) will have to be plotted against the times required for one ionization (eq. 9.6) and for pumping from the source volume (eq. 9.8). If the source design allows a high f factor, a good efficiency can be obtained if the half-life is comparable to the ionization time; otherwise, if f is small (<0.1) and the half-life is small compared to the pumping time, the ionization efficiency for the radioactive isotope can be significantly smaller compared to the one of the stable isotope(s) of the same element.

9.2 The VADIS concept.

9.2.1. **Customization of the source design for specific ISOL requirements.**

VADIS already represents the name of the new ion source series introduced at ISOLDE, following the successful developments described in chapter 8, but the "versatile" term in the source name was chosen to express that this development means more than a new and better fixed design to replace the old one. The accumulated information on the FEBIAD behavior, occurring phenomena and performance limitations described in this thesis can allow the implementation of the goal announced in section 2.4: reaching better performances through the optimization of the source design for specific ISOL requirements (which would not be possible with a fixed design), through the adaptation of the nominal operation parameters or plasma properties to the values required for that specific application.

The introduction of this "versatile source" concept required the establishment of a set of performance indicators for estimating what can be gained through the respective development (additional to just a number for the maximum ionization efficiency). We review in section 9.2.2 these indicators, as they have already been introduced in the previous chapters.

9.2.2. **Diagnose of the source performance.**

The following source diagnostics can be used for the characterization of the performance of a given source design. If this performance is found to be insufficient for the specific application, the design can be optimized with the help of the model developed in the present work.

The first diagnostic (point a) is the most important quality factor defined in the present work, as it provides the global figure of the source performance and allows the estimation of the maximum ionization efficiency that the investigated design can provide; the following diagnostics (points b and c) are referring to the maximum variation range of the operation parameters, which can require adjustment for some applications (see section 9.3); the last diagnostic provides important information on the source selectivity and contamination level.

a) *The f factor.*

For a given design, it can be accessed either through direct experimental measurement, either through simulation:

- Experimentally: the global f factor can be obtained, by employing the eq. (4.26) for a given set of operation parameters and the measured ionization efficiency. The geometrical factor f_0 can be then obtained through one of the methods described in section 7.1.4 (for example, through eq. 7.13).
- Simulation: CPO (for example) can map the equipotential lines inside the source, which can serve to the estimation of the active volume and consequently of the geometrical factor f_0. The global f factor can be then deduced for any element, depending on their neutral residence time (eq. 7.13).

As the f factor cannot be higher than 1 (due to the lack of confinement for the primary electrons, see section 4.2), it defines the maximum ionization efficiency available for a given design.

Also, the geometrical factor f_0 provides information on the plasma density inside the source.

An example on how the f factor can be improved was presented in chapter 8.

b) *The maximum operation temperature.*

It was pointed out in this work that above a given temperature, the ionization efficiency can drop (fig. 5.14) or just saturate (fig. 8.17).

In the first case, the design was not optimized for efficient ionization (due to the presence of an important amount of impurities inside the source) and therefore it is of no use to employ it again for ISOL. In the second case, the source presents a very good ionization efficiency for the medium and heavy elements (see table 8.1), but there is still place for improvement for the light elements. Therefore this design is good for ionizing a part of the elements produced through the ISOL method (see also sections 9.3.1 and 9.3.2), but a modified design is required (and is possible) for the ionization of the light elements (more details in section 9.3.6).

It may be of interest to also lower the operation temperature, while maintaining the best source performances. An approach for doing this is presented in section 9.3.3.

c) *The variation range of the operation pressure.*

It was found during the present work that the FEBIAD sources can be operated with similar efficiencies both at low and at high pressures (see figure 5.21). Between the two operation regions, there is almost one order of magnitude for the operation pressure (approximately between 10^{-4} and 10^{-3} mbar) where the ionization efficiency decreases continuously before regaining the previous values.

The efficiency saturation in the low pressure region can be seen in figure 5.19, while the transition between the two operation modes can be seen in figure 5.22.

The two operation regions are corresponding respectively to the rarefied plasma, allowed by the accelerating grid introduced by Kirchner, and to the high density plasma appearing above Bohm's threshold pressure (specific to the Nielsen sources and, more generally, to any volume discharge source). The selection between the two operation modes has to be made according to the specific application, but the transition region should be avoided. The operation in the low density mode presents the advantage of a low total current extracted from the source, while the high density mode presents the advantage of a increased selectivity for the light ions (due to the preferential transition through the plasma boundary of the lower masses).

The source design does not affect the threshold pressure, but it affects the maximum gas load that will produce the threshold pressure inside the source.

It is therefore important to measure the dependence of the ionization efficiency on the gas load.

As long as the equivalent conductance between the target and the ion source allows the reduction of the (eventual) high pressure from the target container and the ion source is only exposed to an increased gas load that can be evacuated efficiently for not increasing the pressure in the plasma chamber, the design can be adapted for allowing the operation in the low density mode at higher gas loads (see section 9.3.5).

d) *Mass scan.*

The investigation of the full mass scan provides important information on the source selectivity, the impurities present inside the source at that respective pressure and their partial pressures. If the total current becomes too high due to these impurities, the ionization efficiency is affected (see figures 8.12-13 and the corresponding explanations in the text). The same geometrical design can provide different source performances, depending on the ratio between the useful current and the total current. The mass scan is an indispensable diagnostic towards the source optimization.

9.3. Examples of VADIS applicability.

We present here the most important optimizations of the FEBIAD sources that became available through the results presented in this thesis. A part of them has already been implemented with positive results; for the rest, we only give the principle description and the critical aspects that will have to be optimized.

9.3.1. **Noble gases.**

The ionization efficiency of the noble gases is the result of the optimization of the ionization time versus the total confinement time of the neutral atoms inside the source volume. Starting from the old ISOLDE design, this implied the increase of the fraction of the ions extracted after one ionization, which reduced the losses due to the gas pumping from the source volume.

This development has already been successfully implemented and was presented in chapter 8. The design presented therein was adopted as the new ion source for the noble gas ionization at ISOLDE and became this way the first source from the VADIS series (called VD7, for historical reasons, as it replaced the old MK7 design).

9.3.2. **Refractory elements.**

As the VD7 design (developed for the ionization of the noble gases) has the nominal operating temperature of 2000°C, it can also provide the ionization of the refractory elements that are sufficiently volatile at this temperature. The only difference is that the design for the noble gases integrates a water-cooled transfer line, while the design for refractory elements presents a transfer line at high temperature. The available ionization efficiencies are nevertheless similar.

This design is already implemented at ISOLDE, as the second source from the VADIS series (named VD5, as it replaced the old MK5 design).

9.3.3. **Enabling different chemistry approaches. Reduction of impurity level.**

It is useful for some experiments to extract the isotope of interest as a molecular compound, either for providing sufficient selectivity (through the shift of the position in the mass spectrum from the isotope mass to the mass of the molecule), either for providing sufficient volatility (so that the respective isotope will not decay before extraction from the source).

Typically, the employed molecular compounds are fluorides and sulfides, obtained through the injection into the ion source (as support gases) of CF_4 or SF_6. These gases are optimum for the operation of the source at around 2000°C. For other temperature ranges, these molecular compounds can either no longer be stable or not form at all. The gain of changing the nominal operation temperature is that other compounds can become available, allowing the development of new refractory beams.

A first solution for lowering the nominal temperature from 2000°C down to ~1500°C has been proposed, implying the change of the emissive surface of the cathode from tantalum (Ta) to thoriated tungsten (ThW).

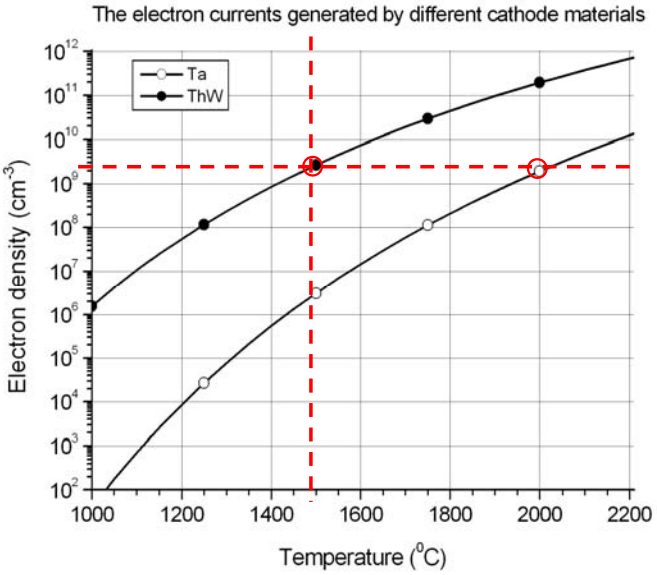

Figure 9.2. The electron densities generated inside the source (V_{anode}=150V) for different cathode emissive surfaces (Ta and ThW).

It can be seen in figure 9.2 that the same electron density generated by a tantalum cathode at 2000°C can be obtained using a thoriated tungsten cathode at only ~1500°C.

Additional to the motivation for the molecular compounds, the operation of the source at lower temperatures (without sacrificing the ionization efficiencies) will also provide a significant reduction of the background pressure generated by the evaporation of the source materials. Contaminants like CO (specific to the old MK series) and BF_2 (specific to the sources with insulators in boron nitride, BN) can practically be eliminated.

This design will be implemented at ISOLDE in the near future.

Also, one should not forget that the ISOL hot sources (and the FEBIADs in particular) are small chemical factories, affected by all the materials present in the source enclosure. Even without changing the operation temperature, the occurring chemical reactions can be controlled through the selection of the other source materials (grid, anode, insulators).

9.3.4. **Short isotope lifetimes.**

During the present investigations, it was observed that the ionization efficiency is not strongly affected by the internal magnetic field of the ion source for the MK5 and MK7 designs (figure 5.8 c and d). This also applies to the VD5 and VD7 designs. This means that the solenoid magnet is not indispensable to the source design for achieving good performances (though it may be sometimes useful for improving the source selectivity [88]).

The removal of the source magnet from the source design can allow even more compact TIS units and/or smaller sources, leading to better overall efficiencies for the short-lived radioactive isotopes.

This is not valid for the design of the MK3 source (as can be seen in figure 5.4 a), presenting 2 anodes and a stronger expansion of the electron beam.

9.3.5. **Higher gas loads.**

As was presented in figure 6.9 and detailed in section 7.1.1, the highest ionization efficiencies for the VD5 and VD7 designs are available at operation pressures of up to 10^{-4} mbar (or only 10^{-5} mbar, if the ionization of the light elements is required, as they are the first ones affected by the pressure increase).

This translates for the VD5/7 design in a gas load of ~275 μAp (or respectively 27.5 μAp for the light ions).

This pressure limitation is given by the transition between the two operation modes that are possible for the FEBIAD sources (detailed in section 9.2.2 c) and represents the best case for the VD5/7 design.

This value can be reached if no other limitations (specific to a fixed design) are reached:

- The impurity level inside the source should be sufficiently low (the fraction of the useful beam in the total extracted current should be at least 0.3 – see figures 8.12-13);
- The electron cathode from the cathode should not be space charge limited at the accelerating grid, for allowing a sufficiently short ionization time;
- The extracted current should not be space charge limited (due to the relatively thick plasma boundary characterizing the low density discharge – see section 7.2.5), for allowing the efficient extraction of the ions from the source (every ion recombination contributes to the increase of the pressure inside the source, through the increase of the effective residence time of the particles inside the source).

The relation between the maximum pressure and the maximum gas load depends on:

- the outlet conductance of the ion source (towards the separator).
- the extraction time of the generated ions (itself depending on the ionization time and on the extraction factor f).

Higher gas loads can therefore be allowed for the same maximum pressure value inside the source, through the reduction of the extraction time (which can also allow the increase of the outlet conductance without increasing the neutral losses).

We also remind that the FEBIAD/VADIS sources can be operated also above this threshold pressure (see section 9.2.2. c), but only with a corresponding (high) amount of injected buffer gas (required for the source stabilization) and consequently a density of the extracted current starting from 1 mA/cm^2.

9.3.6. **Light elements.**

As was presented in table 8.1, the VD5 and VD7 designs are already providing excellent ionization efficiencies for the elements heavier than Argon. The ionization efficiencies of the light elements can only be little improved (by further reduction of the background pressure inside the ion source), due to the fact that the limitation comes from the space charge limitation of the primary electron current (see section 7.2.6). Only a limited improvement can be obtained through the reduction of the gap between the cathode and the grid (approach limited by the risk of short-circuit between the cathode and grid) or through the increase of the grid potential (approach limited by the decrease of the ionization cross section with the increase of the energy of the primary electrons).

A solution providing significantly higher ionization efficiencies for the light elements is the operation of the source at high pressures, when the cathode emission is no longer limited due to the space charge compensation provided by the plasma. Of course, this solution is no longer requiring the presence of the grid in front of the cathode, but that doesn't mean that the source design has to regress towards the Nielsen source; the improved ISOLDE cathode can still be used and the extraction system should be improved (to a triode or pentode design) for insuring a good beam quality for the high intensities that will be generated (current densities $\geq 1 mA/cm^2$).

9.3.7. **Laser ionization (RILIS).**

The coupling of the VD7 or VD5 design with the RILIS system can be efficient due to the high f factor characterizing the VADIS series, insuring the extraction of an important fraction of the ions generated by the laser pulse. The main issue can be the source selectivity (compared to the surface ionizers, all the elements reaching the source enclosure will be ionized, not only the alkalis), but as can be seen in figures 8.11 and 8.19, the VADIS designs already implemented (VD5 and VD7) are providing high values for the f factor even at low temperatures, where the ionization through electron beam impact (and surface ionization too) is strongly reduced. This can even be transformed in an advantage, as the variation of the source temperature allows the on-line control of the selective condensation of different elements on the source walls (similar to the approach of Kirchner, who already confirmed the element bunching capacity of the FEBIAD sources [98][101]).

Additionally, the source selectivity can be improved with the better comprehension of the loss phenomena appearing at the filling of the source trap capacity (described in section 7.2.3): the fast generation of the ions through resonant ionization (in the central part of the source) will affect the densities of the other ions present in the source volume and can temporarily reduce the extraction of the contaminants. The VORPAL code can be employed for this kind of investigation.

The use of the lower temperature design proposed in section 9.3.3 can further improve the selectivity (and allow the extension of the operation temperature range), provided that the element to be ionized is still sufficiently volatile at the lower temperature.

CONCLUSIONS

C1. GENERAL CONCLUSIONS

With the aim of finding a solution for the efficient operation of the ISOL ion sources coupled with 100 kW targets (which will generate increased gas loads to the ion sources of the future ISOL facilities, as was presented in table 2.1), a detailed study of the standard ISOLDE FEBIAD ion sources has been done. Through experimental, analytical and numerical investigations, several results have been obtained:

- The detailed dependence of the FEBIAD performances on the operation parameters;
- The characterization of the FEBIAD plasma properties (composition, temperatures, densities, potential);
- The identification of the FEBIAD limitations, together with the corresponding theoretical justifications and solutions for their removal;
- An analytical model for the FEBIAD ionization efficiency, inferred from the experimental results and valid all over the investigated variation range of the operation parameters;
- The proposal of a customizable series of ion sources (VADIS), which can take advantage of the developed model to optimize the ion source design for the different chemical classes of produced isotopes.
- The implementation at ISOLDE of two of the proposed VADIS designs: one dedicated to the ionization of the noble gases (which improved the 1+ ionization efficiencies for the noble gases by 5 to 20 times - depending on element - and reaching 60% for Radon) and one dedicated to the ionization of the refractory elements (improving the efficiencies by a factor of ~3).

Starting from 2009, the VADIS sources replaced the old "MK" series of FEBIAD ion sources and are now the new standard ion sources in use at ISOLDE.

The performance improvement was confirmed by the new production units for all the investigated noble gas radioactive isotopes.

C2. ORIGINAL CONTRIBUTIONS

The improvement of the ISOLDE FEBIAD sources efficiencies was possible due to an original development approach: the experimental investigation of the performance of the existing sources for the widest variation range of the operation parameters, to validate the theoretical model and identify the best developments possible without the radical change of the source design.

This approach produced the original results listed in section C1.

My personal contributions to the results presented in the thesis are:

- The investigation of the available simulation codes, the proposal for CPO and VORPAL acquisition; use of the codes for the applications quoted in Chapter 3.
- The theoretical analysis of the FEBIAD plasma properties and the inference of the new model for the ionization efficiency, significantly different to the existing ones

and based on clearly identified elementary physical phenomena contributing to the overall source efficiency (Chapter 4);
- The proposal and planning of all the experimental investigations of the previous ISOLDE FEBIAD sources (MK series), the data measurement and treatment (Chapters 5 and 6);
- The identification, analysis and solution proposal for the FEBIAD limitations (Chapter 7);
- The proposal and justification of the two prototypes described in Chapter 8; the follow-up of their realization, the experimental investigations and data treatment;
- The proposal of the VADIS ion source series, together with the possible applications described in Chapter 9.

C3. FUTURE PERSPECTIVES

The new VADIS series has a long lifetime perspective at ISOLDE, as the achieved efficiency increase is expected to significantly improve all the previous yields of produced radioactive isotopes (the expected multiplication factors are presented in table 8.1, with similar reliability).

Also, the new VADIS designs are of great interest to many of the ISOL facilities worldwide (some of them being technically compatible with the ISOLDE equipment and/or already employing sources of FEBIAD type).

The extensive source performance characterization provided by the present work validated the VADIS sources as a candidate for the future facilities dealing with increased gas loads.

Several other possible applications - of equal interest - of the VADIS designs have been detailed in section 9.3:

- The increase of the overall ISOL efficiency for the short-lived isotopes through a further simplification of the source design (and of the TIS unit);
- Improvement of the ionization efficiencies of the light elements;
- The modification of the nominal operation temperature of the source to produce beams of the elements of interest as molecular compounds; also, the background pressure inside the source can be reduced this way;
- The coupling of the VADIS sources with laser ionization (RILIS) systems. The optimal configuration of the electrical field inside the VADIS can guarantee the extraction of a high fraction of the ions produced through laser ionization. Also, the selectivity of such a system can be tuned on-line.

ANNEXES

A1. LIST OF PUBLICATIONS

Publications in peer-reviewed journals:

- **L. Penescu**, T. Stora, J. Lettry, G. Cata-Danil and R. Catherall, "Arc Discharge Ion Source Development at CERN ISOLDE", accepted for publication in the Scientific Bulletin of the University POLITEHNICA of Bucharest (2009);
- **L. Penescu**, R. Catherall, J. Lettry and T. Stora, "*Development of high efficiency Versatile Arc Discharge Ion Source (VADIS) at CERN ISOLDE*", accepted for publication in Rev. Sci. Instrum. (2009).
- D. Neidherr, G. Audi, D. Beck, K. Blaum, Ch. Bohm, M. Breitenfeldt, R.B. Cakirli, R.F. Casten, S. George, F. Herfurth, A. Herlert, A. Kellerbauer, M. Kowalska, D. Lunney, E. Minaya-Ramirez, S. Naimi, E. Noah, **L. Penescu**, M. Rosenbusch, S. Schwarz, L. Schweikhard and T. Stora, "*Discovery of ^{229}Rn and the Structure of the Heaviest Rn and Ra Isotopes from Penning-Trap Mass Measurements*", Phys. Rev. Lett. 102 (2009) 112501.
- **L. Penescu**, R. Catherall, J. Lettry and T. Stora, "*Numerical simulations of space charge effects and plasma dynamics for FEBIAD ion sources*", Nucl. Instrum. and Meth. in Phys. Res. B 266 (2008) 4415-4419.
- C. Huet-Equilbec, P. Jardin, M.G. Saint Laurent, C. Barué, C. Canet, J.C. Cornell, M. Dubois, M. Dupuis, C. Eléon, J.-L. Flambard, G. Gaubert, P. Lecacheux, N. Lecesne, P. Lehérissier, F. Lemagnen, R. Leroy, J.Y. Pacquet, and **L. Penescu**, "*Radio frequency injection system for electron-cyclotron-resonance ion source in a hostile environment*", Rev. Sci. Instrum. 77 (2006) 03A343.
- P. Jardin, C. Barué, C. Canet, J. Cornell, M. Dubois, M. Dupuis, J-L. Flambard, G. Gaubert, C. Huet-Equilbec, N. Lecesne, P. Lehérissier, F. Lemagnen, R. Leroy, J.Y. Pacquet, **L. Penescu**, M.G. Saint Laurent, O. Tuske and A.C.C Villari, "*Recent developments in the target-and-ion-source station for the SPIRAL II project at GANIL*", Nucl. Instrum. and Meth. in Phys. Res. B 241 (2005) 940-946.

Other publications:

- T. Stora, E. Bouquerel, L. Bruno, R. Catherall, S. Fernandes, P. Kasprowicz, J. Lettry, S. Marzari, B.S. Nara Singh, E. Noah, **L. Penescu** and R. Wilfinger, "*Oxide Target Designs for High Primary Beam Intensities for Future Radioactive Ion Beam Facilities*", AIP Conf. Proc. 1099 (2009) 764-768.
- E. Bouquerel, R. Catherall, J. Lettry, S. Marzari, E. Noah, **L. Penescu**, T. Stora and R. Wilfinger, "*Design and test of a two-body target unit for 100kW solid targets*", EURISOL DS report 03-25-2008-0009 (2008).
- E. Bouquerel, P. Bricault, L. Bruno, R. Catherall, M. Dombsky, S. Fernandes, J. Lettry, M. Lindroos, E. Noah, **L. Penescu**, P. Schmor, T. Stora and R. Wilfinger, "*High Power Oxide Target Tests at TRIUMF*", EURISOL DS report 03-25-2007-0007 (2007).

- T. Stora, J. Lettry, R. Catherall, E. Noah, R. Wilfinger, **L. Penescu**, E. Bouquerel, S. Fernandes, M. Santana-Leitner, L. Zanini, I. Guenter and F. Groeschel, "*Feasibility study for the 100kW direct targets*", EURISOL DS report 03-25-2006-0005 (2006).
- **L. Penescu**, "*Évaluation de la méthode ISOL par fusion-évaporation à partir des faisceaux d'ions lourds stables de LINAG*", GANIL Report R05 02 (2005).

A2. RESULTS DISSEMINATION AT CONFERENCES AND WORKSHOPS

Oral presentations:

- ICIS 09, 13th **International Conference on Ion Sources**, Gatlinburg, Tennessee, September 2009: "*Development of high efficiency Versatile Arc Discharge Ion Source (VADIS) at CERN ISOLDE*".
- **ISOLDE Workshop and Users Meeting** 2008, CERN, Geneva, November 2008: "*FEBIAD ion source development at ISOLDE: efficiency improvement for all the elements*".
- **ISOLDE Workshop and Users Meeting** 2007, CERN, Geneva, December 2007: "*FEBIAD ion source operation modes for tuning its selectivity: physics processes, numerical simulations and experimental data*".
- **Marie Curie Conference**: Putting the Knowledge Based Society into Practice, Manchester, UK, April 2006: "Ion source development for higher intensity radioactive ion beam production".
- The Interdisciplinary **TARGISOL Winter School** 2005, El Escorial, Madrid, February 2005: "*First simulations for N=Z radioactive beams for SPIRAL2*".

Posters:

- ICIS 09, 13th **International Conference on Ion Sources**, Gatlinburg, Tennessee, September 2009: "*Ion sources for MedAustron*".
- **EURISOL DS & EURONS Town Meeting** 2007, Helsinki, September 2007: "*Modeling of an ISOLDE FEBIAD ion source: plasma dynamics calculations and transversal emittance Measurements*".
- EMIS 07, XVth **International Conference on Electromagnetic Isotope Separators and Techniques Related to their Applications**, Deauville, France, June 2007: "*Numerical simulations of space charge effects and plasma dynamics for FEBIAD ion sources*".
- **EURISOL Town Meeting 2006**, CERN, November 2006: "*Characterization of a plasma ion source using numerical simulations*".

REFERENCES

[1] *P. Van Duppen et al.*, Nucl. Instr. and Meth. in Phys. Res. B 70 (1992) 393-397.
[2] Special Issue on Research Opportunities with Accelerated Beams of Radioactive Ions, Nuclear Physics A 693 (2001) n.1 and 2, Editor I. Tanihata.
[3] Proceedings of the Seventh International Conference on Radioactive Nuclear Beams, Cortina d'Ampezzo Italy 2006, EPJ Special Topics 150 (2007).
[4] Proceedings of 15th International Conference on Electromagnetic Isotope Separators and Techniques Related to their applications, Deauville France 2007, Nucl. Instrum. and Meth. in Phys. Res. B 266 (2008).
[5] *H.R. Ravn and B.W. Allardyce*, "On-Line Mass Separators", in Treatise on Heavy-Ion Science, Edt. D. A. Bromley, Plenum Press, New York, 1989, ISBN 0-306-42949-7.
[6] *B. Harss et al*, Rev. Sci. Instrum. 71 (2000) 380-387.
[7] *L.Penescu*, GANIL Report R-05-02 (2005).
[8] *J. Äystö*, Nucl. Phys. A 693 (2001) 477-494.
[9] *J.R.J. Bennett et al*, NuPECC Report by The NuPECC Working Group on Radioactive Nuclear Beam Facilities, April 2000.
[10] *M. Lindroos*, CERN Report CERN-AB-2004-086 (2004).
[11] TARGISOL Webpage: http://www.targisol.csic.es/facilities.html
[12] ISOLDE website: http://isolde.web.cern.ch/ISOLDE/
[13] *B. Jonson, H.L. Ravn and G. Walter*, Nuclear Physics News, Vol. 3, No. 2 (1993).
[14] *D. Voulot et al*, Nucl. Instrum. Meth. B 266 (2008) 4103-4107.
[15] *K. Peräjärvi et al*, Nucl. Instrum. and Meth. in Phys. Res. B 204 (2003) 272-277.
[16] *S. Sundell and H. Ravn*, Nucl. Instrum. and Meth. in Phys. Res B70 (1992) 160-164.
[17] *R. Kirchner*, Nucl. Instrum. and Meth. 186 (1981) 275-293.
[18] *B. Vosicki et al*, Nucl. Instrum. and Meth. 186 (1981) 307-313.
[19] *V.I. Mishin et al*, Nucl. Instr. and Meth. B 73 (1993) 550.
[20] *U. Koster, V. Fedoseyev et al*, Nucl. Instr. and Meth. B 204 (2003) 347.
[21] *F. Wenander and J.Lettry*, Rev. Sci. Instrum. 75 (2004) 1627-1629.
[22] *G. Gaubert et al*, Rev. Sci. Instrum. 74 (2003) 956-960.
[23] *G.D. Alton et al*, Nucl. Instrum. and Meth. B 170 (2000) 515-522.
[24] *P. Jardin et al*, Nucl. Instr. and Meth. in Phys. Res B 241 (2005) 940-946.
[25] *P. Jardin et al*, Rev. Sci. Instrum. 73 (2002) 789-791.
[26] *C. Huet-Equilbec et al*, Nucl. Instrum. and Meth. in Phys. Res. B 240 (2005) 752-761.
[27] *C. Eléon et al*, Nucl. Instrum. and Meth. B 266 (2008) 4362-4367.
[28] *P. Bricault et al*, Nucl. Instrum. and Meth. in Phys. Res. B 204, 319 (2003) 319-324.
[29] *P. Bricault*, Rev. Sci. Instrum. 77 (2006) 03A710.
[30] *K. Jayamanna et al*, Rev. Sci. Instrum. 73, (2002) 792.
[31] *J. Lassen et al*, Rev. Sci. Instrum. 77 (2006).
[32] *P. Bricault et al*, Proceedings of the 18th International Conference on Cyclotrons and their Applications 2007, Giardino Naxox Italy, p.499-504.
[33] *H.K. Carter and D.W. Stracener*, Nucl. Instrum. and Meth. B 266 (2008) 4702–4705.
[34] *G.D. Alton*, Nucl. Instrum. and Meth. A 382 (1996) 207-224.
[35] *P. Decrock et al*, Nucl. Instrum. and Meth. in Phys. Res. B 58 (1991) 252-259.
[36] *C. Barué et al*, Rev. Sci. Instrum. 69 (1998) 764-766.
[37] *J. Arje et al*, Phys. Rev. Lett. 54 (1985) 99-101.
[38] *P. Taskinen et al*, Nucl. Instrum. and Meth. A 281 (1989) 539.
[39] *R. Beraud et al*, Nucl. Instum. and Meth. A 346 (1994) 196.

[40] *K. Peräjärvi et al*, Nucl. Instrum. and Meth. A 546 (2005) 418.
[41] *P. Karvonen et al*, Nucl. Instrum. and Meth. in Phys. Res. B 266 (2008) 4454-4459.
[42] Report of the Working Group on Nuclear Physics, OECD Global Science Forum, May 2008, http://www.oecd.org/dataoecd/35/41/40638321.pdf
[43] *B.M. Sherrill*, Nucl. Instr. and Meth. B 204 (2003) 765-770, http://www.phy.anl.gov/ria/index.html and http://www.nscl.msu.edu/ria/index.php
[44] EURISOL Website: http://www.eurisol.org
[45] *L.Penescu et al*, Nucl. Instrum. and Meth. in Phys. Res. B 266 (2008) 4415-4419.
[46] *T.Stora et al*, Feasibility study for the 100kW direct targets, EURISOL DS report 03-25-2006-0005 (2006).
[47] *R. Kirchner and E. Roeckl*, Nucl Instrum and Meth 133 (1976) 187-204.
[48] *R. Kirchner*, Nucl. Instrum. and Meth. in Phys. Res. B 204 (2003) 179-190.
[49] *J. Lettry*, Proc. of the 20th Int. Linac Conference, Monterey, CA, USA, 2003, p.346-350.
[50] *G.D. Alton et al*, Rev. Sci. Instrum. 77 (2006) 03A711.
[51] *N. Lecesne*, NIM B 266 (2008) 4338-4345.
[52] *P.G. Johnson et al*, Nucl. Instr. and Meth. 106 (1973) 83.
[53] *G. Beyer et al*, Nucl. Instr. and Meth. 96 (1971) 347.
[54] *A. Latuszynski et al*, Nucl. Instr. and Meth. 125 (1975) 61.
[55] *M. Huyse*, Nucl. Instr. and Meth. 215 (1983) 1.
[56] *R. Kirchner*, Nucl. Instr. and Meth. A 292 (1990) 203.
[57] *O. Almen and K.O. Nielsen*, Nucl Instrum 1 (1957) 302-322.
[58] *G. Sidenius*, Nucl. Instrum. and Meth. 38 (1965) 19-22.
[59] *I. Chavet and R. Bernas*, Nucl. Instrum. and Meth. 51 (1967) 77-86.
[60] *J.M. Nitschke*, Nucl. Instrum. and Meth. A 236 (1985) 1-16.
[61] *D. Bohm et al*, The Characteristics of Electrical Discharges in Magnetic Fields, McGraw-Hill Inc.,New York, 1949.
[62] *A.G. Drentje*, Rev. Sci. Instrum. 74 (2003) 2631-2645.
[63] *P. Van Duppen*, Nucl. Instr. and Meth. B 126 (1997) 66.
[64] *J. Lettry et al*, Nucl. Instr. and Meth. B 126 (1997) 130-134.
[65] *W. Lotz*, Z. Phys. 216 (1968) 241.
[66] *A. Muller and E. Salzborn*, Phys. Lett A 62 (1977) 391.
[67] *H. Bethe and E. Salpeter*, Atome I, edit. S. Fliigge, Handbuch der Physik Vol.35, Springer-Verlag, Berlin, 1957.
[68] *D. Kamke and HJ. Rose*, Z. Phys. 145 (1956) 83.
[69] *O. Tarvainen, P. Suominen and H. Koivisto*, Rev Sci Instrum 75 (2004) 3138.
[70] *C. Nieter and J.R. Cary*, Journal of Computational Physics 196 (2004) 448-473.
[71] CPO programs, www.electronoptics.com
[72] *L. Tonks and I. Langmuir*, Phys. Rev. 34 (1929) 876.
[73] *I. Langmuir and K.T. Compton*, Reviews of Modern Physics 3 (1931) 191.
[74] *S. Gammino et al* – Rev. Sci. Instrum. 67 (1996) 4109.
[75] *Z.Q. Xie*, Rev Sci Instrum 69 (1998) 625.
[76] *C. Perret et al*, Physics of Plasmas 6 (1999) 3408.
[77] *R. Geller*, "Electron Cyclotron Resonance Ion Sources and ECR Plasmas" (IOP, Bristol, 1996).
[78] *P. Spaedtke*, Rev. Sci. Instrum. 75 (2004) 1643.
[79] *R. Becker and W.B.Herrnannsfeldt*, Rev Sci Instrum 63 (1992) 2756.
[80] *S.M. Elliott et al*, Proc. of ECRIS08, Chicago, IL USA.
[81] *S. Biri et al*, HEP & NP 31 (2007) 156.
[82] *M.C. Vella*, Nucl. Instrum. and Meth. 187 (1981) 313.
[83] *B.M. Penetrante et al*, Phys. Rev. A 43 (1991) 4861.
[84] *I.V. Kalagin et al*, Plasma Sources Sci. Technol. 7 (1998) 441.
[85] *O. Almen and K.O. Nielsen*, Nucl. Instrum. 1 (1957) 302-322.

[86] *G.D. Alton and C. Williams*, Rev. Sci. Instrum. 67 (1996) 1626.
[87] *D. Fang et al*, Phys. Rev. A 47 (1993) 1861.
[88] *L.Penescu*, ISOLDE Workshop and Users Meeting, CERN Geneva, December 2007 (unpublished).
[89] *R. Kirchner et al*, Nucl. Instr. and Meth. 186 (1981) 295-305.
[90] *J. Lettry*, Proc. of the 1999 Particle Accelerator Conference, New York, 1999.
[91] *C.D. Child*, Phys. Rev. (Ser.1) 32, 492 (1911).
[92] *I. Langmuir and K.T. Compton*, Rev. Mod. Phys. 3, 251 (1931).
[93] *E. Bouquerel*, PhD Thesis, University Paris XI, Orsay, 2009.
[94] *U.C. Bergmann et al*, NIM B204 (2003) 220-224.
[95] *U. Köester*, PhD Thesis, Technical University of Munich, 2000.
[96] CERN experiment IS467, H.Fynbo, B.Blank and col. (to be published).
[97] *D. Niedherr et al*, Phys. Rev. Lett. 102 (2009) 112501.
[98] *R.Kirchner et al*, Nucl. Instrum. and Meth. in Phys. Res. A 247 (1987) 265-280.
[99] *H. Bakker*, Enthalpies in Alloys, Miedema's Semi-Empirical Model., TransTech Publications, Switzerland (1998).
[100] *B. Eichler et al*, Adsorption flüchtiger Metalle auf metallischen Oberflächen und Möglichkeiten ihrer Anwendung in der Kernchemie – Berechnung der Adsorptionsenthalpien der Actinoide. Tech. Rep. ZfK-560, Zentralinstitut für Kernforschung, Rossendorf, 1985.
[101] *R. Kirchner*, Nucl. Instrum. and Meth. in Phys. Res. B 26 (1987) 204-212.